NEI-NO--1021
NO9905058

Håkon Bergem

Sulfur tolerant zeolite supported platinum catalysts for aromatics hydrogenation

NTNU Trondheim
Norges teknisk-naturvitenskapelige universitet

Doktor Ingeniøravhandling 1997:41
Institutt for industriell kjemi
Trondheim

The Norwegian University of

Science and Technology

The Department of Industrial Chemistry

SULFUR TOLERANT ZEOLITE SUPPORTED PLATINUM CATALYSTS FOR AROMATICS HYDROGENATION

by

Håkon Bergem

A Thesis submitted for the Degree

DOCTOR OF ENGINEERING

April 1997

DISCLAIMER

Portions of this document may be illegible in electronic image products. Images are produced from the best available original document.

ACKNOWLEDGMENTS

First of all I wish to thank Professor Anders Holmen for giving me the opportunity and encouragement to engage myself in this work. Associate Professor Edd A. Blekkan is greatly acknowledged for his guidance, helpful suggestions, and valuable comments on the manuscript.

In addition, I want to thank Dr. Arne Grønvold ,Siv.Ing. Marit S. Brownrigg, Stud.tech. L. Bednarova, and V. Mala for invaluable contributions in the preparation and characterization of the catalyst samples.

My colleagues at the Department of Industrial Chemistry, NTNU and The Department of Catalysis and Kinetics, SINTEF Applied Chemistry are also appreciated for their support and friendship.

A special thank to Siv and my parents for their interest, support and encouragement throughout these many years of schooling.

This work was made possible by the financial support from the Norwegian Research Council and Statoil under the MILRAF program. The Department of Industrial Chemistry is acknowledged for financial support during the last year of this work.

ABSTRACT

An experimental study of sulfur tolerant zeolite supported platinum catalysts for aromatics hydrogenation.

Platinum catalysts supported on Y-zeolite have been prepared and characterized in various ways, including the hydrogenation of toluene in a high pressure fixed bed reactor. The effect of sulfur adsorption on the kinetic behaviour of the catalysts has been investigated. The effect of different sulfur compounds on the catalyst activity has also been studied. Platinum supported on Y-zeolite gives considerably more sulfur-tolerant catalysts compared to Al_2O_3 as support.

Catalyst preparation and characterization. Noble metal catalysts supported on Y-zeolite were successfully prepared by ion-exchange. The metal content was 0.3 wt% and the Si/Al ratio of the zeolite supports varied in the range between 2.6 and 40. Characterization of the catalyst samples were performed utilizing several techniques. Ammonia TPD profiles showed wide desorption peaks indicating a large distribution in acid strength. The metal function was characterized by chemisorption (H_2-O_2 titration in the pulse mode, and H_2 chemisorption in a volumetric apparatus), TEM, and toluene hydrogenation. The results indicated the presence of reduced metal in both supercages and mesopores. The location and size of the metal particles depended on the temperatures of pretreatment and on the zeolite support itself. Toluene hydrogenation revealed differences in diffusion properties resulting from coke formation, different metal distribution, and the absent of mesopores.

Hydrogenation of toluene. The effects of temperature and pressure on the kinetic behaviour of the platinum catalysts were studied in a high pressure fixed bed micro reactor. The reaction orders in toluene and hydrogen were determined at 240°C and 31 bars total pressure. An order close to 0 in toluene and 1.5 in hydrogen was found. A temperature dependent maximum in the reaction rate was also found. The temperature of maximum reaction rate varied with catalyst support and reaction pressure.

Hydrogenation of sulfur-spiked toluene. When sulfur is added to the toluene feed there is a strong decrease in the catalyst activity due to sulfur adsorption. The kinetics of the catalysts is also altered. Both a change in the reaction orders in toluene and hydrogen, and a different temperature response is observed. Three different sulfur compounds; benzothiophene, dibenzothiophene, and dimethyldisulfide were studied. There were no clear differences in the effect of these sulfur components on the catalyst activity. Pre-sulfiding of the same catalysts in 5% H_2S/H_2 resulted in catalysts with lower hydrogenation activity but similar kinetic behavior.

Sulfur-tolerance. Platinum supported on Y-zeolites gives considerably more sulfur-tolerant catalysts compared to Al_2O_3 as support. As an example the most active zeolite supported catalyst shows a turnover frequency five times that of Pt/Al_2O_3 at a sulfur level one order of magnitude greater. High Si/Al ratios give high specific activty due to higher Pt dispersion, while the intrinsic activity (TOF) in the presence of sulfur is highest at low Si/Al ratio. The sulfur tolerance defined as the ratio of the TOF for hydrogenation of sulfur-spiked toluene over the TOF for hydrogenation of clean toluene seems to be independent of the SiAl ratio.

TABLE OF CONTENTS

LIST OF PAPERS

The results which this thesis is based on are presented in the following papers.

I. Bergem H, Gitlesen A, Holmen A, Blekkan EA. *Sulfur Resistance of Supported Noble-Metal Catalysts: Cyclohexane Dehydrogenation over Y-Zeolite-Supported Pt, Pd, Ir, and Ru in the presence of Thiophene.* Environmental Catalysis. Proceedings of the 1st World Congress.: May 1, 1995-May 5, 1995; Pisa (Italy). Rome: Societa Chimica Italiana; (1995), 411.

II. Bergem H, Holmen A, Blekkan EA. *Toluene Hydrogenation over Supported Noble Metal Catalysts: Benzothiophene Poisoning of Pt/Y-zeolite Catalysts with Different Si/Al Ratios.* EuropaCat-II, Book of Abstracts.: September 3, 1995-September 8, 1995; Maastricht, The Netherlands. (1995), 779.

III. Bergem H, Holmen A, Blekkan EA, Grønvold A. *Toluene Hydrogenation over Supported Noble Metal Catalysts: Sulfur Tolerance of Pt/Y-Zeolite Catalysts with Different Si/Al Ratios.* 11th International Congress on Catalysis.: June 30, 1996-July 5, 1996; Baltimore. USA: (1996), Poster no. 058.

IV. Bergem H, Blekkan EA, Holmen A. *Aromatics hydrogenation over supported platinum catalysts: the influence of sulfur on the kinetics of toluene hydrogenation over Pt/Y-zeolite catalysts.* Amsterdam: Elsevier Science;. Froment GF, Delmon B, Grange P; Stud. Surf. Sci. Catal.; *106* (1997), 391

V. Bergem, H, Blekkan EA, Grønvold A, Holmen A. *Toluene Hydrogenation over Supported Noble Metal Catalysts: Sulfur Tolerance of Pt/Y-Zeolite Catalysts with Different Si/Al Ratios,* in preparation.

SYMBOLS AND ABRIVATIONS

A	- Catalyst activity [μmol/s, g cat.]
AAS	- Atomic Absorption Spectroscopy
BE	- Binding energy
C	- Concentration
CN	- Cetane Number
CI	- Cetane Index
d_p	- Particle diameter
D	- Dispersion
E_a	- Apparant activation energy
ESR	- Electron Spin Resonance
eV	- electron volt
FCC	- Fluid Catalytic Cracking
FID	- Flame Ionization Detector
GC	- Gas Chromatograph
H	- Hydrogen atoms
h	- Planck constant [J s]
IR	- Infrared spectroscopy
K	- equilibrium constant
k	- Rate constant
LCO	- Light Cycle Oil
LEED	- Low-energy Electron Diffraction
LGO	- Light Gas Oil
LHSV	- Liquid Hourly Space Velocity [ml reactant/ml catalyst, h]
m	- Reaction order in hydrogen
NMR	- Nuclear Magnetic Resonance
n	- number of moles of hydrogen
n	- Reaction order in toluene
PAH	- Polycyclic Aromatic Hydrocarbons
P_i	- Partial pressure of component i
Re_p	- Particle Reynolds number

r	- Reaction rate
T_C	- Temperature of calcination [°C]
TEM	- Transmission Electron Microscopy
TGA	- ThermoGravimetric Analysis
TPD	- Temperature Programmed Desorption
TOF	- Turnover Frequenzy [s^{-1}]
TOS	- Time on Stream [h]
T_R	- Temperature of reduction [°C]
UV	- Ultraviolet
WHSV	- Weigth Hourly Space Velocity [g reactant/g catalyst, h]
XPS	- X-ray Photoelectron Spectroscopy
XRD	- X-ray Diffraction
Y_i	- mole fraction of component i
$\Delta G°_f$	- Standard Gibbs free energy of formation [kJ/mol]
ΔH	- Enthalpy of formation [kJ/mol]
θ	- ratio of sulfur atoms to surface metal atoms
ν	- frequency [Hz]

1. INTRODUCTION

Motivation and aims for the present work.

The increasing demand for transportation fuels at the expense of heavier fuel oil has forced the refinery industry to expand their conversion capacity with hydrotreating as one of the key processes. A shift towards more diesel powered vehicles along with tightening fuel regulations demanding cleaner fuels has lead to increasing interest in catalytic processes for the manufacturing of such environmentally acceptable fuels.

History

Information on the historical background for this work is given in Chap. 1.1. Hydroprocessing is playing an increasingly important role in order for the refinery industry to comply with governmental and market demands for cleaner and environmentally more acceptable products. Transportation fuels with better ignition quality, higher H/C ratio, less aromatics, and sulfur requires extensive upgrading with hydroprocessing as one of the key processes.

Outlook

Some thoughts on future transportation trends are presented in Chap. 1.2. Diesel vehicles are achieving a growing share of the ligth duty vehicle market. Its inherently high efficiency, low operating cost, durability, and reliability have contributed to its increasing role especially in areas where fuel cost are high. Continued growth are raising concerns regarding the health and environmental effects of the high NO_x and particulate emissions leading to increasingly tightening diesel regulations.

Scope of the work

A description of the aims and premises are given in Chap. 1.3. The production of middle distillates and diesel from refractory feedstocks requires extensive reduction of the sulfur and aromatic content in the final product. Catalysts capable of maintaining high hydrogenation and desulfurization activity in the presence of increased levels of sulfur will be of great interest and hence motivates a detailed study of possible such materials.

1.1 HISTORY

1.1.1 TRADITIONAL HYDROPROCESSING

A review of its importance in petroleum refining.

Hydroprocessing rank among the most important catalytic processes worldwide today. **Hydroprocessing or hydrotreating include a variety of catalytic hydrogenation processes resulting in the saturation of unsaturated hydrocarbons and the removal of S,N,O, and metals from petroleum streams. Environmental legislation and the increased need for conversion of heavier refinery fractions into light distillates for transportation use are major factors contributing to the increased role of hydrotreating.**

The development of catalytic hydrotreatment was closely related to other refinery processes, especially catalytic reforming. Naphta reforming were commercialized during the 1940's for the production of high-octane gasoline [1] resulting in huge amounts of hydrogen becoming available to the refineries. The success of catalytic reforming again depended on the crucial removal of sulfur from the naphta feed resulting in a win-win situation for the two processes.

Importance of hydroprocessing

Today hydroprocessing of oil fractions or coal-derived liquids rank among the most important catalytic processes worlwide accounting for close to 10% of annual sales of catalysts in the world [2]. Hydroprocessing is used both for improving final products and in the pretreatment of feeds utililzed in other refinery processes like catalytic reforming, fluid catalytic cracking (FCC), and hydrocracking. The result of this beeing that over 50% of all refinery streams undergo hydrotreating.

The caracteristics of hydroprocessing

Hydroprocessing catalysts consist of base metal sulfides on alumina carriers (e.g. $CoMo/Al_2O_3$ or $NiMo/ Al_2O_3$). The choice of catalyst depends on which reaction is targeted. Hydrotreating includes a variety of catalytic hydrogenation processes like the removal of heteroatoms (sulfur, nitrogen, oxygen, and metals), hydrocracking, hydrogenation, and

isomerization. The sum of these reaction determine the overall change in the molecular structure of the product.

The role of hydrotreating today

The decrease in the consumption of fuel oil coupled with the ever increasing demand for ligh distillates for transportation use have lead to the need for conversion of these heavier refinery fraction. This is illustrated in Figure 1.1 showing the change in demand for various oil products during the last decades. Environmental legislations have imposed stringent regulations on the emissions from both the refinery itself and from its products. In the last case hydrotreating have played and will play an increasing role in the future.

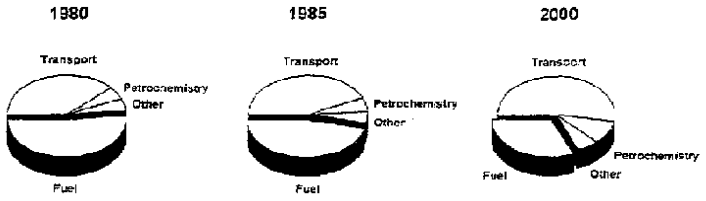

Figure 1.1: Changes in demand for various oil products [2].

1.2 OUTLOOK

1.2.1 REGULATIONS ON TRANSPORTATION FUELS

Views on factors shaping fuel requirements.

The combustion engine will also in the foreseeable future be the main instrument for moving vehicles. The goal for current and future engine and fuel technologies then becomes a combined strategy leading to better overall performance of such vehicles. Several factors influence the demands put on transportation fuels, among them the need for clean and efficient fuels to meet advanced emission control and fuel economy goals.

The combustion engine

Since the beginning of this century the thermal engine has been the main instrument for moving vehicles. The immense success of the combustion engine, due to its low cost and high reliability, has built up tremendous industries to satisfy the transportation demand: vehicles, fuels, equipment, and roads. With this in mind one can safely predict that this picture will not change in the foreseeable future resulting in a continuing evolution of these technologies.

Future technologies

The emphasis of engine technology will be in terms of fuel economy and emission control. Engines like the diesel engine are widespread in Europe and have a clear fuel economy advantage over the traditional four-stroke engine. Other engines under development are the lean burning gasoline engines and the two-stroke direct gasoline injection engine. These are all characterized by their low fuel consumption and they can be optimized for conventional fuels [3].

Clean fuels

The need for clean and efficient fuels have lead to the implementation of reformulated gasoline (in the U.S.) and reformulated diesel (in the E.U.). Although this is a complex subject the positive effects on emissions of some gaseous species and particulates are well documented [3]. Some present environmental specifications and likely trends for

transportation fuels are outlined in Table 1.1.

Table 1.1: Some present environmental specifications and likely trends for transportation fuels [2].

	Present specifications (<1993)					Expected future (1993-2000)			
	Europe	Sweden	Japan	US	Calif.	Europe	Japan	US	Calif.
Gasoline (unleaded)									
Max. S[a]	0.05-0.1	0.1		0.1		0.01		0.04	0.003
Max. aromatics[b]								25	22
Max. benzene[b]	5			5		1-3		1	0.8
Diesel									
Min. cetane No.	45-50	45-50[c]	45	40	40	50	50	45	50
Max. S	0.2-0.3	0.001-0.2[c]	0.2	0.5	0.05	0.05	0.05	0.05	0.05
Max. aromatics		5-25[c]							10

[a] wt%, [b] vol%, [c] lower and higher values represent Class I and Class III, respectively.

Future demand for diesel fuel quality

The emissions of carbonmonoxide (CO) and unburned hydrocarbons (HC) from diesel engines are very low [4], infact they are about the same level as an Otto engine equipped with a 3-ways catalyst. In these engines the efforts are concentrated on reducing nitrogen oxides (NOx) and particulates including polycyclic aromatic hydrocarbons (PAH). The interrelationship between these emissions and fuel characteristics are therefore important. The combustion in the engine is affected by changes in the physical and chemical properties of the diesel fuel. The main characteristics of a more stringent classification of diesel are:

- ignition quality
- density and viscosity
- distillation range
- low temperature operability
- cleanliness and stability
- sulfur content

The most significant property is the ignition quality characterized by the cetane number and an expected increase in the minimun requirements of this property is clearly seen in Table 1.1.

1.3 SCOPE OF THE WORK

1.3.1 SULFUR TOLERANT HYDROGENATION CATALYSTS

An experimental study with the purpose of describing and explaining catalyst properties.

The main objective of the present work was the study of possible catalysts active for desulfurization, hydrogenation, and ring-opening of aromatics all in the presence of sulfur. A close examination of the physical properties and kinetical behavior of the choosen catalysts was to be performed. In connection with this a high pressure reactor setup was constructed and built as part of this work enabling activity measurements to be performed.

This work was performed as a part of the "MILRAF" program initiated and funded by the Norwegian Research Council. The program was aimed at studying the production of clean fuels with this work focusing on hydrotreating of middle distillates. More specific the main objective of this work was the study of catalysts active for desulfurization, hydrogenation, and ring-opening of aromatics all in the presence of sulfur. The task was further narrowed down and limited to the investigation of noble metals supported on Y-zeolites.

Noble metals supported on Y-zeolites have been a field of research at the Department of Industrial Chemistry at the Norwegian University of Science and Technology (NTNU) and SINTEF Applied Chemistry for several years. Fields of interest have been the incorporation of metals, the effects of pretreatment conditions, the application of various techniques for characterization, and the study of different chemical reactions over such systems. A Ph.D work on the deactivation and regeneration of such catalysts is also in progress.

The catalysts were to be characterized in terms of their physical properties. Due to the bifunctional nature of these catalyst systems this meant a close examination of both the metallic and acidic function. Toluene hydrogenation was chosen as a suitable model reaction and the activity and kinetic behavior of the catalysts in question for this reaction were studied.

To be able to perform the probe reaction at close to realistic conditions a high pressure reactor setup was constructed and built.

Method of writing

This thesis is written according to a relatively new way of organizing the process of writing developed by the two Norwegians Per and Tormod Bjørnstad called the Method of Levels [155]. The material is organized in a way that goes from a general overview at the top level down to underlying levels where the topics are treated in a more specific and expanded manner. By doing so the reader can explore the written material to the extent of his/her abilities and needs.

2. LITERATURE AND PRINCIPLES

Survey of literature and principles, the present status.

Knowledge of the thermodynamic and kinetic behavior of aromatic hydrogenation is a prerequisite for the successful upgrading of diesel fuel. Due to the great importance of hydrotreating processes in the refining industry, much work in understanding how hydrotreating catalysts operate has been done. Sulfur compounds are present in all petroleumderived feedstocks with the potential of poisoning metal catalysts. Characterization of catalyst properties is essential in the study of these reactions.

Aromatic saturation

A description of aromatic saturation, basic and industrial aspects are given in Chap. 2.1. Diesel fuel quality and aromatic content are closely related. Fuel upgrading via aromatic hydrogenation require extensive knowledge of the thermodynamic and kinetic behavior of these reactions. The literature on both model aromatic compounds and industrial feedstocks is rewieved. Finally available options in manufacturing high quality diesel meeting stringent fuel specifications are outlined.

Catalysts in hydrotreating

A description of hydrotreating catalysts with emphasize on hydrogenation activity and sulfur tolerance is outlined in Chap. 2.2. The immense importance of hydrotreating processes in the refining industry has motivated the great efforts in understanding how hydrotreating catalysts works. Metal sulfide catalysts in form of their active phases are now well understood. The growing demand for high quality diesel fuel underlines the need for high activity catalysts for aromatic hydrogenation in the present of sulfur. Noble metals on various supports together with transition metal sulfides, carbides and nitrides are all interesting systems in this respect.

Sulfur poisoning of metal catalysts

Studies on sulfur poisoning, the fundamental characteristics are outlined in Chap. 2.3. Due to the strong chemisorption bond between sulfur and all metallic catalysts high toxicities of sulfur for different reactions are encountered. The adsorption of other molecules is modified by the presence of adsorbed sulfur on the catalyst surface. Interactions between the metal, the hydrocarbon and the sulfur compound affect the catalyst activity and selectivity. Regeneration schemes performed at moderate temperatures to avoid sintering of highly dispersed catalysts are essential.

Catalyst characterization

A brief description of catalyst characterization, the applied methods and the principles and procedures related to them are given in Chap. 2.4. Chemisorption of hydrogen is an extensively used method for measuring the dispersion of supported metals due to the well-defined adsorption stoichiometries. Toluene hydrogenation is classified as a structure-insensive reaction and as such can be used to assess the metal particle size. To measure the acidity of zeolites, temperature programmed desorption of ammonia is a simple and much used technique.

2.1 AROMATIC SATURATION

2.1.1 THE CHEMISTRY OF DIESEL BLENDING COMPOUNDS

Explanation of the chemistry of diesel blending compounds and their impact on diesel fuel quality.

The Cetane Number (CN) is the prime measure of the diesel fuel quality and the cetane quality depends on the paraffinicity of the molecular structures that constitute the fuel. Refinery streams high in aromatic rings and with little or no alkyl-side chains have poor cetane quality. To be able to follow the progress of aromatic removal in hydroprocessing, understanding the relationship between cetane quality measurements and the numerous analytical techniques for measuring aromatics are important.

Diesel

Diesel compounds generally fall in the boiling range of 200°-360°C and the carbon-number of the molecules roughly lies between C_{12}-C_{25} and they are comprised of aromatics, naphthenes, n- and iso-paraffins, olefins or molecular combinations of them all. Because of the great number of refinery streams available for blending into the final fuel, the proportion of the different molecules varies conciderably. An illustrative example of the structural composition of a light LGO is given in Table 2.1 An overview of typical structures of mono-, di- and triaromatic compounds found in middle distillate is shown in Table 2.2.

Cetane Number

The cetane number is the prime measure of the ignition properties of diesel fuel. The paraffinicity of the fuel and the cetane quality are closely related as can be seen by studying Fig. 2.1.

Table 2.1: Composition of Ligth LGO [5].

Paraffines:	High levels of n-paraffines ranging from C_{12} to C_{19}
Naphthenes:	Evenly distributed isomers of monocyclonaphthenes with side chains ranging from C_5 to C_{12}. Bicyclonaphthenes (decalines) are practically absent.
Mono-aromatics:	
Mono-substituted	n-alkyl benzenes present with the alkyl group ranging from C_3 to C_{11}. The largest concentration (approx. 70%) are the alkyl benzenes with C_6-C_8 alkyl groups.
Di- and tri-substituted	Substituted benzenes where the length of one of the n-alkyl substitution groups differs.
Alkyl indanes	Low concentrations
Alkyl tetralines	Low concentrations
Di-aromatics:	
Naphthalenes	Predominantly alkylated naphthalenes where the alkyl group ranges from C_1-C_4.
Tri-aromatics:	
Fluorene	Traces
Anthracene	Traces

About 90% of the saturates are paraffines.

The n-paraffins possess high cetane quality increasing with the chain-lenght of the molecule (CN = 100 for n-C_{16}). Highly condensed aromatic structures lie at the other end of the scale with CN below 20. From this we clearly see the beneficial effect of saturating the aromatics followed (if possible) by an opening of the formed naphtenic rings.

Table 2.2: Typical structures of some aromatic compounds present in petroleum fractions [6].

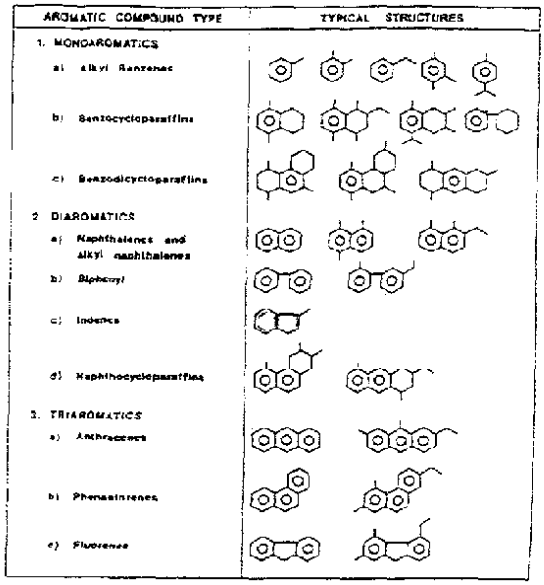

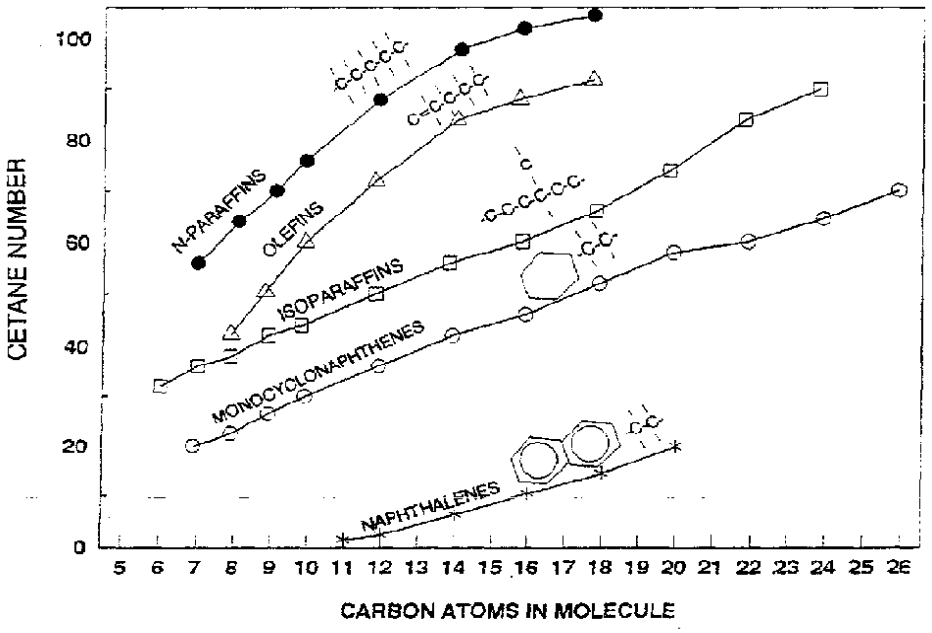

Figure 2.1: Cetane number vs. hydrocarbon type [7].

The cetane / aromatics relationship

As stated above, reduction in the aromatics content improves the cetan number of the fuel. Unzelman reported a linear correlation of aromatics content versus cetane number for light cycle oils and straight-run gas oils as illustrated in Fig.2.2.

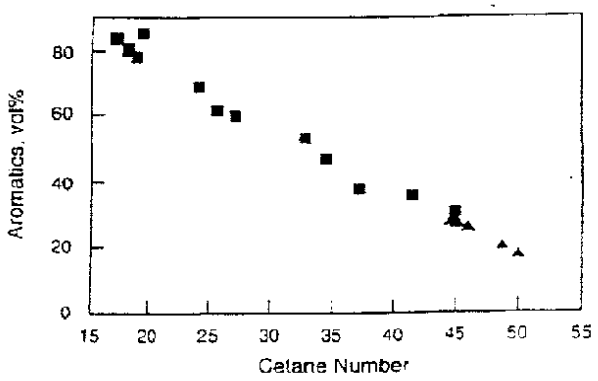

Figure 2.2: Cetane number vs. aromatic content: (■) LCO and SR distillates: (▲) diesel fuel [8].

2.1.2 THE THERMODYNAMICS OF AROMATIC HYDROGENATION

Information on the thermodynamic limitations in hydrogenation of aromatics.

Aromatic saturation is the only group of conversions that gives rise to thermodynamic limitations within the operating range of hydrorefining. These reactions are strongly exothermic and subsequently the level of aromatic saturation achievable with a given feedstock goes through a maximum with increasing reaction temperature. Polyaromatics are hydrogenated via successive steps, saturating one aromatic ring at a time, each of which is a reversible reaction.

Hydrotreating conditions

Hydrotreating is conducted within a wide operating range depending on the feedstock and the desired conversion. Reaction temperatures generally lie between 300°C and 400°C, and the partial pressure of hydrogen varies from 5 to 120 bar.

Equilibrium limitations

Aromatic hydrogenation reactions are highly exothermic with heats of reaction in the range between 17 and 63 kJ/mol H_2 [9]. Consequently these reactions are favored by lower temperature. Given the reaction:

$$Aromatics + nH_2 \Leftrightarrow Naphtenes \qquad (2.1)$$

it has been shown [10] that the equilibrium concentration of the aromatic species can be approximated by:

$$\frac{Y_A}{Y_A + Y_{AH}} = \frac{1}{1 + K_a \times \left(P_{H_2}\right)^n} \qquad (2.2)$$

where Y_A and Y_{AH} denotes the mole fraction of aromatic and naphthene species respectively; K_a is the equlibrium constant, and P_{H_2} the partial pressure of hydrogen. From this it can be seen that high pressures favor high conversion (low equilibrium concentration of aromatics).

This is especially the case for reactions where the number of moles of hydrogen, n, needed for complete saturation is high. An example of this behavior is shown in Fig.2.3 for an industrial feedstock.

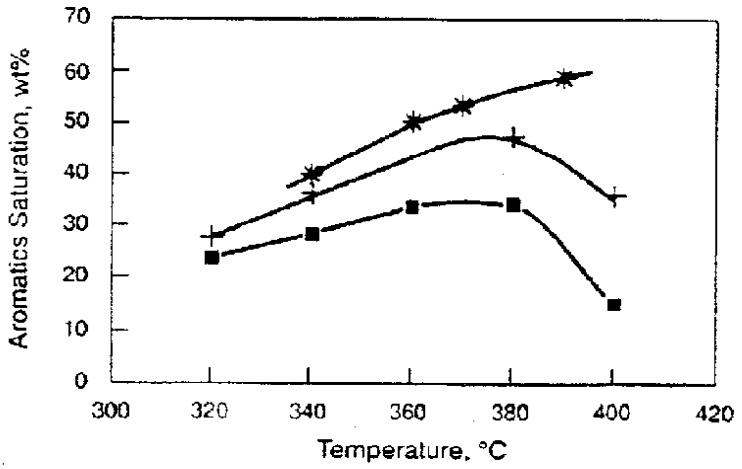

Figure 2.3: Effect of temperature and pressure on the aromatic saturation in an industrial feedstock. (■) 4.5 Mpa, (+) 6.5 Mpa, (✳) 12.5 MPa [11].

Effect of molecular structure on the thermodynamics

The value of the equilibrium constant differs conciderably from one family of aromatic hydrocarbons to another. For the benzene homologues the value of the equilibrium constant decreases when the number of side chains and the number of carbon atoms in each side chain increases as shown in Fig. 2.4. The same general rule applies to multi-ring aromatics.

Hydrogenation of polyaromatics proceeds via successive steps one ring at a time, each of which is reversible. The equilibrium constant is usually higher for the hydrogenation of the first ring, decreasing for the subsequent steps as the molecule attain a more naphthenic character. In spite of this, saturation of the first ring is thermodynamically less favorable at typical hydrotreating conditions because of the larger number of moles of hydrogen involved in the final ring hydrogenation as shown in Fig. 2.5.

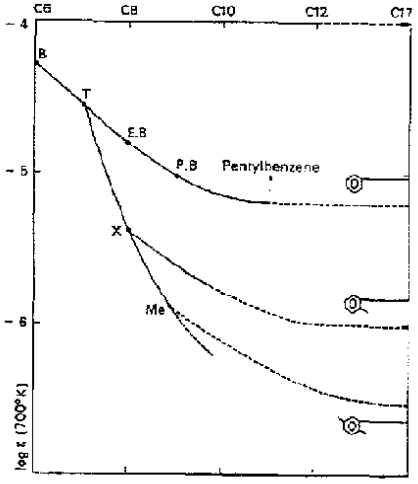

Figure 2.4: Equilibrium constants for the hydrogenation of the benzenic series [12].

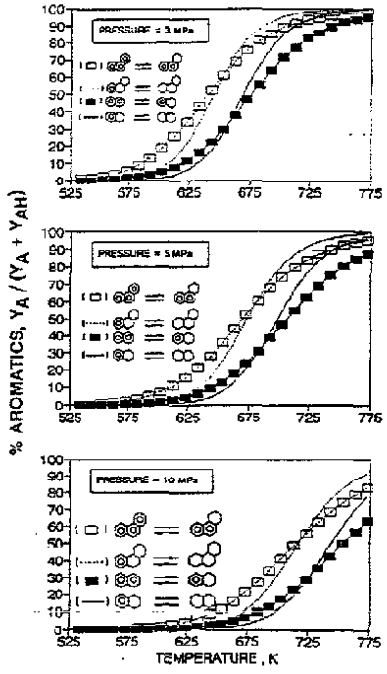

Figure 2.5: Equilibrium concentration for first- and last-ring hydrogenation of phenanthrene and naphthalene as a function of hydrogen pressure [6].

A general observation is also that the quilibrium constant for saturating polyaromatics is lower than that for hydrogenating benzene. Thus, higher hydrogen partial pressures are needed to convert high molcular weight polyaromatics to fully hydrogenated products. This demonstrates the necessity of developing more active catalysts which can operate at lower temperatures, taking advantage of the thermodynamics.

2.1.3 KINETICS AND REACTION MECHANISMS FOR AROMATIC HYDROGENATION

Studies on kinetics and reaction mechanisms of model aromatic compounds and industrial feedstocks.

For simple monoaromatics a reaction order close to 1 in both the reactants on metal sulfides is generally found. Over Group VIII metals an order of reaction close to zero for the reacting hydrocarbon is observed. Multi-ring aromatics are hydrogenated one ring at a time. The ring with the lowest aromaticity is hydrogenated first at a much higher rate than the monoaromatics. For industrial feedstocks information is scarce due to the complexity of the reactions.

Studies of the mechanisms and kinetics of chemical reactions are important for several reasons: These tools give insight into how chemical bonds are made and broken and in estimating their energies and strenght. Knowledge of molecular structure of compounds can be obtained and the satisfactory design of chemical reactors for performing reactions on a technical scale is possible. For catalytic reactions insight into the role of the catalyst in altering the rate (via the reaction mechanism) is of crucial importance.

Model aromatic compounds / monoaromatics

The hydrogenation of benzene and simple alkylbenzenes on both hydrotreating catalysts (metal sulfides) and Group VIII metals (Ni, Pt, Pd) has been the subject of many experimental studies.

On metal sulfides (CoMo, NiMo, NiW) close to first order in both the reactant hydrocarbon and hydrogen is generally observed [12,13]. Sulfur-compounds converted to H_2S are known to inhibit the reaction [14,15]. For toluene hydrogenation on MoS_2/Al_2O_3 a complex behavior of H_2S is found [16]. At medium partial pressure of H_2S an inhibiting effect is observed, while at high H_2S partial pressure (above 60000 Pa) the hydrogenation activity seems to stabilize.

On Group VIII metals studies of the hydrogenation of benzene, toluene, xylenes and ethylbenzene have revealed orders of reaction close to zero [17-20]. These low orders of reaction of the aromatics are explained by a strong adsorption of the aromatic compound. The

apparant activation energies are low (50-60 kJ/mol). The aromatic compounds are bonded to the metal surface via π-bonds involving an electron transfer from the aromatic ring to the unoccupied d-metal orbitals. A probable mechanism is a stepwise addition of hydrogen (scheme 2.1) proposed by Van der Steen et al. [21].

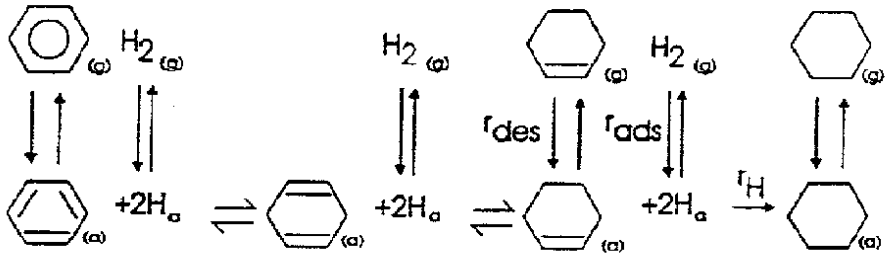

Scheme 2.1: Mechanism for the heterogeneous catalytic hydrogenation of benzene over group VIII metals [21].

A temperature-dependent maximum in the hydrogenation activity occuring round 200°C is frequently reported [17-19,22,23]. This is not due to thermodynamic limitations but rather attributed to the formation of hydrogen-deficient surface carbonaceous species inhibiting the hydrogenation reaction [24].

Model aromatic compounds / multiring aromatics

Sapre and Gates studied hydrogenation of naphthalene, biphenyl and phenylnaphthalene over hydrotreating catalysts ($CoMo/Al_2O_3$) and found it to be a first order reaction [25]. The reaction pathways are shown in scheme 2.2. The rings are saturated sequentially and the rate data in the network suggest that the hydrogenation of the first ring is considerably faster than hydrogenation of the last. Recent studies on hydrogenation of fused diaromatics (naphthalene and 1-methylnaphthalene) over metal sulfides by Kokayeff [26] and Bouchy et. al. [27,28] respectively, confirm this with a rate of hydrogenation for the first ring roughly one order of magnitude faster than the rate of the monoaromatics. They also found compounds containing nitrogen to reversibly deactivate the hydrogenation. The partial resonance energy or aromaticity of the different rings in fused multiring aromatics are not the same. The ring with the lowest aromaticity will be hydrogenated first.

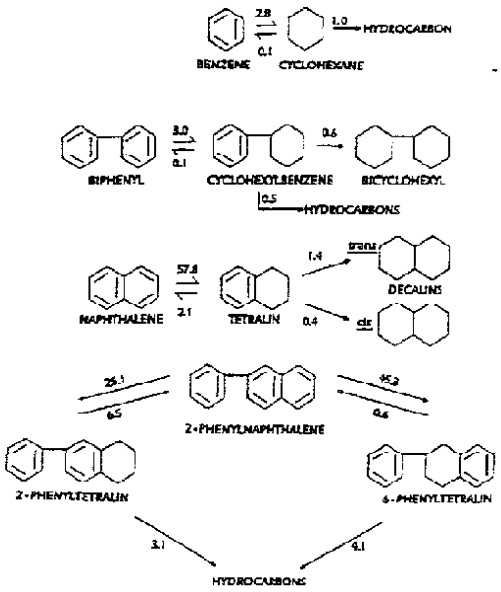

Scheme 2.2: Reaction networks for hydrogenation of benzene, biphenyl, naphthalene, and 2-phenylnaphthalene in the presence of sulfided CoO-MoO/γ-Al_2O_3 at 325°C and 75 atm [25].

Industrial feedstocks

Kinetic studies of industrial feedstocks regarding aromatic hydrogenation are few in numbers most likely due to the complexity of the reactions. Several workers [29,30] have developed kinetic models based on simple first-order reversible reactions:

$$Aromatics + nH_2 \Leftrightarrow Naphtenes \qquad (2.1)$$

Assuming pseudo-first-order for the forward reaction and also first-order in naphthenes for the reverse reaction, the rate expression becomes:

$$-\frac{dC_A}{dt} = k_f C_A P_{H_2}^n - k_r C_N \qquad (2.3)$$

where: C_A = fractional aromatic content; C_N = fractional naphthene content; t = time; k_f = forward rate constant; k_r = reverse rate constant; P_{H_2} = hydrogen partial pressure; and n = reaction order with respect to hydrogen partial pressure. Integrating with suitable substitutions gives the expression:

$$\ln\frac{C_A - C_{Ae}}{C_{A0} - C_{Ae}} = -k_R t \tag{2.4}$$

where C_A, C_{A0} and C_{ae} is related to product, feed and equilibrium consentration of aromatics in the reacting mixture and k_R is the hydrogenation rate constant.

At lower temperatures where the effect of equilibrium is insignificant, the simplifying assumption of irreversible kinetics can be made:

$$\ln\frac{C_A}{C_{A0}} = -k_R t \tag{2.5}$$

Wilson et al. [30] used this expression on data from aromatic hydrogenation of a middle-distillate fraction from Alberta syntetic crude over a presulfided Ni-W/γ-Al_2O_3.

Yui and Sansford [31] used a similar approach and arrived at this rate equation after integration:

$$\ln\frac{C_A - C_{Ae}}{C_{A0} - C_{Ae}} = -\frac{1}{C_{Ae}}\left(\frac{k_r}{LHSV}\right) \tag{2.6}$$

The model was used to calculate kinetic parameters from published data and a good fit between observed and calculated results were obtained (Fig. 2.6).

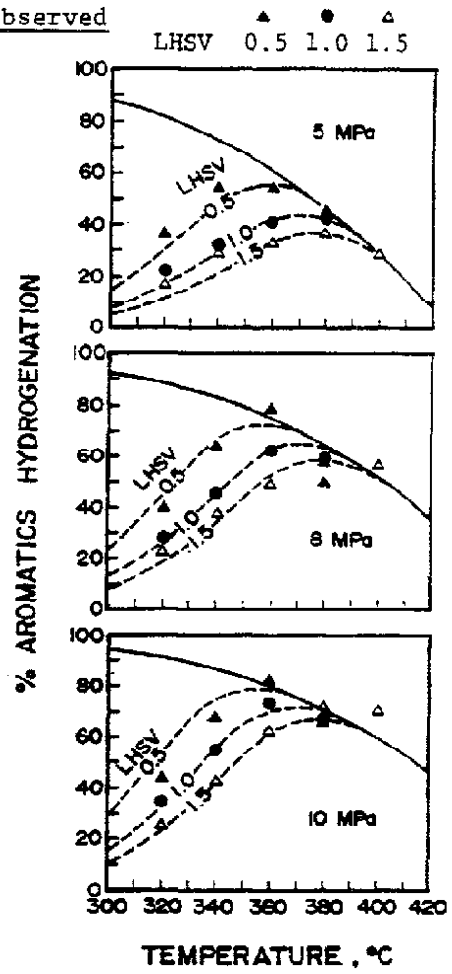

Figure 2.6: Observed and calculated percent aromatics hydrogenation at various operating conditions of Arabian Light Gas Oil [31].

Cooper et. al conducted a study on aromatic hydrogenation of North Sea gas oils over two noble metal catalysts [32,33]. Fitting the results using simple power law expressions based on total aromatics content gave the best fit to first-order for the non-zeolite supported catalyst (TK907). The zeolite-supported catalyst (TK908) fitted zero-order kinetics. This is illustrated in Fig. 2.7. The apparent order of reaction for hydrogen was 1 and 2.5 respectivly. The low

order of reaction for the zeolite-based catalyst indicated inhibition by adsorption of unconverted aromatic compounds and suggests that the kinetics is better described with a Langmuir-Hinshelwood type rate equation.

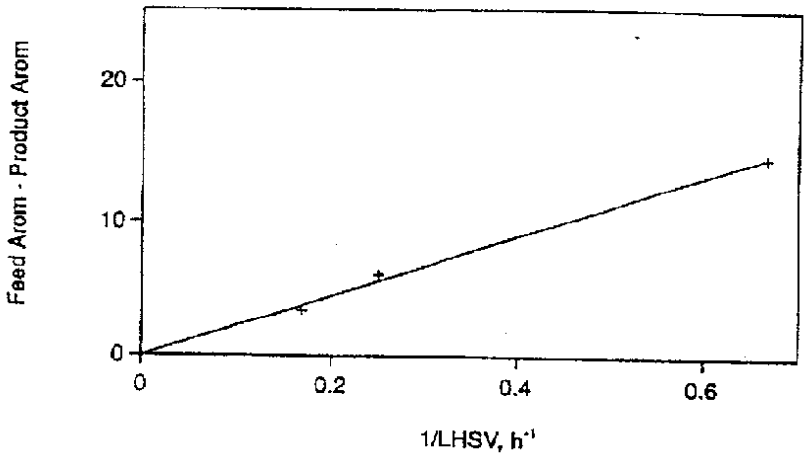

Figure 2.7a: Hydrogenation of North Sea gas oil over noble metal supported on zeolite support. Fit to zero order kinetics [33].

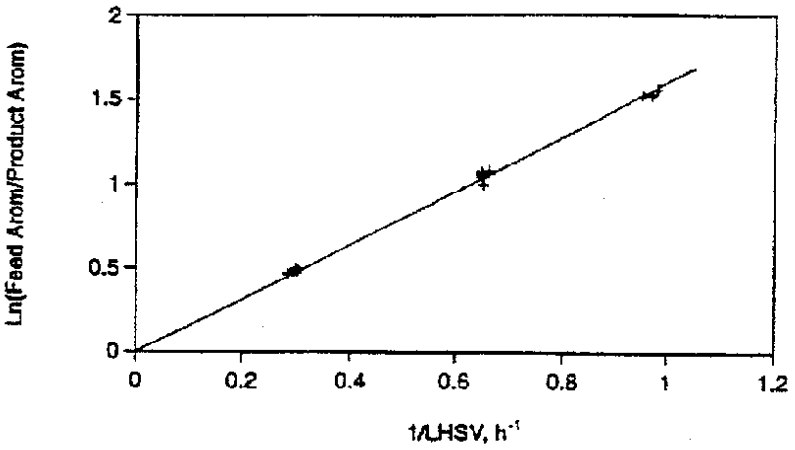

Figure 2.7b: Hydrogenation of North Sea gas oil over noble metal supported on non-zeolite support. Fit to first order kinetics [33].

2.1.4 PROCESSING SCHEMES FOR THE PRODUCTION OF ENVIRONMENTALLY IMPROVED DIESEL FUEL

Description of processing schemes for the available options in manufacturing middle distillates meeting new fuel quality requirements.

Single stage hydrotreating over mixed sulfides requires high pressures and long contact times to achieve acceptable levels of aromatics saturation. Processes based on a dual-stage configuration with deep hydrotreating in the first stage followed by deep hydrogenation in the second stage using a sulfur-tolerant hydrogenation catalyst show better promise. A second stage hydrocracker is an attractive alternative for feeds rich in aromatics. Feedstock properties govern factors like process severity, catalysts cycle lengths and the degree of aromatics saturation obtainable.

Feedstocks

Regulations on emissions and in connection with that, requirements on diesel fuel quality, have been considerably tightened during the last few years. At the same time the increasing demand for distillates force refineries to increase their conversion capacity. The avilable conversion processes can be divided into two groups: thermal and catalytic conversion. Thermal conversion processes, like visbreaking and coking give poor quality products, middle distillates included. Fluid Catalytic Cracking (FCC) is optimized for producing gasoline and the properties of the FCC middle distillates are extremely poor. At the other end of the scale one find the hydroconversion processes such as Mild hydrocracking and conventional hydrocracking giving high quality products. Characteristics of refinery gasoil streams are illustrated in Fig. 2.8. Extensive upgrading of the low cetane quality feedstocks high in sulfur and nitrogen content to comply with future specifications is "a must" for modern refineries. Various options in dealing with this development are discussed in the following.

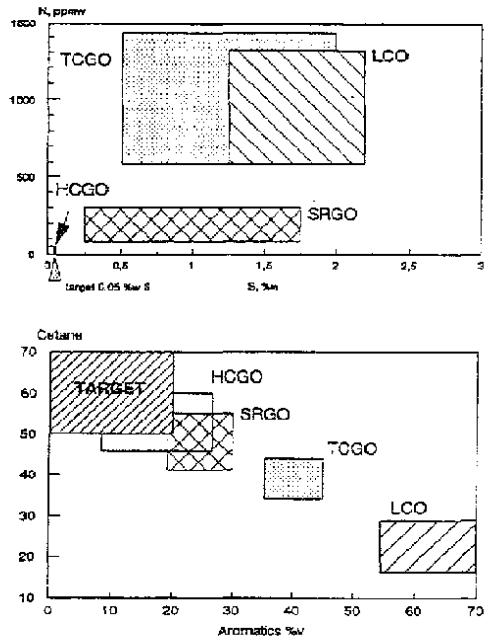

Figure 2.8: Feedstock characteristics for refinery gasoil pool [34].

High severity single stage concept

Mixed sulfides of Ni-Mo and Ni-W are preferred for applications were enhanced hydrogenation activity is needed. In hydrogenation of diesel conversion of the mono-aromatics to saturates (naphthenes) is the rate-determining step. Due to the low activity of these systems, high severity hydrotreatment (+ 100 bars, large reactor volumes) is necessary to reach acceptable levels of saturation [5,11,34-36]. An example of the effect of hydrogen partial pressure is given in Fig.2.9. The influence of feed refractiveness on the aromatics saturation level is also shown. Heteroatoms inhibit the hydrogenation of aromatics to a certain extent and the more bulky mono-aromatic molecules in feeds like LCO introduce steric effects which decrease the reactivity of such feeds.

Since aromatic hydrogenation is a reversible reaction thermodynamically favored by low temperature, the temperature operating window is limited. In summary the singie stage

concept requires high capital investments and gives only limited flexibility especially when processing cracked feedstocks.

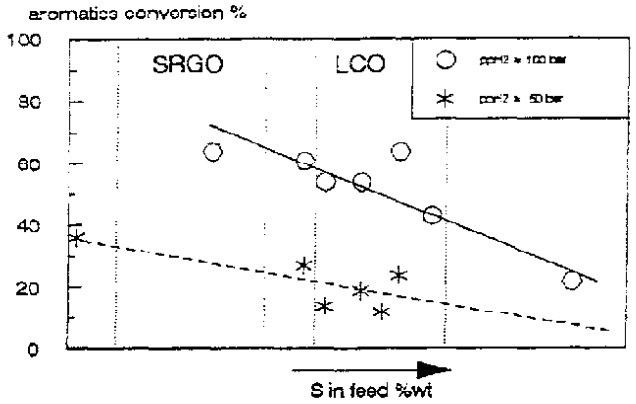

Figure 2.9: Effect of hydrogen partial pressure and feed refractiveness on maximum arimatics saturation level [34].

Dual-stage operation

Group VII metal catalysts exhibit much higher hydrogenation activity compared to metal sulfide catalysts. These catalysts can operate at low pressure and temperature hence avoiding the problem of thermodynamic limitations. Because the conventional metal catalysts (e.g. Pt or Ni on Al_2O_3) are extremely susceptible to sulfur and nitrogen in the feedstock, operation in a two-stage unit where the heteroatoms are removed in the first stage is necessery. Excisting industrial applications is the production of low aromatic solvent, medicinal oils and jet fuels [37].

The most common method in low aromatics diesel production is the use of a Ni-Mo/Al_2O_3 catalyst in the first stage, followed by a sulfur-tolerant noble metal/zeolite catalyst in the second stage. An overwiev of publications on two stage middle distillate hydrogenation processes is given in Table 2.3.

Table 2.3: Two-stage middle distillate hydrogenation processes [34].

Year	Company	Own catalyst	Process line-up	Reference
1988	Shell	1: NiMo	Integrated two-stage	
		2: NMet/Z	Co-current downflow	[38]
1990	OUP		Integrated two-stage	
			Co-current downflow	[39]
1990	Criterion	1: NiMo	SYNSAT:	
	Lummus	2: mixed sulphides	Integrated two-stage	
		Nmet	Counter-current	[40]
1991	IFP	1: NiMo	Two-stage	
		2: NMet	Co-current downflow	[41]
1992	Topsøe	1: NiMo	Two-stage	
		2: NMet/Z	Co-current downflow	[42]
1992	Akzo	1: NiMo	Two-stage	
		2: Pt, Pd/Support		[43]
1995	Mobile	1: NiMo	Two-stage	
		2: NMet/Z		[44]

According to the claims made in the literature these second-stage catalysts tolerate relativly high levels of sulfur and nitrogen in the feedstock (up to 1000 ppm sulfur and 50 ppm nitrogen) and still maintains high activity and stability.

A flow diagram of the Topsøe process is shown in Fig. 2.10. It can be divided into four sections: initial hydrotreating, intermediate stripping (H_2S and NH_3), final hydrotreating and product stripping. An example of feed and product properties in the manufacturing of Swedish Urban Diesel I is shown in Table 2.4.

An alternative approach is to install a hydrocracker as the second stage. Hydrocracking is characterized as the "ultimate sledghammer" for aromatics reduction of diesel boiling range streams [7]. These units carry a high investment cost and is best utilized on feeds rich in aromatics (e.g. FCC cycle oil). High yields of premium quality jet and diesel fuel is produced in this configuration.

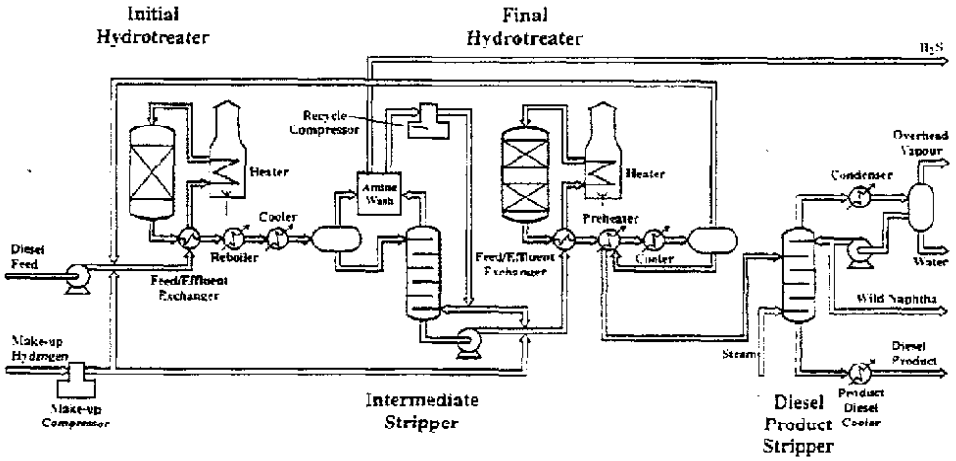

Figure 2.10: Two-stage process for diesel aromatics removal [15].

Table 2.4: Industrial operation to produce Swedish Urban Diesel I [15].

	Feedstock	1st-stage Product (Urban Diesel II)	2nd-stage Product (Urban Diesel I)
Density (kg/m^3)	825	814	805
S (ppm wt)	3500	10	< 1
N (ppm wt)	20	< 1	< 1
Aromatics (vol%)(IP 391-91)	24	18	4
Diesel yield (vol%)	-	99	97
Naphtha yield (180°C-, vol%)	-	1	3
Cetane index (ASTM D4737-90)	49	52	55.5
Saybolt color (ASTM D156)	-	-	+ 30

2.2 CATALYSTS IN HYDROTREATING

2.2.1 STRUCTURAL MODELS FOR SULFIDE CATALYSTS

Explanation of structural models for the nature and role of active phases in hydrotreating catalysts.

Various attempts have been made to elaborate models explaining the nature and role of the active phases in hydroprocessing catalysts. The "contact synergism" or "junction model" states that the system is bi-phasic and synergism is the consequence of contact between separate sulfide particles of molybdenum and cobalt. The "Co-Mo-S phase model" links the activity to a phase consisting of two-dimentional slabs of MoS_2 in which Co atoms are located at the edges. Different types of catalytic sites for hydrogenation and hydrogenolysis has been proposed.

Sulfide catalysts

Hydrotreating catalysts are made by impregnation of salts of the relevant metals on γ-Al_2O_3 in aqueous solution followed by intermediate drying and calcination. The oxidic precursor is transformed into the working catalyst by a sulfiding step involving treatment in a mixture of H_2S (thiophene) and H_2, or in a liquid feed of sulfur-containing compounds and H_2. The MoO_3 (WO_3) is transformed into MoS_2 and the promotor ions (Co, Ni) have passed into a sulfidic environment.

Structural models

The first important model, called the "monolayer model" was proposed by Schuit and Gates [45]. It describes the calcined catalysts, but since the oxcidic monolayer is completely sulfided during pretreatment, this model is not applicable to the working catalyst.

Observations that the S/Mo (S/W) ratio is close to 2 has lead to several proposals on the presence of Mo as MoS_2 in active catalysts. One such model based on this assumption is the "intercalation model" developed by Voorhoeve and Stuiver [46]. MoS_2 (and WS_2) crystallizes in layered structures of slabs consisting of a Mo(W) layer with close packed sulfur layers on each side. Bulk sulfides are made up of numerous slabs stacked on top of each other in certain

stacking sequences. Metal atoms (promotor) can enter (intercalate) between the slabs. Farragher *et al.* restricted this to occur at surface positions [47].

Another model based on the presence of MoS_2 is the socalled "contact synergism model" proposed by Delmon [48]. The active phases are separate crystallites of Co_9S_8 and MoS_2 in close contact with each other as shown in Fig. 2.11. The role of the promotor is to activate and provide hydrogen atoms via spill-over to MoS_2. These compounds are thermodynamically stable under real reaction conditions.

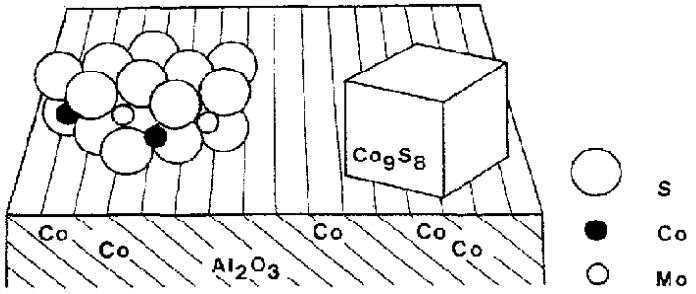

Figure 2.11: Structures of the different forms in which cobalt ions can be present in Co-promoted MoS_2/Al_2O_3 [48].

Mössbauer studies combined with catalytic activity studies lead Topsøe *et al.* to conclude that the promotor effect of Co (Ni) is related to the promotor atoms adsorbed on MoS_2 [49]. The promotor atoms are located around the edges of the MoS_2 crystallites. A schematic picture of a couple of the models is shown in Fig. 2.12.

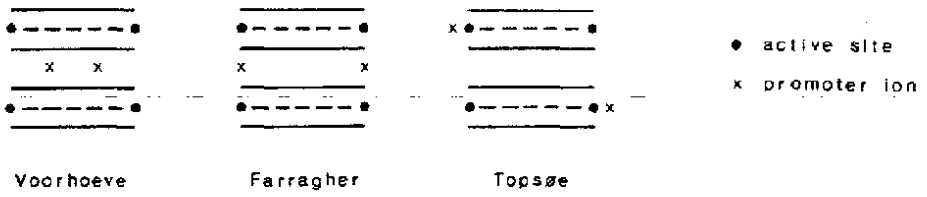

Figure 2.12: Schematic picture of the location of the Co promoter ions in MoS_2 according to the models of Voorhoeve, Farragher, and Topsøe [50].

The catalytically active sites for hydrotreating reactions is generally visualized as sulfur (anionic) vacancies. Whether hydrogenation and hydrogenolysis occur on the same type of sites or on different sites have been widely debated. It has been suggested that H_2S can transform hydrogenation sites on the catalyst surface into hydrogenolysis centers [51]. This is shown in scheme 2.3.

Scheme 2.3: Interconversion of hydrogenation and hydrogenolysis sites on hydrotreating catalysts [6].

2.2.2 NOBLE METAL CATALYSTS WITH SULFUR-TOLERANT FEATURES

Description of noble metal catalysts and the nature of active sites.

Noble metals in Y-zeolite catalysts are industrially important as catalysts for aromatics hydrogenation. Their high sulfur tolerance is suggested to originate from the small bonding energy of the electron acceptor sulfur atoms with the electron-deficient metal clusters within the zeolite cavities. The zeolite support alters the electronic state of the small, highly dispersed metal particles and thereby weakens the metal-sulfur bond. The preparation and pretreatment of the catalysts is crucial in determining the activity, selectivity and the resistance to poison.

Zeolites

Zeolites are crystalline microporous solids, more particular aluminosilicates, with well defined pore and cage structures. The basic building block is a tetrahedron made up of a central cation surrounded by four O^{2-}-ions. Each tetrahedron is linked to four others with two adjacent tetrahedra sharing one O^{2-}-corner. The structural framework of *Y-zeolite* is shown in Fig. 2.13

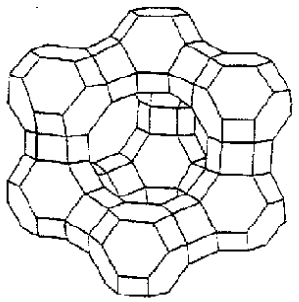

Figure 2.13: Framework of zeolite Y [52].

The framework carries a negative charge which is balanced by cations who together with water molecules occupy the void space. These alkali metal and alkaline earth ions move freely through the channels and in aqueous salt solutions they undergo ion-exchange. Replacement by protons (via NH_4^+ exchange and calcination) creates strong Brönsted acid sites.

Zeolites are used industrially as molecular sieves, ion-exchange agents and as catalysts. In the following zeolites containing reduced particles of one or more transition metals dispersed inside the cavities are discussed in terms of their catalytic properties (e.g hydrogenation activity and sulfur tolerance).

Sulfur tolerance of metal clusters in zeolites

It has been known for many years that highly (close to atomic) dispersed platinum in Y zeolite can be prepared and that these catalysts possess higher resistance to sulfur poisoning than other Pt catalysts [53]. Dalla Betta and Boudart found that this catalyst showed an anomalously high activity for reactions like hydrogenation, isomerization and hydrogenolysis [54]. It was suggested that the resistance to sulfur poisoning came from the small bonding energy of the electron acceptor sulfur atoms with the electron-deficient metal clusters within the zeolite cavities [54,55]. Investigations of these catalysts by techniques like x-ray photoelectron spectroscopy (XPS), electron spin resonance (ESR) and infrared spectroscopy (IR) have confirmed the electron-deficient nature of the small metal particles [55,56]. The fact that small Pt agglomerates ineracts strongly with Lewis bases such as NH_3 which deactivates the metal also supports this [55].

Role of the support

The electron-deficiency of Pt particles is seemingly intimately related to the proton concentration of the zeolite. Indeed it disappeares when the protons are neutralized.

The competitive hydrogenation of toluene and benzene on Pt particles in zeolites of different proton concentration was used as a probe reaction in determining the electronic properties of the metal [57]. The ratio of the adsorption coefficients of toluene and benzene b_T/b_B obtained from an analysis of the hydrogenation rate data, increased with increasing acidity, likewise the electron-deficiency. This was understood by concidering that toluene is a stronger electron donor than benzene.

The close dependency between the electron deficiency of the noble metal (Pt and Pd) particles and the proton concentration of zeolites imply intimate interaction and direct bonding between metal particles and some protons forming *metal-proton adducts* [58]. These complexes share the positive charge of the protons with the metal atoms. In these adducts e.g., $[Pd_nH_m]^{m+}$, the protons may act as "chemical anchors" between the metal particle and the zeolite wall and

thus stabilize the small metal particles. This means that high metal dispersions, even monoatomic metal atoms is obtainable in zeolites with high proton concentrations [59]. Studies by X-ray photoelectron spectroscopy (XPS) have shown that the binding energy (BE) of the Pd $3d_{5/2}$ electrons of the palladium atoms in Pd/NaHY is significantly increased with respect to the Pd reference as shown in Fig. 2.14.

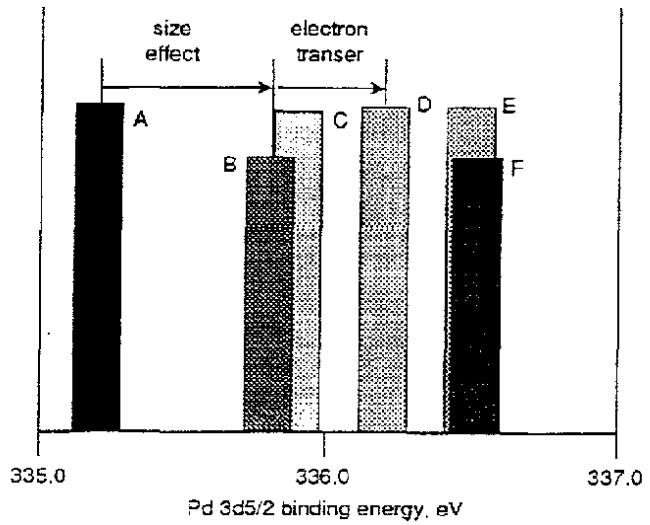

Figure 2.14: Positions of Pd $3d_{5/2}$ for (A) bulk Pd, (B) Pd/NaY neutralized with NH_3, (C) Pd/NaY neutralized with NaOH, (D) Pd/NaY reduced at 350°C, (E) Pd/MgY reduced at 350°C, and (F) Pd/HY reduced at 350°C: width of the bars corresponds to error bar [58].

The differerence in BE between Pd/NaHY and Pd/NaY (and Pd/HY) is dued to the difference of Na^+ and H^+ as ligands to the Pd cluster. H forms the stronger bond and makes the metal particle more electron deficient.

These metal-proton adducts are *bifunctional* and hence reaction intermediates can undergo multiple reaction steps being adsorbed to the same adduct. There is no desorption/adsorption steps and shuttling of the reaction intermediates between metal and acid sites. As a result the reaction rate for such multistep reactions is much higher for catalysts containing these adducts than physical mixtures of zeolites containing only one type of site [60].

Preparation of Metal Zeolites

The preparation of metal zeolites consists of several steps, including the loading of metal or metal compound inside or on the external surface of the zeolite and the treatments determining the final metal dispersion. The metal loading can be performed by impregnation (e.g. "incipient wetness") or by ion-exchange of the desired cation. Adsorption of neutral metal complexes like metal carbonyls into dehydrated zeolites is a suitable metod for elements which undergoes ion-exchange at a slow rate. These complexes are volatile and so vapor-phase adsorption is applicable. Ion-exchange in solution is the most common method in preparing zeolite-based metal catalysts [61].

Dilute aqueous solutions of ionic precursor is slowly added to the zeolite slurry. To avoid hydrolysis of the transition metal ions prior to their exchange, control over the pH in the slurry is imperative [59]. Neutral ligands like NH_3 are coordinatively stronger than H_2O and can therefore be utilized in neutral solution to prevent hydrolysis. In fact, $Pt(NH_3)_4^{2+}$ and $Pd(NH_3)_4^{2+}$ are stable toward hydrolysis over a wide pH range and are predominantly used in ion-exchange of Pt^{2+} and Pd^{2+}. Coexchange of multivalent cations (Fe^{2+}, Ca^{2+}, La^{3+}) is a strategy often used to prevent (by blocking) the migration of transition metal ions into the small sodalite cages and hexagonal prisms which is detrimental in obtaining high metal dispersion [62].

Calcination in air or O_2 removes water molecules and destroys the ligands, e.g. the ammine groups of $Pt(NH_3)_4^{2+}$ ions. As Pt^{2+}-ions lose their ammine ligands, migration from supercages towards the smaller sodalite cages is thermodynamically favorable. Here the highest negative charge density in the zeolite framework exist thus favoring coordination of the bare Pt^{2+}-ions with O^{2-}-ions of the cage wall [63]. Studies on the ammine removal from $Pd(NH_3)_4^{2+}$/NaY during temperature-programmed oxidation revealed no bare Pd^{2+}-ions in the supercages. Instead $Pd(NH_3)_4^{2+}$- and $Pd(NH_3)_2^{2+}$-ions were found [64]. At temperatures above 250°C the third ammine ligand is destroyed and migration of the mono-ammine Pd^{2+}-ion into adjacent sodalite cages takes place immediately. Ion migration is an activated process proceeding to an increasing extent with increasing calcination temperature.

Choosing the optimum calcination temperature for metal/zeolite catalysts is thus very important, because it controls the cation locations and by that the metal particle growth mechanism during the following reduction. This in turn decides the final metal dispersion [54,62,63,65]. As a rule low temperature calcination leaves partially complexed metal ions (Pd) or naked metal ions (Pt) in the supercages, while high temperature calcination initiate migration of metal ions to the sodalite cages. Calcination temperature of 300°C is found to be optimum for high metal dispersion on Pt/NaY [66-69]. For Pt/NH_4Y a higher temperature is found to be optimum [67,68,70].

Release or decomposition of ammine ligands during calcination create a reducing atmosphere inside zeolite cavities resulting in autoreduction giving metal particles and protons. This may lead to metal sintering and formation of large particles. A slow heating rate and a rapid O_2-flow are preferred along with small sample batches to prevent this uncontrolled reduction [66].

Reduction of transition metal ions in zeolites is usually performed in flowing H_2 following calcination. While reduction of an oxide with hydrogen yields water, hydrogen reduction of metal ions yields protons:

$$M^{2+} + H_2 \leftrightarrow M^0 + 2H^+ \qquad (2.7)$$

High proton concentration shifts the equilibrium to the left. The reducibility of metal ions in zeolites depends on several factors, like location of the ion, its accessibility, its coordination with ligands, effects of other coexisting ions (site blocking or metal anchoring), zeolite structure, proton concentration, zeolite acidity and metal loading [59].

After reduction of ions the thermodynamics works towards locating the metal atoms where they can form M_X particles. Homeyer and Sachtler [63] have proposed the following sequence of steps for reduction of metal (Pt) ions (bare and complexed) located in the supercages:

1. Formation of a neutral nucleus Pt_n ($n = 1, 2 ....$);
2. Migration of the complexed or bare ions to a supercage containing a nucleus;

3. Adsorption of the cation on the nucleus;
4. Release of the ligands;
5. Dissociative adsorption of dihydrogen;
6. Release of two protons which become attached to oxide ions of the cage wall;
7. Migration of the primary particles and their coalescence to larger particles.

The final dispersion is governed by the relative rates of nucleation (1) and particle growth, the latter limited by the rate of the migration step (2) up to the point where particle growth in step (7) is limited by the apertures between supercages. The rate of the ion migration step (2) is controlled by the mobility of the metal ions which in turn depends on the degree of complexation. Bare metal ions migrate slowly due to strong electrostactic interactions with the zeolite lattice. On the other hand tetraammine ions have a low charge density, are coordinatively saturated and as a consequent move much faster through the supercage network.

Temperature-programmed desorption (TPD) gives information on the type of particles formed after reduction. Keeping in mind that only surface atoms adsorb hydrogen the TPD spectra reveal the metal dispersion and the activation energy of the desorption process. The effect of both calcination and reduction temperature on the dispersion is shown in Fig. 2.15 [65]. Low calcination temperature T_C gives small metal particles in supercages (Fig. 2.15a). High T_C force the metal ions into sodalite cages and the subsequent lack of nucleation sites in the supercages as the reduced metal atoms leave their positions results in migration out to the exterior surface and the formation of large particles (Fig. 2.15c). At intermediate T_C ions exist in both supercages and sodalite cages and sufficient nucleation sites in the supercages makes particle growth possible (Fig. 2.15b). Formation of "grape shaped" particles larger than the supercages by growing through the windows is observed [61]. In the case of Pt trapped in sodalite cages the high temperature required for migration makes reoxidation of Pt atoms by protons in the same cages possible:

$$Pt^0 + 2H^+ \rightarrow Pt^{2+} + H_2 \qquad (2.8)$$

This release of H_2 is observed in Fig. 2.15 for samples redused at 400°C with a peak near 450°C (dotted lines).

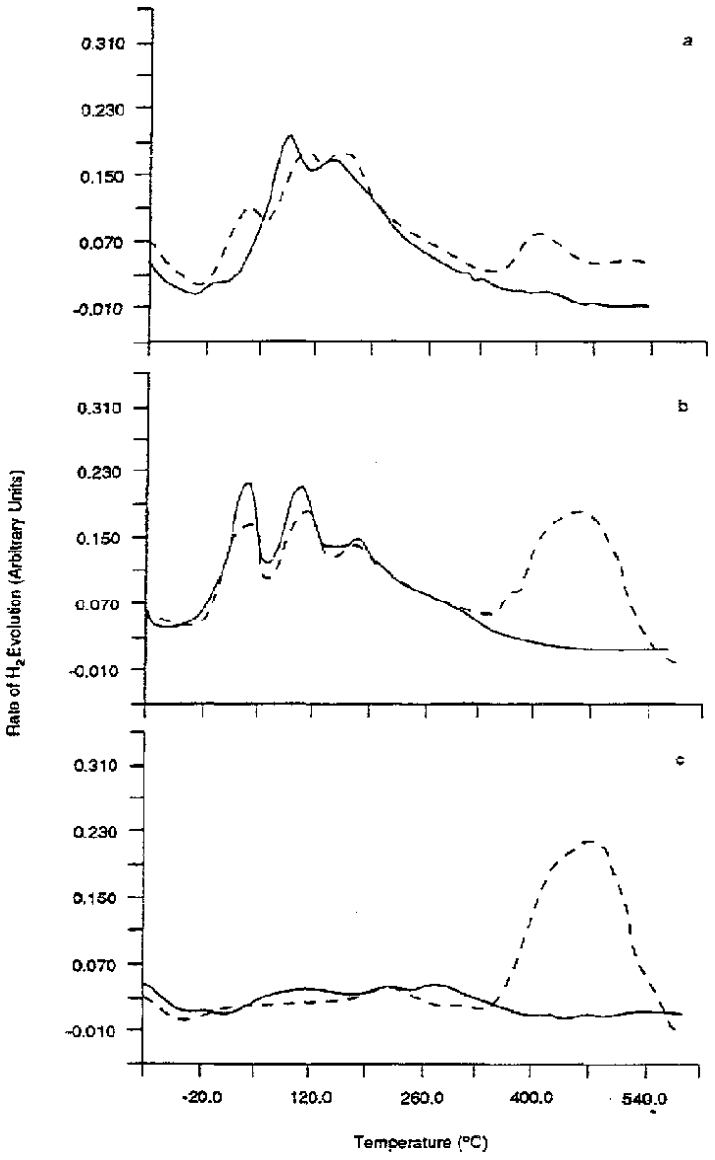

Figure 2.15: Temperature-programmed hydrogen release profiles of Pt/NaY (7.4 wt% Pt) calcined at (a) 360°C, (b) 450°C, (c) 550°C. Solid lines, after reduction at 550°C; dotted lines, after reduction at 400°C. The peaks at high temperature for the dotted lines are attributed to reoxidation of Pt atoms by protons [65].

A summary of the elementary steps in the synthesis of metal/Y catalysts is shown in Fig. 2.16 Some of the processes are: 1) destruction of ligands, 2) migration of complexed or bare metal ions from supercages to sodalite cages and the reverse process, 3) reduction of ions in various locations and different degree of complexation, 4) reoxidation of metal atoms in sodalite cages and 5) migration of these atoms to supercages, where they might be attached to existing clusters, forming grape-shaped particles.

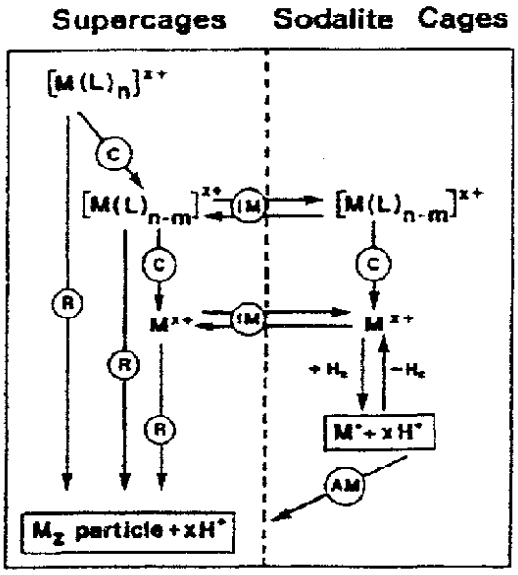

Figure 2.16: Fundamental processes in metal/NaY synthesis. C: calcination in O_2; R: reduction by H_2; IM: metal ion migration; AM: atom migration; M(L): metal ligand [63].

2.2.3 ALTERNATIVE CATALYST SYSTEMS

Information on alternative catalyst systems and their catalytic properties in hydroprocessing including hydrogenation reactions.

Studies have demonstrated that other transition metal sulfides beside the commercially used in hydrotreating possess higher specific activities in HDS and hydrogenation. Transition metal carbides and nitrides are catalytically active for many hydrogen transfer reactions where they are behaving like Group VIII metals also exhibiting sulfur resistans features. Noble metals dispersed on specially modified carriers, like doped titania exhibit enhanced hydrogenation activity and improved sulfur tolerance.

The trend toward hydroprocessing heavier crudes of decreasing quality together with the increasing interest in syntetic hydrocarbon liquids derived from coal and tar sand impose significally more challenging requirements on existing catalysts. These feeds contain substantial quantities of highly unsaturated aromatic compounds and heteroatoms like sulfur, nitrogen and oxygen. The production of clean burning fuels from these feedstocks requires better catalysts for hydrotreating.

Transition metal sulfides

Comparison of catalytic properties of various unsupported transition metal sulfides (TMS) in hydrotreating reactions has shown that some other systems beside molybdenum and tungsten present high activities [71]. Ruthenium sulfide is one example of an effective catalyst in HDS and hydrogenation reactions. Studies by Kuo and Tatarchuk on alumina supported ruthenium catalysts in hydrotreating reactions have demonstrated the importance of the sulfidation process in obtaining high activity catalysts [72,73]. They found that presulfidization at high H_2S/H_2 ratios resulted in sulfur uptakes of more than 0.5 monolayer necessitating the incorporation of sulfur below the plane of the surface. This *"bulk sulfidization"* produces crystalline RuS_2 extending to the surface. It was found that this RuS_2-like surface chemisorb much larger quantities of hydrogen and possess higer H_2-D_2 exchange rates compared to metallic ruthenium surfaces covered by partially monolayers of adsorbed sulfur produced by

mild presulfurization treatment and that this could contribute to the higher hydrogenation rates observed.

Breysse et al. studied the activities and selectives of vanadium, niobium and ruthenium sulfides (unsupported) in hydrotreating reactions of representative model compounds [74]. For hydrogenation and hydrodesulfurization reactions for which the active sites are anionic vacancies the most active catalyst was RuS_2 (7 and 15 times higher than MoS_2 respectively) in terms of intrinsic rates.

Ledoux et al. investigated sulfided vanadium, palladium and ruthenium supported on uranium modified alumina in hydrogenation and ringopening reactions [75]. Compared to an industrial NiW catalysts all catalysts were god HDS catalysts, but they were not able to hydrogenate aromatic rings and subsequently open these rings to a significant degree under realistic reaction conditions.

Transition metal carbides and nitrides

Due to the incorporation of carbon and nitrogen in the metal lattice of the parent metals (Fig. 2.17), transition metal carbides and nitrides possess altered physical and chemical properties. Materials of high surface area can be prepared by temperature-programmed reaction of the oxidic precursors in a reactant gas stream (CH_4/H_2 for the carbides and NH_3 for the nitrides) [76].

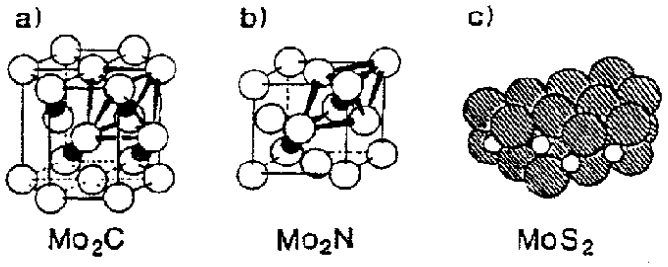

Figure 2.17: Crystal structures of catalysts. (a) Mo_2C and (b) Mo_2N, the large open circles represent molybdenum, the dark circles represent carbon or nitrogen. (c) MoS_2, the small circles represent molybdenum, the large hatched circles represent sulfur [77].

These catalytic materials are active for several hydrogen transfer reactions including benzene hydrogenation [78]. The carbides and nitrides have shown excellent hydrodenitrogenation activity in quinoline treatment compared to commercial sulfided $NiMo/Al_2O_3$ with high selectivities for the formation of the aromatic products [76,79].

Sajkowski and Oyama conducted hydrotreating of a coal-derived gas oil over molybdenum carbide and nitride catalysts [77]. Pseudo first-order rate constants for desulfurization, denitrogenation and aromatic saturation relative to a commercial $NiMoS/Al_2O_3$ are given in Table 2.5. XPS analysis of spent catalysts showed little incorporation of sulfur in the surface region of the catalysts, supporting the observation that these materials are tolerant of sulfur.

Table 2.5: Estimated relative first-order rate constants[a] per "active site[b]" [77].

Catalyst	Desulfurization	Denitrogenation	Aromatic saturation
Mo_2N	1.3	3.4	3.4
Mo_2C/Al_2O_3[c]	2.1	5	3.1
Mo_2S/Al_2O_3	0.67	0.98	0.41
$Ni\text{-}Mo\text{-}S/Al_2O_3$	1	1	1

[a]: Calculated by $[\ln(CO/C)]/[\ln(CO/C)_{Ni\text{-}Mo}]$.

[b]: As titrated by CO for the carbide and nitride and by O atoms for the sulfides.

[c]: Rate constant corrected by 718/268, the ratio of μmol O uptake by Ni-Mo to CO uptake by Mo_2C/Al_2O_3 in the reactors.

Noble metals dispersed on titania carriers

Koussathana et al. have performed extensive studies of slurry-phase hydrogenation of aromatic compounds over monometallic and bimetallic noble metal catalysts supported on γ-Al_2O_3 or TiO_2 [80-82]. In most cases, bimetallic formulations exhibited significantly higher hydrogenation activity compared to the monometallic counterparts. The greatest enhancement factor was found on TiO_2-supported samples which induced improved metal dispersions [80]. Bimetallic catalysts exhibit improved sulfur tolerance especially when rhenium and palladium is employed.

Doping of the TiO_2 support with cations (W^{6+} and Ta^{5+}) of valence higher than the parent cation by high temperature diffusion into the lattice of the carrier results in increased hydrogen adsorption capacity, enhanced hydrogenation activity and sulfur tolerance for Rh, Ru and Pd. [81]. For platinum the opposite trends are observed. These effects are a function of the dopant concentration in the support and are interpreted as an electronic interaction developing at the metal-support interface resulting in a lowering of the work function of surface metal atoms.

The activity of bimetallic catalysts on doped TiO_2 in the hydrogenation of a coal-liquid distillate cut was found to be superior to undoped catalysts and also a commercial $CoMo/Al_2O_3$ catalyst [82].

2.3 SULFUR POISONING OF METAL CATALYSTS

2.3.1 SULFUR ADSORPTION ON METALS

Description of sulfur adsorption on metals, the structure and bonding.

The contact of a metal with H_2S leads to a widely covered surface without any sulfur dissolution in the metal. Sulfur compounds chemisorb dissociatively on the metal surface and the rate of adsorption is rapid with a initial sticking coefficient close to 1.0. Sulfur adsorption under reaction conditions is a complex phenomenon leading to various stoichimetries at saturation coverage. Due to the high stability of surface sulfides monolayer coverage is inevitable in the presence of only minute amounts of H_2S.

Catalyst poisoning is one of the major obstacles facing the commercial use of catalysts for industrial purposes. Poisoning of metal catalysts by adsorption of sulfur-containing species is a severe problem due to the abundance of sulfur compounds in all industrial feedstocks derived from natural sources. Sulfur poisoning has a profound impact on catalyst activity, selectivity and life and some of the characteristics of sulfur adsorption on metals is highlighted her.

The metal-sulfur bond

Because sulfur has an electronegativity comparable to most metals of catalytic interest, bulk metal sulfides possess covalent bonds. They are nonstoichiometric compounds with the existence of many phases stable over a limited range of sulfure pressure and temperature [83]. The free energy of formation of bulk metal sulfides for common catalytic metals like Pt, Ni, Ru, Rh, Ag, Fe, Co and Ir is rather low necessitating relativly large gas-phase H_2S concentrations for stable bulk sulfides to exist. The extreme susceptibility of most metals to sulfur poisoning under reaction conditions where stable bulk sulfides does not form, suggest that surface structures are formed. This is confirmed by studies of MacCarty and Wise on metal-sulfur interactions (Ni, Ir) showing the stability of the adsorbed state [84,85]. For Ni catalysts they found sulfur coverages close to half a monolayer with extremely low partial

pressures of H_2S (1-10 ppb) at temperatures ranging between 373 and 873 K. This illustrates the problems of avoiding sulfur poisoning in catalysis by metals.

For adsorption reactions thermodynamics give:

$$\Delta H_{ads} = E_a - E_d \qquad (2.9)$$

ΔH_{ads} is the enthalpy of adsorption, E_a is the activation energy of adsorption and E_d is the activation energy of desorption. For metallic catalysts the activation energy for adsorption of sulfur is neglible and binding energies is therefore obtainable from adsorption or desorption studies. The use of Van't Hoff equation on these isotherms makes evaluation of the chemisorption energy for a given sulfur coverage possible [86]. Since the heat of adsorption decreases with increasing sulfur coverage, due to chemisorption of undissociated sulfur-species for coverage near one monolayer, comparison of sulfur binding energy on different metal surfaces must be done at the same coverage. McCarty and Sancier found that on Pt sulfur chemisorb weakly, consistence with the greater sulfur-resistance of Pt compared to Ni [87].

Adsorption of H_2S on supported catalysts were studied by Menon and Prasad, [88] and by Apesteguia *et al.* [89]. They showed that while the adsorption on pure alumina is completely reversible at 500°C in a hydrogen atmosphere, H_2S adsorbed on Pt/Al_2O_3 desorbs only a small fraction during the initial stage of the same treatment as shown in Fig. 2.18. Thus two distinctly different forms of adsorbed sulfur exist: One "reversible" form and one "irreversible" form associated with the interaction of adsorbed sulfur and the metal. Apesteguia and Barbier found the same behavior for other metals and also bimetallic catalysts [90]. The irreversible sulfur coverage varies in the range of 0.4 - 1 sulfur atom for each accessible metallic atom indicating the strength and lifetime of adsorbed sulfur on metal catalysts.

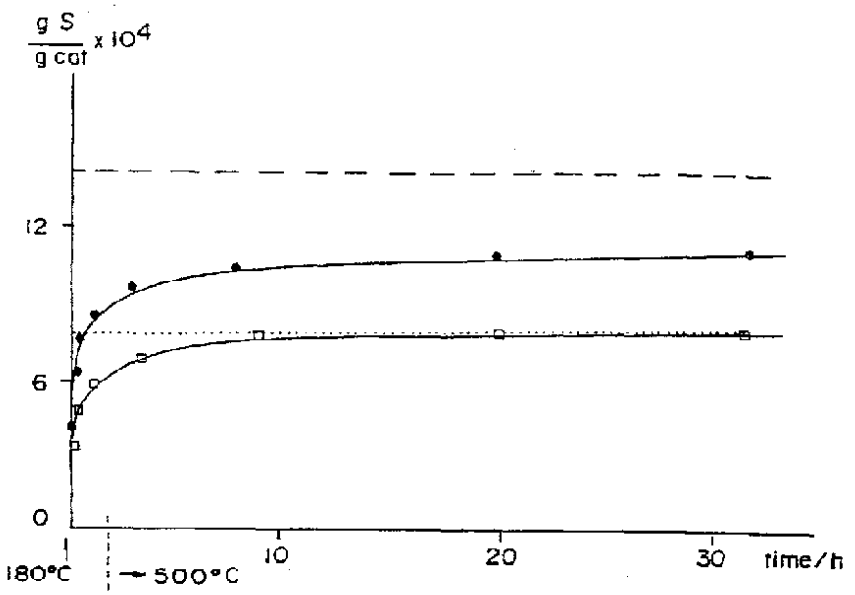

Figure 2.18: Desorption of H_2S by heat treatment under hydrogen. (●) Pt/Al_2O_3, ---- initial quantity of sulfur on Pt/Al_2O_3, (□) Al_2O_3, and ..... initial quantity of sulfur on Al_2O_3 [89].

The toxic effect of a molecule on a catalyst is related to its ability to create a strong chemisorption bond with the catalyst (metal) surface. Many sulfurcontaining compounds possess doublets of free electrons in its valence layer allowing bonding with the metal. Electronic properties of the metal also influence the chemisorption strength of sulfur. A charge transfer between the metal (adsorbent) and the sulfur species (adsorbate) can occure, depending on the difference in electronegativity between the metal and the adsorbate [91].

Barbier *et al.* made use of the difference in electronic affinities between sulfur and the metal to explain the adsorption behavior of sulfur on noble metals [92]. Small differences in this parameter give predominantly covalent metal-sulfur bonds. An example is the Pt-S bond (electronic affinities of 2.12 and 2.08 eV respectively)[86]. Larger differences yield polarized bonds e.g. sulfur on iridium is adsorbed at a negative oxidation state, hence metals of low

electronic affinities enhance the adsorption of sulfur which is an electron-acceptor [55]. The coverage of "irreversible" sulfur on such metals increase as the electronic affinities decrease. It is well known that for supported catalysts acidity of the carrier along with metal dispersion can modify the electronic state of the metal [93]. The electronic deficiency of highly dispersed platinum on very acidic supports is well documented [55,56]. The effects of dispersion and the support act independently of each other and the affinity of the catalyst for sulfur is determined by these two phenomena. On acidic supports (reforming alumina, Y-zeolite) the support effect prevail and small platinum particles are more sulfur-resistance than bulky catalysts [92]. Iridium on low-acidity supports adsorbs larger amounts of sulfur on small metallic crystallites than on larger ones, hence the size effect is controlling with sulfur adsorbing on sites of low coordination (edges and ledges). Replacing Ir with Pt on the same low-acidity support results in the two effects canceling each other giving almost the same sulfur coverage, regardless of platinum dispersion.

Mechanisms and kinetics

At high temperatures and under reducing conditions sulfur-containing compounds adsorb dissociatively on metals (foil, film, or supported metals) leaving a strongly bonded reduced sulfur atom. The sulfiding is restricted to the metal surface atoms with no incorporation into the metal bulk. Hence the poisoning reaction is given by:

$$S_{ads} + H_2 \leftrightarrow H_2S \qquad (2.10)$$

This means that at these conditions the initial structure of the sulfur molecule no longer effects the deactivation of the catalyst. As a consequent of this, adsorption studies using H_2S as the sulfiding agent are numerous [83]. At lower temperatures the sulfur molecule maintain its structural identity upon adsorption. The free rotation of the carbon-chain inhibits the adsorption of other reactans on adjacent sites and thus the specific toxicity increase with the size of the molecule [94].

As mentioned above under reductive conditions all sulfur compounds undergo some degree of dissociation on the metal giving the coresponding hydrocarbon and adsorbed sulfur. The extent and rate of dissociation depend on the sulfur species. The formation of butane from the

adsorption of a number of sulfur compounds over dispersed palladium catalysts is shown in Fig. 2.19.

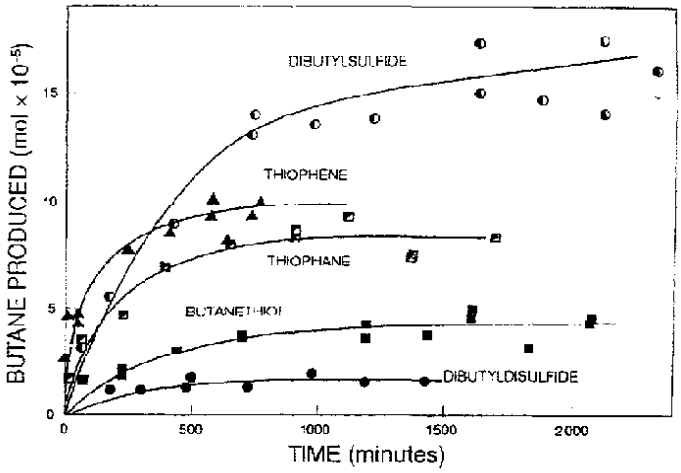

Figure 2.19: Formation of butane as a function of time, during the dissociative chemisorption of different sulfur compounds on Pd/Al_2O_3 (T=20°C, P=1 bar, solvent=heptane) [86].

The Figure shows that thiols and disulfides undergo little dissociation into butane opposed to high-level dissociation of thiophene, thiophane and dibutylsulfide. The initial slope of the curves suggests that the rate of dissociation of thiophene to be the highest. The mechanism of thiophene dissociation most likely proceeds via immediate breaking of the two C-S bonds, leaving the unsaturated hydrocarbon strongly chemisorbed (Fig. 2.20). Before desorption can take place, hydrogenation to butane is necessary.

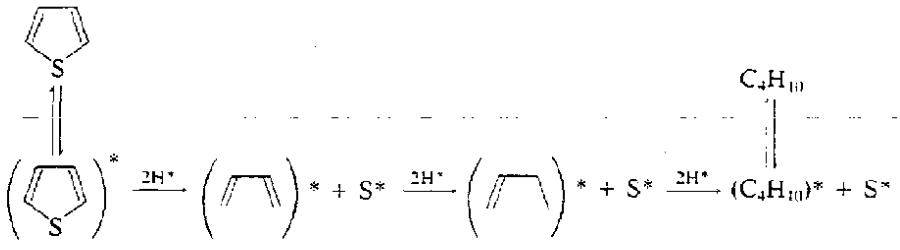

Figure 2.20: Mechanism of thiophene dissociation [86].

Kinetic studies of the rate of sulfur adsorption on metals are few. It seems like the adsorption and dissociation of H_2S on metals is very fast with a sticking coefficient close to 1.0 at low coverage decreasing with increasing sulfur coverage [83]. Aguinaga *et al.* [95] studied the poisoning kinetics by thiophene on supported Ni catalysts and found that sulfur initially was completely retained by the catalyst. Later, the decreasing slope of sulfur atoms retained per nickel atom suggest a slower adsorption rate of sulfur.

Adsorption stoichiometries

On the basis of relative areas of sulfur and nickel (0.11 and 0.060 nm^2/atom respectively) roughly 0.5-0.6 atoms of sulfur chemisorbed per nickel atom (θ) on a clean nickel surface is expected at saturation coverage [83]. This is also generally the case for metals important in catalysis at high reaction temperatures (>400°C) and low H_2S concentrations (<0.1 ppm). At higher concentrations and lower temperatures values of θ = 0.5-1.0 are possible [83].

At realistic reaction conditions with additional reactants present the complexity of sulfur adsorption is greatly increased. This is probably why few studies of sulfur adsorption in hydrocarbon mixtures have been conducted. Boitiaux *et al.* studied the dissociative chemisorption of thiophene on Pd/Al_2O_3 in a mixture of thiophene and 3 mol% isoprene in heptane [96]. The C_5 composition of the effluent along with the butane formation from thiophene are shown as a function of time in Fig. 2.21.

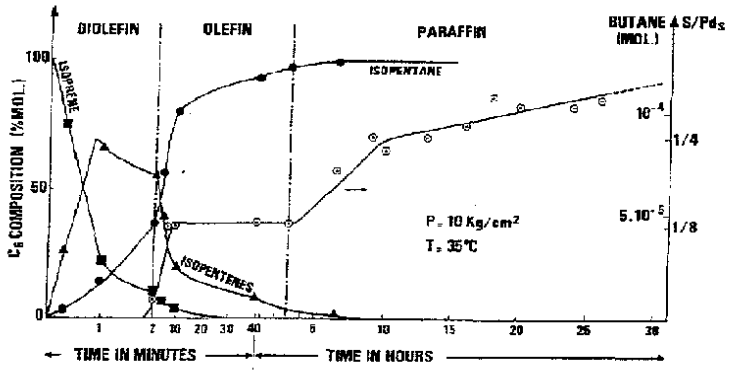

Figure 2.21: Dissociative adsorption of thiophene on Pd/Al_2O_3 as a function of the nature of hydrocarbon on Pd/Al_2O_3 (T=35°C, P=10 kg/cm^2) [96].

During the conversion of isoprene no butane is formed before nearly all of the isoprene is fully hydrogenated, Then a rapid formation of butane takes place reaching a plateau of 1 sulfur atom for every 8 surface palladium atoms. When the isopentenes have almost disappeared, formation of butane increases further reaching a ratio of S/Pd close to 0.25. This exemplify the effect of different adsorbing hydrocarbons on the state of the sulfided surface.

Stability of the metal-sulfur bond

As stated earlier in this chapter surface sulfides are considerably more stable than bulk metal sulfides. In general the heats of sulfur adsorption are 20-40% higher than the heats of formation of the most stable bulk sulfides [83]. The decreased metal-sulfur surface bond length compared to bond lengths in bulk sulfides as measured by LEED confirm this further [97]. For Eq. (2.10) ΔG° is defined as:

$$\Delta G^\circ = RT \ln(P_{H_2S} / P_{H_2}) \qquad (2.11)$$

Stability of surface sulfides can be determined from Eq. (2.11) utilizing experimental values of P_{H_2S} / P_{H_2} at equilibrium with fixed values of temperature and θ. As an illustration: for ΔG° = -84 kJ/mol and a temperature of 500K, 1.81 ppb H_2S in H_2 is sufficient to form a stable surface sulfide. From Eq. (2.11) the temperature sensitivity of surface sulfides are also apparent.

2.3.2 INFLUENCE OF SULFUR ON ADSORPTION OF OTHER MOLECULES

Studies on the influence of sulfur on adsorption of other molecules and their contributions in understanding the poisoning process.

Sulfur adsorption on metal surfaces modifies the adsorption characteristics of other molecules by blocking of the active surface (geometric effects, negative) or by inducing structural alterations caused by strong metal-sulfur interactions (electronic effects, negative or positive) with the latter giving rise to changes in the binding energy. The binding energy can decrease (H_2, CO, saturated hydrocarbons) or increase (olefins, aromatics).

Because chemisorption of reactans is an essential step in the catalytic cycle on heterogeneous catalysts, studies on the effects of adsorbed sulfur on the coadsorption of other molecules are of great importance in shedding light on characteristics of the poisoning process. Adsorption of CO and H_2 on sulfided metal catalysts has been widely studied because of their use in many important industrial reactions. They are also used as selective titrants in the measurement of metal surface areas.

H_2-adsorption

Numerous studies on presulfided nickel (supported and single-crystals) show a lowering in the H_2-adsorption capacity compared to the clean metal surface [83]. For polycrystalline and supported Ni there is a linear decrease proportional to the mean sulfur coverage as depicted in Fig. 2.22 [98,99]. Sulfur poison H_2 adsorption by blocking chemisorption sites making parts of the metal surface inaccessible. At low coverage one sulfur atom can prevent hydrogen adsorption on several metal atoms (electronic effect), while at complete coverage dissociation of H_2 is impossible due to the lack of required metal ensembles and thus a simple blocking mechanism can explain the deactivation.

Mahoungou studied the hydrogen chemisorption on presulfided Pt and Ir supported catalysts by thermodesorption of molecular hydrogen [100]. Both the hydrogen adsorption capacity and hydrogen binding energy decreased as shown in Table 2.6.

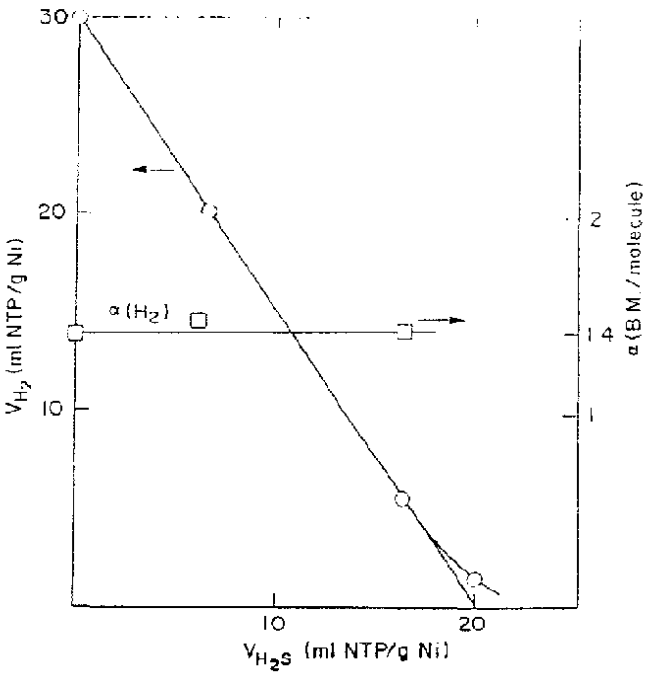

Figure 2.22: Volume of adsorbed H_2 at room temperature and ca. 5 torr and $\alpha(H_2)$ versus the volume of preadsorbed H_2S. *B.M.* denotes *Bohr* magnetons [98].

Table 2.6: Effect of sulfur on the hydrogen adsorption capacity and the hydrogen binding energy of platinum- and iridium-supported catalysts [100].

	Atoms H/g catalyst × 10^{-18}		ΔH_{ads} (kJ mol^{-1})	
Catalyst	Fresh catalyst	Sulfurized catalyst	Fresh catalyst	Sulfurized catalyst
0.6 Pt/SiO_2	14.24	1.72	44.7	32.2
0.6 Pt/Al_2O_3	16.93	3.33	38.5	32.6
0.6 Ir/SiO_2	12.60	1.72	61.9	43.9
0.6 Ir/Al_2O_3	24.88	3.00	47.6	27.6

CO-adsorption

The effects of sulfur poisoning on CO adsorption are complex, especially in the case of supported metals [83]. Depending on the adsorption pressure of CO two sets of behavior are observed on Ni/Al_2O_3 as shown in Fig. 2.23.

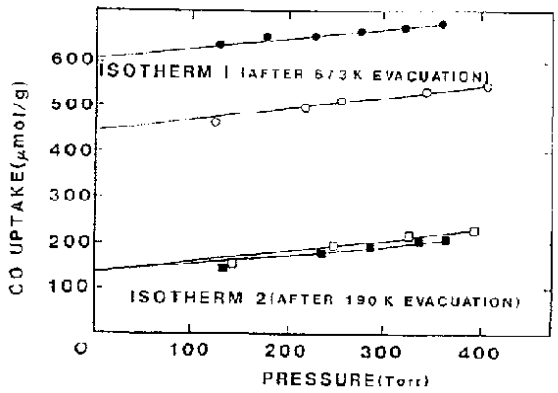

Figure 2.23: Effects of H_2S on CO adsorption on 8% Ni/Al_2O_3 (open symbols denotes fresh sample; closed symbols denotes poisoned sample) [83].

At pressures less than 0.1 kPa CO adsorption (total and irreversible) is decreased, while at higher pressure (13-53 kPa) a huge increase in both total and irreversible CO uptakes take place. The large increase is explained by the formation of subcarbonyl species, e.g. $[Ni(CO)_x$, x=2-3] and $Ni(CO)_4$ migrating to the gas phase or the support exposing new nickel sites.

Chang *et al.* studied the effect of sulfur on aromatic hydrogenation over Pt catalysts using FT-IR spectroscopy and found a weakening in the bond strength between CO and platinum resulting from the decreased electron density of the platinum clusters [101,102].

Adsorption of other molecules

Compounds of high electronic densities like olefins and aromatics bond stronger to sulfur poisoned metals. Sulfur acts as an electron-acceptor and decrease the electron density of the unpoisoned metallic surface area [86].

Chang *et al.* found that the bonding strength between aromatics and Pt increased with the severity of sulfur poisoning [101,102]. Marécot *et al.* studied the effect of sulfur on the competitive hydrogenation of benzene and toluene on platinum and iridium catalysts [103]. Sulfurization increased the adsorption coefficient ratio b_T/b_B (toluene stronger electron donor) indicating a modification in the electronic properties of the metal.

Apesteguia and Barbier conducted a kinetic study of cyclopentane hydrogenolysis on Pt/Al_2O_3 and sulfurized Pt/Al_2O_3 [104]. They found an increase in the reaction order with respect to cyclopentane upon sulfurization indicating inhibition of the hydrocarbon adsorption. A simultaneous decrease in the ratio of the adsorption equilibrium constants of cyclopentane and hydrogen also showed that sulfur deposition inhibited cyclopentane adsorption more strongly than hydrogen.

2.3.3 EFFECT OF SULFUR ON ACTIVITY AND SELECTIVITY

Studies on the effect of sulfur on activity and selectivity identifying sulfur resistance and sulfur tolerance properties of metal catalysts.

The toxicity of sulfur during catalytic hydrogenation is the result of interactions between the metal, the hydrocarbon and the sulfur compound. Sulfur resistance (rate of deactivation) is a function of both catalyst properties and reaction conditions, while the sulfur tolerance is more of an intrinsic property of the metal through the strenght of the metal-sulfur bond.

Sulfur adsorbs strongly on metallic catalysts and hinders or modifies the adsorption of other reactant molecules. Adsorbed sulfur deactivates the catalyst surface in a substantial way resulting in significant or complete loss of activity. For multiple reactions leading to more than one product, selectivity is influenced because the poisoning reduces the rates of the different reactions to a varying extent. Studies of these effects caused by sulfur poisoning provide knowledge on rates and extends of poisoning, in other words the sensitivity to poisoning of a catalyst.

Definitions

Before proceeding any further a closer definition of some important concepts and terms frequently used in the discussion of this topic is in order. Some of these concepts were first introduced and used by Maxted [94].

According to Maxted: "Substances are in practice only regarded as *poisons* if they exert an appreciable inhibitive effect on catalysis even when they are present in very small concentrations". *Toxicity* is a term refering to the extent of inhibition of a poison for a given reaction and catalyst. *Initial toxicity* is defined as the number of accessible metal atoms deactivated through adsorption of the first molecule of poison [105].

Catalyst susceptibility to poisoning relates to the sensitivity of a catalyst to poisoning under specified conditions. Poisoning susceptibility is often characterized using the terms of poisoning *resistance* and *tolerance*. Poisoning resistance is related to the rate of catalyst

deactivation. Slow deactivating catalysts is hence more resistance to poisoning than a catalyst which undergo fast deactivation. Poisoning tolerance is defined as the degree of which a catalyst retains its activity after adsorption of a steady-state amount of poison under specified reaction conditions. An alternative definition is the ultimate amount of poison a catalyst can adsorb and still maintain a specific activity. It is important to bear in mind that even though the sulfur tolerance of a catalyst is close to nil, the sulfur resistance can vary considerably (catalyst life accordingly) with catalyst configuration, composition and support.

Toxicity

A prerequisite to the concept of toxicity is associative adsorption of the sulfur molecule. For most reactions including hydrogenation that means low temperature conditions. Maxted state that under such conditions toxicity depends on electronic configuration, molecular structure and size and length of stay on the surface [94]. Toxic elements shielded against formation of chemisorptive bonds with the catalyst by saturation of its normal valency orbitals by stable bonding to other atoms are less toxic than unshielded ones. Thus SO_4^{2-} is a less toxic structure compared to H_2S. The toxicity per atom of sulfur increases with the the molecular weight of the compound, e.g., the size of the moiety attached to the sulfur atom.

Maurel and Barbier determined the initial toxicity of sulfur for various hydrocarbon reactions as tabulated in Table 2.7. This illustrates the huge variation in sulfur toxicity between different reactions.

Table 2.7: Determination of the initial toxicity of sulfur for different reactions [105].

Reaction:	Initial toxicity of sulfur[1]
Hydrogenation of benzene	2.0
Monoexchange of benzene	0.2
Epimerization, dimethylcyclohexane (453K)	1.7
Hydrogenolysis of cyclopentane	9.0
Monoexchange of cyclopentane	0.5
Multiple exchange of cyclopentane	9.0
Epimerization, dimethylcyclohexane (383K)	8.9

[1]: number of accessible metal atoms deactivated through adsorption of the first molecule of poison.

Sulfur susceptibility

Sulfur resistance is dependent on several factors: the composition of the catalyst (one or more metals, promoters, supports), physical properties (surface area, pore structure) and reaction conditions. Sulfur tolerance also depends on the above except physical properties as it is a intrinsic property of the metal surface. In hydrogenation reactions the nature of the unsaturated hydrocarbon also influences the action of the adsorbed sulfur.

Associating two metals having different catalytic properties sometimes produce a synergetic effect. Addition of palladium to platinum catalysts is claimed to improve the sulfur resistance of such catalysts [38, 102,106, ,107]. Lin *et al.* speculated on the basis of FT-IR spectroscopy that the enhanced sulfur resistance stems from the decreased electron density on Pt induced by the Pt-Pd bimetallic interaction resulting in the inhibition of H_2S adsorption [102]. Larsen *et al.* found that Ni in a Pt-Ni /L-zeolite aromatization catalyst stabilize the Pt particles against sulfur induced particle growth and migration out of the zeolite channels [108].

Pt-Re/Al_2O_3 reforming catalysts is an example of the beneficial effects of sulfur adsorption. Although this catalyst is more sensitive to sulfur poisoning than monometallic Pt/Al_2O_3, presulfiding of the catalyst is performed to improve the selectivity and stability. Presulfiding modifies hydrogenation, dehydrogenation and isomerization reactions to a less degree than hydrogenolysis (cracking) reactions resulting in coke formation [1].

Many workers investigating the effect of sulfur deactivation have found that the support influence the sulfur tolerance in hydrogenation and dehydrogenation reactions. The strong interaction between metal and proton centers in zeolites results in enhanced sulfur tolerances [53-55,57,61]. Huang and Kang also ascribed the higher thioresistance of Pt/aluminium borate compared to Pt/Al_2O_3 for aromatic hydrogenation to increased support acidity [109]. Seoane *et al.* studied thiophene poisoning of supported palladium hydrogenation catalysts and underlined the importance of the nature of the support (chemical nature, texture, pore structure, surface state etc.) for the thioresistance of the catalyst [110].
Increasing reaction temperature will favor the reversible adsorption of sulfur resulting in increased sulfur tolerance [83].

The chemical nature of the unsaturated hydrocarbon is able to modify the poisonous action of sulfur. Boitiaux *et al.* examined the influence of palladium sulfurization on the hydrogenation and isomerization of 1-butene, 1,3-butadiene and 1-butyne [96]. The resistance to sulfur for the hydrogenation reaction decreased in the order: 1-butene > 1,3-butadiene > 1-butyne. In the case of 1-butyne the rate becomes independent of the degree of sulfurization at higher conversions as illustraded in Fig. 2.24. This is due to the destabilization of the metal-sulfur bond through the strong chemisorption of unsaturated reactants.

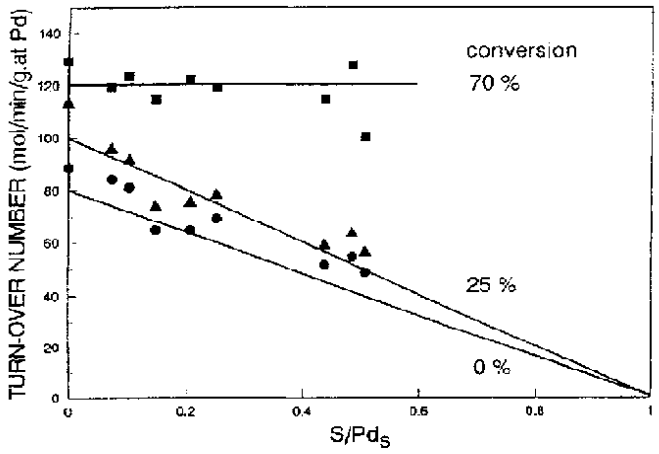

Figure 2.24: Effect of the degree of palladium on the hydrogenation rate of 1-butyne, for different conversions (T=20°C, P=10 bars) [96].

2.3.4 REGENERATION OF SULFUR-POISONED METALLIC CATALYSTS

Studies on regeneration - the effect of different regeneration schemes.

High temperature regeneration of sulfur-poisoned hydrogenation catalysts using various sulfur-free atmospheres is impossible dued to detrimental sintering of the highly dispersed metal phase of these catalysts. Displacement of reversibly adsorbed sulfur by poly-unsaturated molecules in the presence of hydrogen and therebye recovering (partly) the hydrogenation activity without altering the metal dispersion seems more promising.

Regeneration of deactivated catalysts is performed in many large-scale processes and thus is of great industrial importance. In catalytic processing of sulfurcontaminated feedstocks the possibility of reactivating the catalysts by desorption of the sulfur adlayer is of vital importance likewise. The capability of the catalyst to respond to regeneration in separate steps or to self-regenerate after dynamic changes in the sulfur concentration is a sought after property.

Regeneration by O_2/air and steam

Studies on the regeneration of sulfur poisoned Ni catalysts in oxygen have shown a complex behavior where the competition between sulfur removal and oxide formation is both pressure and temperature dependent [83]. Regeneration using steam was shown effectful in removing adsorbed sulfur from steam reforming catalysts [111]. The high temperatures necessary to achieve sulfur removal in these regeneration schemes is of little practical value in the case of high-surface area hydrogenation catalysts due to the detrimental sintering accompanying such conditions.

Regeneration by H_2 and unsaturated hydrocarbons

As discussed earlier poly-unsaturated molecules are able, due to their high heat of chemisorption on metallic catalysts, to displace reversible adsorbed sulfur and therbye recover (partly) themselves the hydrogenation activity. Oudar *et al.* found that butadiene chemisorption at 100°C on Pt(110) and Pt(111) induced a partial desorption of sulfur

[112,113]. Figoli *et al.* studied the regenerating role of 2-butyne + hydrogen on Ni/SiO_2 poisoned with carbon disulfide [114]. The results are given in Table 2.8. They found that the treatment lead to the elimination of reversible adsorbed sulfur and a recovery of the catalytic activity. The regeneration scheme induced no significant change in the metal dispersion.

Table 2.8: Relative activity of unpoisoned, CS_2-poisoned and regenerated catalysts in the selective hydrogenation of styrene [114].

Catalyst	Relative activity
Without poison	1.00
100 ppm CS_2	0.09
Regenerated toluene	0.09
Regenerated 2-butyne, 5h (P_{hyd}=1.5 kg cm^{-2})	0.21
Regeneration 2-butyne, 10h (P_{hyd}=1.5 kg cm^{-2})	0.22
Regenerated H_2, 1.5 kg cm^{-2}	0.09
Regenerated H_2, 20kg cm^{-2}	0.22

Results of other investigations on sulfur poisoning of supported platinum and palladium catalysts used in aromatics hydrogenation show a partially recovery of activity upon introduction of pure sulfur-free feed [101,109,115]. The results are explained both by irreversible adsorbed sulfur and sulfur induced sintering of metal particles. Hoyos *et al.* postulated that the decontamination level was connected with the sulfur coverage and that the regeneration level correleted with the strength of the metal-sulfur bond [115]. They found that regeneration under pure hydrogen was easier for Pd than for Pt and also more efficient for the more acidic supports.

2.4 CATALYST CHARACTERIZATION

2.4.1 CHEMISORPTION

Description of chemisorption and its use in determining metal dispersion.

Due to the well-defined stoichiometrics of hydrogen adsorption on supported metal catalysts it is an extensively used method for measuring metal dispersions. Flow techniques are fast and inexpensive, while volumetric adsorption techniques are accurate but time-consuming. The hydrogen-oxygen titration technique offers increased sensitivity and simplicity in the determination of metal surface areas.

Chemisorption of hydrogen on the platinum group noble metals is strong and proceedes dissociatively with the formation of about a monolayer of adsorbed H atoms with a stoichiometry of one hydrogen atom per metal surface atom. They are attached to the metal surface in well-defined energy states and the binding energies are not substantially affected by factors like: surface structure, support and dispersion as stated by Bartholomew [116]. On the basis of these characteristics the applicability of hydrogen chemisorption for quantitative determination of assessable sites on metal surfaces becomes apparent.

Pulse chemisorption

Pulse chemisorption is a dynamic technique in which the reduced catalytic sample is subjected to an inert carrier gas, usually argon. The sample is repeatedly exposed to pulses of chemisorbing gas of known quantity injected into the carrier. The exit gas composition is determined using a thermal conductivity detector (TCD). From the number of pulses "missing" at the exit the amount of adsorbed gas can be calculated and with the help of known adsorption stoichiometries the metal dispersion is readily obtained. This is a fast and inexpensive way of retrieving dispersion measurements.

Volumetric chemisorption

Volumetric chemisorption is a static technique in which the hydrogen uptake of the catalyst sample is measured at equilibrium conditions. By varying the adsorption pressure and

allowing suficient time for the catalyst sample to equilibrate an adsorption isotherm is obtained. Extrapolation of the linear part of the isotherm to zero pressure gives the adsorbed amount equivalent to monolayer coverage. It is common practice to measure two isotherms with intermediate evacuation of the sample. The first isoterm gives the total adsorption while the second measure the amount of reversibly adsorbed gas. Substraction gives the strongly asorbed fraction.

The hydrogen-oxygen titration methode

The hydrogen-oxygen titration methode was first used by Benson and Boudart [117]. The stoichiometry of the hydrogen titration of a oxygen-covered Pt surface was put forward as follows:

$$Pt\text{-}O + 3/2\ H_2 \rightarrow Pt\text{-}H + H_2O \qquad (2.12)$$

It offer increased sensitivity in the determination of metal surface areas (H_2 uptake three times that of dissociative H_2 adsorption for each Pt surface atom). There has been differences in opinion regarding the stoichiometry and proper procedure for the H_2-O_2 titration [116], but work by O'Rear *et al.* established the number of II and O atoms adsorbed per Pt atom at 1.1 and 0.71 respectively [118].

2.4.2 TOLUENE HYDROGENATION

Description of toluene hydrogenation and its use in determining metal dispersion.

Toluene hydrogenation is classified as a structure-insensitive (facile) reaction. The specific activity of the catalyst is constant and independent of the metal particle size and of the support used. Hydrogenation of toluene should be a good probe reaction for assessing the metal dispersion of supported noble metal catalysts, although contributions to the specific activity from the support and pretreatment procedure have been reported.

As pointed out earlier (Chap. 2.2.2) the metal particle size is an important parameter closely related to the sulfur tolerance properties of the socalled sulfur-tolerant noble metal catalysts. Control of the metal dispersion is thus of vital importance and the use of a probe reaction for assessing this property is an useful supplement to other methods such as chemisorption and electron microscopy measurements.

Structure insensitivity

The concept of "structure-sensitive" and "structur-insensitive" reactions in heterogeneous catalysis was first developed by Boudart *et al.* [119]. Structure-insensitive or "facile" reactions are distinguished by their specific activity being close to constant, independent of the metal particle size and of the support used. Catalytic reactions involving C-H bonds are seemingly structure insensive. Several investigations reported in the literature state that benzene hydrogenation on platinum catalysts is one such reaction [120-123] as shown in Fig. 2.25.

Work performed by Vannice *et al.* on hydrogenation of aromatic hydrocarbons over supported Pt and Pd catalysts contradict this [19,24]. They consistently found higher turnover frequencies for aromatic hydrogenation over acidic supports such as SiO_2-Al_2O_3 compared to SiO_2. It was proposed that acid sites on the support act as adsorption sites for the aromatic molecules and react with hydrogen spilled over from the metal at the interfacial regions.

Reaction models involving this phenomenon have also been developed by the same group [24,124].

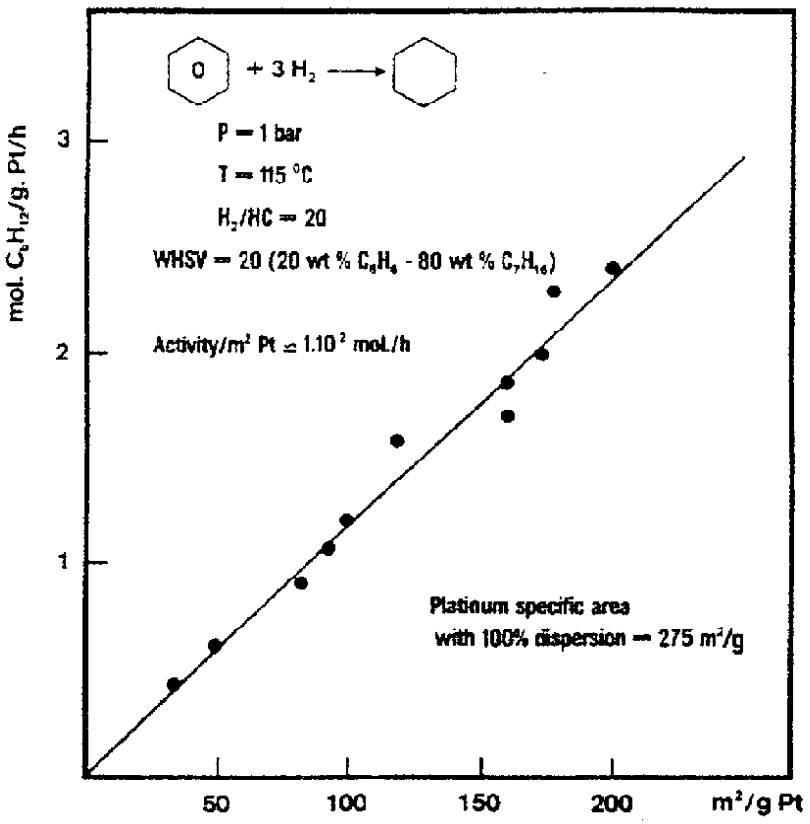

Figure 2.25: Effect of Pt dispersion on activity for benzene hydrogenation [123].

2.4.3 TEMPERATURE PROGRAMMED DESORPTION OF AMMONIA

Description of TPD of ammonia and its use in probing zeolite acidity.

TPD of ammonia is an often used technique for determining the acidity of solids. The basic principle is that when the desorption temperature is linearly increased, the rate of desorption of chemisorbed ammonia will show maximums with temperature or time, each peak representing a group of sites whose energy distribution is continuous in a finite range. The method does not distinguish between Brönsted and Lewis acid sites and diffusional limitations may occur.

To be able to accurately descripe the acidity of zeolites the determination of the nature, the strength and the number of acid sites is required. To perform this task a number of various techniques have been developed: Titration methodes, spectroscopy (IR, NMR, UV) of adsorbed bases, use of model reactions and temperature programmed desorption of chemisorbed bases [125].

The principles of Temperature Programmed Desorption (TPD) of ammonia is illustrated in Fig. 2.26. The sample is equilibrated with adsorbing ammonia and when the desorption temperature is linearly increased the rate of desorption of chemisorbed ammonia will show maximums with temperature or time, each peak representing a group of sites whose energy distribution is continuous in a finite range. The desorption curve and the amount of desorbing ammonia can be acquired using e.g . a TCD.

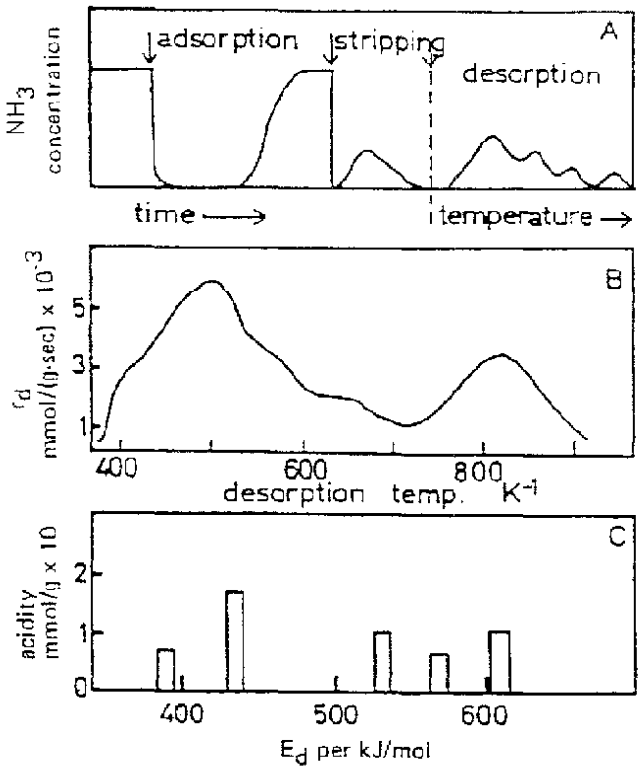

Figure 2.26: Temperature programmed desorption of ammonia from acid catalysts: (A) schematic drawing of the ammonia concentration at the column exit during the whole experiment; (B) actual desorption curve from a sample of HZSM-5 zeolite (desorption rate is 4 K/min.); (C) acid strength spectrum (activation energy of desorption, E_d, against concentration) [125].

3. EXPERIMENTAL

Description of equipment and procedures used in catalyst preparation, characterization, and activity studies.

A number of Pt/Y catalyst samples were prepared for this study. Both the metal function and the support properties were characterized applying several techniques. Toluene hydrogenation was chosen as a suitable model reaction and run in a high pressure fixed bed tubular microreactor. The effects of temperature and different sulfur components in the toluene feed were studied. A simplified kinetic study was also performed.

Catalysts

A description of the preparation and pretreatment is outlined in Chap. 3.1. Commercially available Y-zeolite supports with a range of Si/Al-ratios were impregnated with 0.3 wt% platinum by ion-exchange. The catalyst samples were calcined employing conditions designed to avoid autoreduction and sintering of the metal precursor. The catalysts were reduced *in situ* using flowing H_2 at 1 bar. A standard 0.3 wt% Pt/Al_2O_3 catalyst was used as a reference and given the same pretreatment.

Characterization

A closer description of applied techniques is given in Chap. 3.2. The metal function of the prepared catalyst samples was characterized by chemisorption measurements applying both H_2-O_2 titration and volumetric chemisorption of H_2. Transmission electron microscopy (TEM) was also used to determine the metal particle size. The support acidity was measured using temperature programmed desorption (TPD) of ammonia. Further characterization work was done using the techniques of atomic adsorption spectroscopy (AAS) and thermogravimetric analysis (TGA).

Catalytic activity measurements

A detailed description of apparatus and experimental conditions and procedures used studying toluene hydrogenation are given in Chap. 3.3. The catalytic activity was studied in a high-

pressure tubular fixed bed microreactor designed and built as a part of this work. The hydrogenation of sulfur free and sulfur-spiked toluene was performed under conditions close to realistic industrial conditions. A range of different catalyst samples were tested on feeds containing various sulfur compounds at different levels of contamination. The effects of temperature and pressure were also examined.

3.1 CATALYSTS

3.1.1 CATALYST PREPARATION

Description of the method used for introduction of metal into zeolites.

Y-zeolite supports with Si/Al-ratios ranging from 2.6 to 40 were impregnated with 0.3 wt% platinum by ion-exchange. The ion-exchange was performed at room temperature under vigorous stirring followed by settling, filtering, washing and drying. On one of the samples a competitive ion-exchange technique was used. A commercial 0.3 wt% Pt/Al_2O_3 sample was used as a reference.

Loading of metals inside zeolite supports can be performed by several different techniques (see Chap. 2.2.2). In this work the metal was introduced into the zeolite by ion-exchange.

The zeolite supports

The zeolite Y supports were manufactured by PQ Zeolites B.V. The supports were in the H- or NH_4-form and were used as received. Some properties of the supports are listed in Table 3.1.

Table 3.1: Properties of the used zeolite supports.

Product	Si/Al[a]	Na_2O[b]	Unit Cell Size[c]	Surface area[d]
	mole ratio	wt%	Å	m^2/g
CBV500	2.6	0.2	24.53	750
CBV712	6.0	0.05	24.33	730
CBV720	15.0	0.03	24.28	780
CBV740	20.0	0.03	24.26	750
CBV780	40.0	0.03	24.25	780

[a]Chemical analysis bulk composition, [b]Ignited basis, 1000°C, [c]ASTM Method D 3942, [d]Nitrogen adsorption measured at $P/P_0 = 0.03$.

Ion-exchange

The zeolite powder (~33 g) was dissolved in ion-exchanged water (125 ml) and placed under vigorous stirring. $Pt(NH_3)_4Cl_2$ (~0.17 g) was then dissolved in an equal amount of ion-exchanged water (125 ml) and added dropwise to the center of the zeolite slurry using a pipette. On some of the samples a competitive ion-exchange technique was used, by adding NH_4NO_3 to the solution. The ion-exchange was performed at room temperature for 24 hours followed by settling for 48 hours. The ion-exchanged zeolite was filtered and washed repeatedly with water until no Cl^- was detected (addition of $AgNO_3$). The sample was dryed at 100°C overnight.

A sample containing 0.3 weight% palladium (3PdC712) was also prepared using the same procedure as described above.

The reference sample

A commercial Pt/Al_2O_3 catalyst (CK303) manufactured by AKZOCHEMIE Nederland B.V. was used as a reference. This catalyst (EUROPT-3) contains 0.3 wt% platinum, approximately 1 percent by weight chlorine, 50 ppm wt sulfur and has a surface area of 183 m^2/g [1]. The received extrudates were crushed and sieved to particles ranging between 250 µm and 600 µm.

3.1.2 CATALYST PRETREATMENT

Description of procedures for calcination and reduction of catalyst samples.

The catalyst samples were calcined in a quarts reactor under "shallow bed" conditions. A high flow of dry air and a slow temperature increase to avoid autoreduction by the evolved ammonia was employed. The catalysts were reduced *in situ* using flowing H_2 at 1 bar following a drying step in flowing N_2.

The proper pretreatment procedures of noble metals in Y-zeolite catalysts are crucial in determining the activity, selectivity and the resistance to poisons as mentioned earlier (see Chap. 2.2.2).

Calcination

After drying the catalyst powder was pressed in an IR press (1 ton), crushed and sieved into particles. The particles were calcined in a quartz reactor placed in a dedicated calcination apparatus shown in Fig. 3.1.

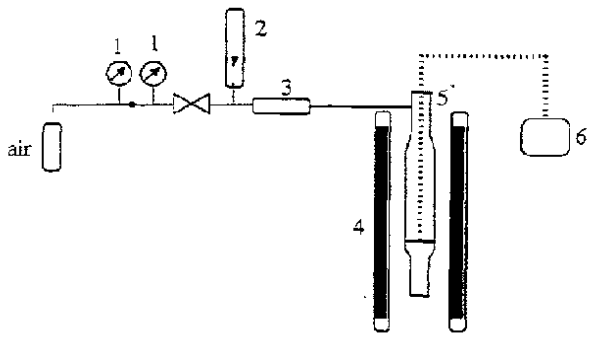

Figure 3.1: Calcination apparatus. (1) manometer, (2) rotameter, (3) molsieve, (4) furnace, (5) quartz reactor with quartz frit, (6) temperature controller attached to thermoelement [126].

The calcination was performed under socalled "shallow bed" conditions (bed hight ~0.5 cm) with a high flowrate of dry air (200 cc/g cat., min.) and a slow temperature increase to avoid autoreduction by the evolved ammonia. The temperature programme was as follows:

1°C/min. to 180°C and hold for 3 hours
1°C/min. to the calcination temperature (T_C) and hold for 6 hours.

Reduction

The catalysts were reduced *in situ* using flowing H_2 at 1 bar. The reduction procedure consisted of a drying step in N_2 (200 cc/g cat., min.), The heating rate was 0.8°C/min. to 240°C and hold for 4 hours followed by the reduction. The gas was switched to H_2 (200 cc/g cat., min.) at 240°C, the heating rate was 10°C/min. to the reduction temperature (T_R) and hold for 2 hours.

The same reduction procedure was employed for the reference catalyst.

3.2 CHARACTERIZATION

3.2.1 CHEMISORPTION

Description of apparatus and procedures.

Chemisorption measurements were conducted on the catalyst samples utilizing both H_2-O_2 pulse titration in a pulse apparatus and volumetric chemisorption of H_2 in a conventional glass apparatus. The measurements were performed on approximately 1 g of sample at ambient temperature following reduction of the precalcined samples.

H_2-O_2 titration, apparatus and procedures

Pulse chemisorption experiments using the H_2-O_2 titration method were performed in a standard apparatus. An outline of the apparatus is shown in Fig. 3.2.

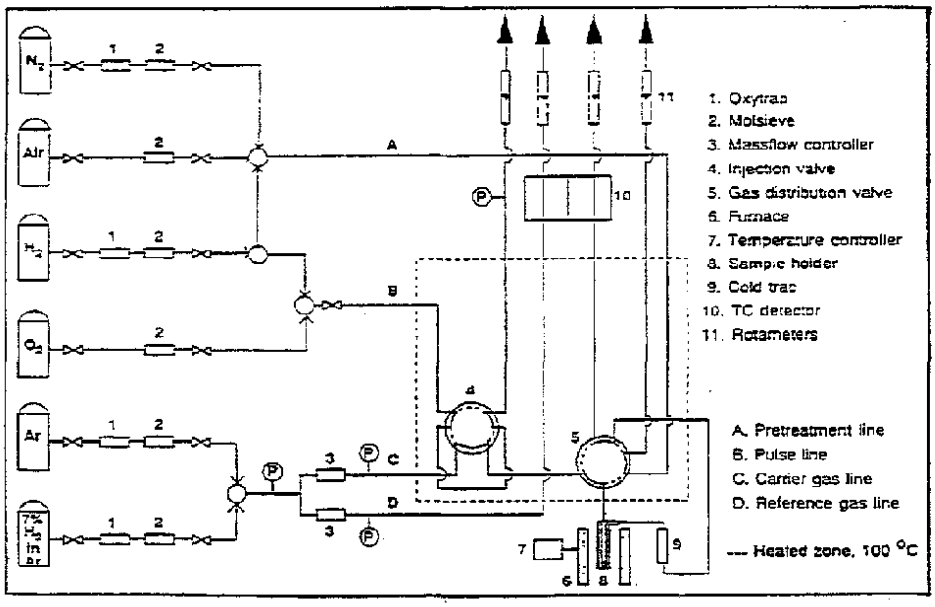

Figure 3.2: Outline of the pulse chemisorption apparatus [127].

The experimental unit consists of gas feed lines equipped with Alltech molsievs and oxytraps for gas purification and with Ili-tec F-100/200 massflow meters/controllers. An adsorbate loop for pulse injections is connected to the carrier gas line before the sample holder. The catalyst sample rests on a quartz frit inside the U-shaped quartz sample holder. The exit gas composition is monitored using a TC detector in a Shimadzu GC-8A gas chromatograph connected to a Shimadzu C-R5A Chromatopac integrator. The heat source is an electrical furnace supplied by Kanthal and controlled by a Eurotherm 818P temperature controller. Two thermocouples placed outside the sample holder are used for furnace control and computer logging of the temperature.

The samples (0.9 g) were reduced in H_2 (50 cc/min.). The heating rate was 10°C/min., up to T_R and hold for 2 hours. After completion of the reduction the sample was flushed with argon and cooled to room temperature for chemisorption measurements. The sample was repeatedly exposed to pulses of O_2 until saturation was reached, subsequently followed by a sequence of H_2-O_2 titrations until stable values were obtained. From the pulse volume, temperature and pressure (50 µl, 100°C, 1.25 bara) the amount of gas in each pulse was calculated to be 53,248 µmol H_2/pulse. The number of pulses adsorbed was estimated by comparing each peak area with the area at "saturation" as reference.

Volumetric chemisorption, apparatus and procedures

The static volumetric chemisorption measurements were performed in a conventional glass apparatus with greased stopcocks shown in Fig. 3.3. The main components in the experimental unit are: the gas supply, the dosing unit, the vacuum unit, and the sample cell. The high vacuum system consist of a rotary vacuum pump and a mercury diffusion vacuum pump cooled with liquid N_2. The pressure in the sample cell is monitored by an electronic pressure gauge calibrated against a Mensor quartz-spring pressure gauge. Some measurements were also performed in a Micromeritics ASAP 2010 unit.

The samples (1.0 g) were reduced in H_2 (12 cc/min.). The heating rate was 10°C/min., up to T_R, and hold for 2 hours. After completion of the reduction, the hydrogen flow was stopped and the sample cell evacuated to a pressure below 10^{-5} torr before cooling to 25°C. Hydrogen was admitted to the sample cell in steps of increasing pressure from approximately 50 torr up to 460 torr. The samples were then evacuated to 10^{-5} torr for 20 minutes before a second

isotherm was obtained as described above and thus the total and the reversible amount of adsorbed hydrogen were obtained. After the last measurement the sample cell was again evacuated and the "dead space" was determined by filling the cell with a known amount of helium and measuring the pressure.

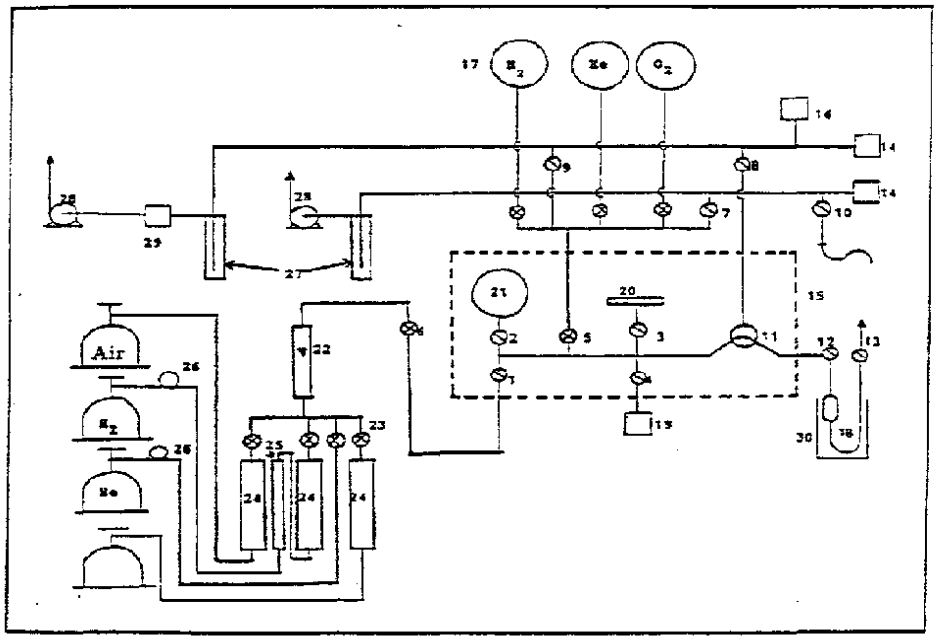

1–4: Glass stopcocks
5: Glass/PTFE stopcock
6: Needle valve
7–13: Glass stopcocks
14: Low-vacuum gauge
15: Parts kept at 298±0.1 K
16: High vacuum gauge
17: Gas reservoirs
18: Adsorption cell
19: Quarts spring pressure gauge
20: Electronic pressure gauge
21: Calibrated volume
22: Gas flow meter
23: Gas inlet valves
24: Gas purifier
25: Indicating oxytrap
26: Oxytrap
27: Liq. N_2-cooled trap
28: Rotary vacuum pump
29: Hg-diffusion pump
30: Furnace

Figure 3.3: Volumetric chemisorption apparatus [128].

3.2.2 TRANSMISSION ELECTRON MICROSCOPY

Description of apparatus and procedures.

Transmission electron microscopy of the catalyst samples were performed on a Philips CM30 electron microscope operating at 300 kV. The micrographs were recorded at around 100.000 times magnification. Several areas of a specimen were studied to get a statistical selection.

The TEM micrographs were recorded by R. Holmestad at SINTEF, Applied Physics, Trondheim. The samples were calcined, reduced and used for H_2-O_2 titration before TEM was performed. The specimens were prepared by grinding the powder under methanol in an agite mortar. The crushed powder was then deposited on to a holey carbon film on Cu grid and placed under the microscope.

3.2.3 TEMPERATURE PROGRAMMED DESORPTION OF AMMONIA

Description of apparatus and procedures.

The acidity of the zeolite supports and one catalyst was measured by gravimetric ammonia-TPD using a traditional microbalance. The samples were placed in a quartz basket with perforated bottom covered with quartz wool. After drying in flowing helium the samples were saturated with ammonia, and flushed in helium before TPD was performed.

Apparatus

The zeolite acidity was measured in a traditional quartz microbalance apparatus. An outline of the experimental unit is shown in Fig. 3.4.

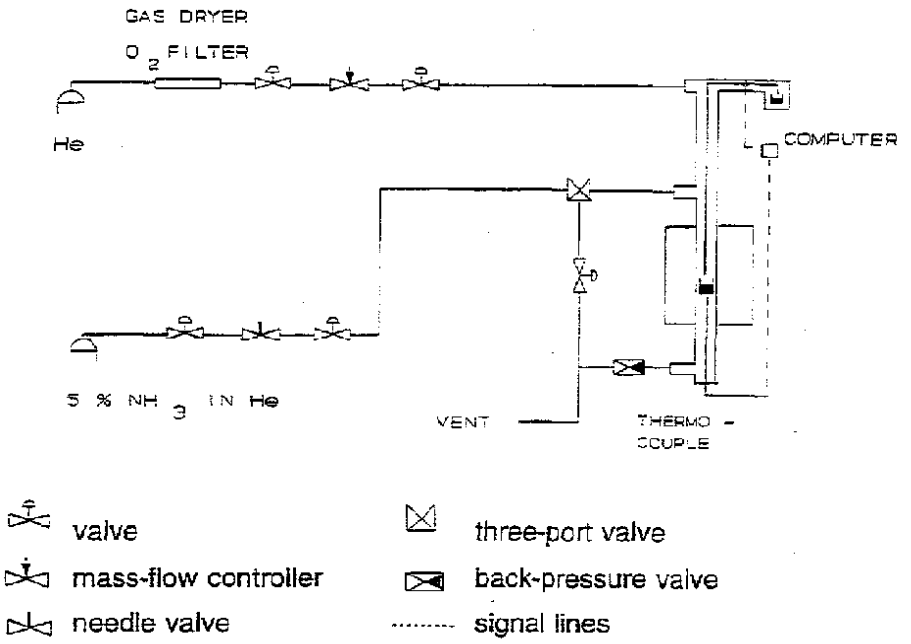

Figure 3.4: Schematic drawing of the TPD apparatus [129].

A tubular quartz reactor (15 mm i.d.) was mounted to a C.I. Electronics Mark 2B microbalance. The samples were placed in a quartz basket (6 mm i.d.) with perforated bottom covered with quartz wool. The basket was suspended with quatrz fibers from one arm of the balance. The weight was continuously recorded using a computer. A thermocouple for temperature measurement and control was placed under the basket. Gas feed lines for He and 5% NH_3 in He were connected to the microbalance reactor and the flow regulated with a Hi-tec massflow controller and a fine metering needle valve respectively.

Procedure

The samples were dried in flowing helium (60 cc/min.). The heating rate was 10°C/min., up to 500°C, and hold for 12 hours, then 5°C/min., up to 600°C, and hold for 30 minutes. The reactor was then cooled to 120°C, and NH_3 (25 cc/min. of 5% NH_3 in He) was adsorbed until saturation. After flushing the sample with He (60 cc/min..) for 30 minutes, TPD was performed with a heating rate of 10°C/min., up to 550°C, and hold for 30 minutes.

3.2.4 ADDITIONAL TECHNIQUES USED

Description of apparatus and procedures.

The degree of ion-exchange of platinum into the zeolite supports were determined from atomic adsorption spectroscopy (AAS) analysis of the exchanged solution.
The amount of moisture in the starting support material and the catalyst samples was estimated from the recorded weight loss obtained by thermogravimetric analysis (TGA).

Atomic adsorption spectroscopy-apparatus and procedure

Atomic adsorption spectroscopy of the exchanged water solutions of all sample batches was performed on a VARIAN SectrAA-400 by H. Semb at SINTEF Sensor and Analytical Chemistry, Trondheim. The water solutions were analyzed directly by adding a solution of $CuCl_2$ (2%).

Thermogravimetric analysis-apparatus and procedure

The TGA experiments on the catalyst samples were performed using a PERKIN ELMER TGA 7 thermogravimetric analyzer.
The sample (20-25 mg) was heated in flowing nitrogen (50 cc/min.) from the head and in air (30 cc/min.) from the side of the cell. For the starting material the heating rate was 10°C/min., up to 500°C, and hold for 30 minutes.

Sulfur analysis

Sulfur analysis of the liquid samples (feeds and products) were performed using an ANTEK 7000NS Elemental Analyzer from Antek Instruments, Inc..
The sample is vaporized and combined with oxygen at temperature in excess of 1000°C. The oxidation product, SO_2, is exposed to ultraviolet radiation of a specific wavelength (eq. 3.1) causing some electrons to shift to higher energy orbitals. This excess energy is released in the form of light and is detected by a photomultiplier tube. This fluorescent emission is completely specific for sulfur and is proportional to the amount of sulfur in the original sample.

$$SO_2 + h\nu' \rightarrow SO_2 + h\nu'' \qquad (3.1)$$

3.3 CATALYTIC ACTIVITY MEASUREMENTS

3.3.1 APPARATUS FOR HYDROGENATION REACTION STUDIES

Description of its design and use.

The experimental unit can be devided into three main parts: The introduction of the reactants, the reactor, and the pressure regulation and analytical system. Gases and liquids are dosed using mass flow controllers and HPLC pumps respectively. The fixed bed tubular reactor is placed in an oven with temperature control. The pressure is set by a back-pressure regulator and part of the exit stream is connected to a gas chromatograph for on-line analysis. The unit is designed for pressures up to 200 bar.

Reactor choice

The function of a laboratory reactor is to generate reliable information. For catalyst testing no universal reactor exists, and so the reactor selection depends on several factors like: nature of the reaction system, purpose of the work, experience etc..

The choice of a fixed bed tubular reactor for this work was made emphasizing the local available experience, prize, purpose (catalyst screening, kinetic parameters) and reaction system (gas-solid).

Apparatus

The design and construction of the high-pressure reactor-rig for the activity and kinetic measurements were an important and necessary part of this work. A schematic design of the experimental set-up is shown in Fig. 3.5. The unit is built in stainless steel and is designed pressures up to 200 bar.

The feed unit consists of two high-pressure gas feed lines (H_2, N_2) and one low-pressure line used for presulfiding of the catalyst sample (5% H_2S/H_2). The flow rates were metered by Hi-Tec mass controllers and a rotameter respectively. The liquid feed was dosed in two separate lines each equipped with a HPLC pump. Separate reservoirs, pumps, and feed lines for clean feed and sulfur-spiked feed were used to avoid history effects due to strongly adsorbed sulfur

components desorbing into the clean feed. The liquid feed was injected into the gas feed at the reactor inlet.

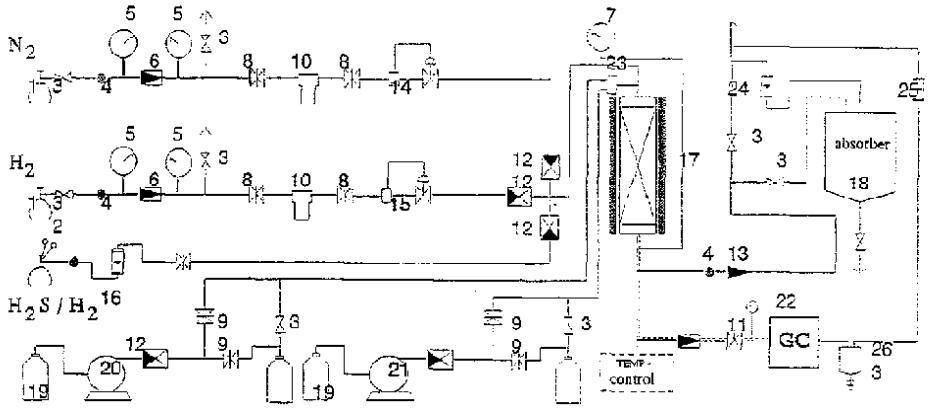

Figure 3.5: Schematic drawing of the high-pressure micro-reactor apparatus. A description of components and parts is given in appendix II.

The fixed bed tubular microreactor is outlined in Fig. 3.6. The reactor was 40 cm long, with an inner diameter of 9 mm. The catalyst was placed on quartz wool on top of a stainless steel frit located 18 cm from the bottom of the reactor. The temperature was monitored by a thermocouple in the catalyst bed. The heat source was an electrical furnace supplied by Kanthal and controlled by a Eurotherm 903P temperature controller.

Directly at the outlet of the reactor a cross-junction leads either to a Tescom back-pressure regulator and a manometer or to a Tescom reduction valve followed by a Hoke metering valve. Downstream of the metering valve the exit stream flows into a injection loop fitted to a Chrompack CP-9000 gas chromatograph equipped with a flame ionization detector (FID) and a 10 m CP-5 (Chrompack) widebore column. Purified helium was used as carrier gas. The products were kept in the gas phase by insulating and heating the lines at 200°C. Finally the hydrocarbon products were collected in a water-cooled condensation pot for sampling and off-line analysis obtaining more detailed composition.

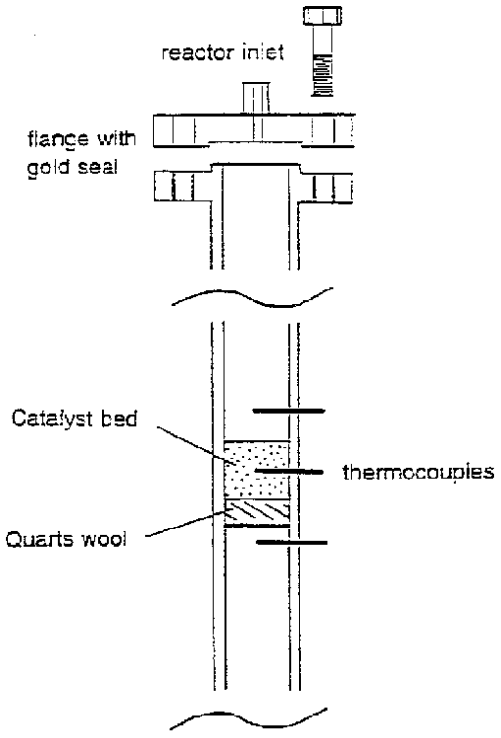

Figure 3.6: The steel reactor [1].

3.3.2 HYDROGENATION OF TOLUENE

Description of the operating conditions for the activity measurements and the kinetic studies.

The hydrogenation of sulfur free toluene was studied under conditions close to industrial conditions. The hydrogenation activity of the prepared catalyst samples was measured under a set of chosen standard conditions and in a range of different temperatures. The pressure dependency of the hydrogenation rate with respect to toluene and H_2 was also studied.

Industrial conditions

The term close to industrial conditions used here strictly reflects the aim of this work to study aromatic saturation at conditions of pressure and temperature similar to those experienced in refinery operations. Requirements like isothermality, ideal flow pattern, and absence of concentration gradients are most desirable features in running a laboratory reactor, while industrially operated reactors are run according to quite different criteria, usually close to adiabatic.

Activity measurements

The standard reaction conditions for the toluene hydrogenation are given in Table 3.1. The catalyst (approx. 0.15 g) was diluted with inert SiC (particle size 53-90 μm) up to 1.3 g total weight, to give a bed hight of approximately 20 mm in the reactor. The SiC particles had a BET surface area of 0.24 m^2/g and were non-porous. Elemental analysis of the SiC revealed small impurities of Al, Fe, K, and Na [130]. Drying and reduction of the precalcined catalyst were performed *in situ* as described in Chap. 3.2.1. The zeolite supported catalysts were all calcined at 400°C and reduced at 500°C, while the alumina supported reference catalyst was calcined and reduced at 450°C. After the completion of the reduction the sample was cooled to the reaction temperature in H_2, then flushed with N_2 and pressurized to the reaction pressure. The gas composition was adjusted to the desired flow before the liquid pumping was started. The hydrocarbon feed was injected into the gas feed at the reactor inlet. The reaction

was run typically for 10 hours until steady-state was established, with GC analysis of the exit stream every 30 minutes.

Table 3.1: Reaction conditions for toluene hydrogenation.

Temperature:	240°C
Pressure:	31 bara
WHSV:	40 h^{-1}
H_2/N_2/toluene:	9/9/1 mol/mol/mol

Temperature effects

The experimental conditions and procedures for the temperature response measurements were the same as described in the preceding paragraph. The toluene hydrogenation activity was measured in the temperature range between 160°C and 400°C. At each investigated temperature the liquid pumping was stopped and the sample flushed in H_2/N_2 for 1 hour before the liquid pumping was resumed and the activity measured.

Pressure effects

The reaction conditions during the kinetic study of these catalysts are given in Table 3.2. The total molflow in the reactor was kept constant along with the partial pressure of either toluene or that of H_2 and varying the pressure of the other component. Differential conditions in the reactor (conversion below 10%) were maintained by adjusting the amount of catalyst loaded into the reactor. Beyond that the procedure was as described in the preceding paragraphs.

Table 3.2: Reaction conditions for the pressure dependency study.

Temperature:	240°C
Pressure:	31 bara (balanced with N_2)
Total molflow:	0.0206 mol/min.
Partial pressure, toluene:	0.8 - 2.0 bara (1.6 bara[1])
Partial pressure, H_2:	10.0 - 20.0 bara (14.7 bara[1])

[1]: center point.

Properties of the chemicals and gases used are listed in Appendix I.

3.3.3 HYDROGENATION OF SULFUR-SPIKED TOLUENE

Description of the operating conditions for the activity measurements and the kinetic studies.

The hydrogenation of sulfur-spiked toluene was studied varying the amount of sulfur and the sulfur compound added to the feed. Feeds spiked with dimethyldisulfide (DMDS), benzothiophene (BT), and dibenzothiophene (DBT) to the equivalent of approximately 20, 100, and 200 ppm wt sulfur were prepared. After a periode of clean liquid feed over the catalyst samples a switch to sulfur-spiked feed was made. The effect of presulfiding the samples in H_2S/H_2 before starting the hydrogenation reaction was also studied.

Sulfur-spiked feeds

To simulate the conditions in real hydrocarbon feedstocks organic sulfur was added to the feed. For simplicity feeds containing only one sulfur compound were prepared. An alifatic sulfur compound (dimethyldisulfide, DMDS) and two different aromatic sulfur compounds (benzothiophene, BT; dibenzothiophene, DBT) were applied. Feeds spiked to the equivalent of approximately 20, 100, and 200 ppm wt sulfur were prepared and used.

Experimental conditions and procedures

The experimental conditions and procedures used during the activity measurements and the study of the temperature and pressure effects are identical to those given in Chap. 3.3.2. After the initial lining out of the system and determination of the catalyst activity with clean feed a switch to sulfur-spiked feed was made and the activity determined at varying sulfur levels.

Presulfiding

After the completion of the reduction the sample was cooled to 400°C in H_2 and sulfided in 5% H_2S/H_2 (60 cc/min.) for 3 hours. The activity measurements over the presulfided samples were performed only on sulfur-spiked feeds in order to maintain the catalysts in the sulfide state.

4. RESULTS AND DISCUSSION

Report of experimental findings.

Nobel metal catalysts supported on Y-zeolite have been prepared and characterized in this study. Characterization of both the metal function and the support was performed utilizing a number of techniques. When studying catalyst activity and kinetics of high specific area materials in laboratory reactors the effect of heat and mass transfer is a potential problem and must therefore be addressed. Toluene hydrogenation at close to realistic conditions was used as a model reaction when assessing the effects of sulfur poisoning on the catalyst activity and kinetic behavior.

Catalyst characterization

A report on the state of metal and support in the prepared catalyst samples is given in Chap. 4.1. Noble metal catalysts supported on Y-zeolite were successfully prepared by ion-exchange. Ammonia TPD profiles shows wide desorption peaks indicating a large distribution in acid strength. The metal function was characterized by chemisorption, TEM, and toluene hydrogenation. The results indicate the presence of reduced metal in both supercages and mesopores. The metal particle size and location depends on the temperatures of pretreatment and on the zeolite support itself.

Transport limitations

Tests for experimental conditions free of temperature and concentration gradients are reported in Chap. 4.2. The correct determination of intrinsic catalyst properties can be, if present, obscured by transport limitations. Ideality of flow pattern and isothermality are two requirements of utmost importance when conducting catalytic reactions in a laboratory reactor. Empirical criteria and tests for ensuring reaction controlled operation of the reactor reveal the strong influence of catalyst properties on the severity of encountered transport limitations.

Hydrogenation of sulfur-free toluene

Experiments with toluene hydrogenation to observe the kinetic behavior of the catalyst samples are described in Chap. 4.3. The effects of temperature and pressure on the kinetic behavior of the platinum catalysts were studied. The reaction orders in toluene and hydrogen were determined at 240°C and 31 bars total pressure. A temperature dependent maximum in the reaction rate was found. The kinetic behavior observed in this study is consistent with reaction models found in literature invoking the presence of carbonaceous species on the metal surface.

Hydrogenation of sulfur-spiked toluene

Report of experiments to measure catalyst performance are given in Chap. 4.4. When sulfur is added to the toluene feed there is a strong decrease in the catalyst activity due to sulfur adsorption. The kinetics of the catalysts are also altered. Both a change in the reaction orders in toluene and hydrogen and a different temperature response are observed. There are no clear differences in the effect of various sulfur compounds on the catalyst activity. The kinetic behavior of reduced and pre-sulfided catalysts show similar features.

4.1 CATALYST CHARACTERIZATION

4.1.1 CATALYST PREPARATION

Report on the moisture content and the degree of ion-exchange.

All the zeolite supports contained various amounts of water absorbed during storage which have to be accounted for in the calculation of the final platinum content. AAS analysis of the exchanged solutions showed metal loadings in excess of 90% on all samples. The use of competitive ion-exchange lead to decreasing levels of platinum exchange with increasing NH_4/Pt ratios.

One of the characteristic properties of zeolites is their ability to accommodate large amounts of water molecules in their void space (zeolites are extensively used as drying agents). Without any special precautions, (air-tight containers etc.) the zeolites will absorb water during storage. This has to be accounted for in the calculation of the final metal content, which then again is used to obtain the H/Pt ratios from the chemisorption measurements.

Moisture content

The moisture content on the Y zeolites delivered from PQ Corp. was measured by TGA and the results are given in Table 4.1.

Table 4.1: Moisture content from TG-analysis of the Y zeolites supplied from PQ Corp.

Zeolite sample	Compensating cation	Remaining material in bottle (%)	Moisture on dry basis (%)
CBV500	NH_4^+	100	30
CBV500	NH_4^+	ca. 0	29
CBV712	NH_4^+	50	17
CBV720	NH_4^+	90	17
CBV740	H_3O^+	20	9
CBV780	H_3O^+	50	29, 34

The moisture content decreases with the SiAl ratio, as expected, except for CBV 780 which has a very high moisture content. Whether parts of the contained material has been used or not does not seem to influence the moisture content.

Metal loading

The moisture content was not taken into account when the zeolites were ion-exchanged with metal. This and the fact that not all of the introduced metal was loaded on the zeolite made it necessary to calculate the metal content based on "dry catatalyst" and the AAS-analysis of the exchanged solution. The results are given in Table 4.2.

Table 4.2: Metal loading on various zeolites corrected for moisture and AAS-analysis.

Sample	NH_4:Metal	Metal added (mg Met./cc)	AAS, exchanged solution (mg Met./cc)	Metal loaded (%)	**Metal (wt%)**
3PtC500	200	401×10^{-6}	31×10^{-6}	92	**0.39**
3PtC712	0	404×10^{-6}	20×10^{-6}	98	**0.35**
3PdC712	0	400×10^{-6}	9.2×10^{-6}	98	**0.34**
3PtC720	0	402×10^{-6}	0.7×10^{-6}	100	**0.35**
3PtC740	0	403×10^{-6}	2.9×10^{-6}	100	**0.33**
3PtC780	0	402×10^{-6}	6.8×10^{-6}	98	**0.39**

Well over 90% of the metal added was loaded on the zeolite supports giving almost identical levels of metal in all the samples. The exception being 3PtC500, and 3PtC780 exhibiting a higher level of metal due to the high water content in the zeolite prior to the ion-exchange.

Competitive vs. non-competitive ion-exchange

Competitive ion-exchange utilizing an aditional cation in the ion-exchange solution is a method used to obtain a more homogenous distribution of exchanged metal in the zeolite crystallites. As a part of the work in optimizing the preparation and pretreatment procedures for the catalyst samples reported in the preceeding chapters of this thesis, the effect of varying the NH_4/Pt ratios (NH_4^+ being the competing cation), was studied. The results are given in Table 4.3.

Table 4.3: Effect of varying the NH_4/Pt ratio on the amount of Pt loaded on the zeolite.

Sample	NH_4:Pt	Pt added (mg Pt/cc)	AAS, exchanged solution (mg Pt/cc)	Pt loaded (%)	**Pt (wt%)**
3PtC500	0	408×10^{-6}	0.1×10^{-6}	100	**0.42**
3PtC500	200	405×10^{-6}	37×10^{-6}	91	**0.39**
3PtC712	0	395×10^{-6}	6.4×10^{-6}	98	**0.29**
3PtC712	50	404×10^{-6}	13.9×10^{-6}	97	**0.30**
3PtC712	200	412×10^{-6}	75.1×10^{-6}	82	**0.26**

It's evident from Table 4.3 that the use of competitive ion-exchange leads to decreasing levels of metal exchange with increasing NH_4/Pt ratios. For the replacement of ammonium-ions sited in the zeolite interior with complexed platinum-ions from the solution a driving force is needed. The main driving force here is the concentration gradients existing between the two locations. Increasing the NH_4/Pt ratio in the water solution flatten these gradients leading to a lower driving force for ion-exchange. As for a chemical reaction this implies a lower rate (of exchange) resulting in reduced platinum loadings for the same exchange time.

4.1.2 TEMPERATURE PROGRAMMED DESORPTION OF AMMONIA

Measurements of Y-zeolite support acidity.

The number of strong acid sites defined here as the amount of NH_3 desorbed above 250°C, decreases with increasing Si/Al ratio. A broad peak centered around 180°C in the TPD profiles are attributed to physically adsorbed NH_3 after comparing with the desorption profile of a non-acidic Y-zeolite. The desorption peaks are wide, indicating a large distribution of acid strength. The amount desorbed is low, and constitutes only about 30-40% of the theoretical number of acid sites based on calculations of framework Al per unit cell.

The NH_3-TPD was performed in the quartz microbalance apparatus described in Chap. 3.2.3. The Y-zeolites were provided by PQ Corporation and the following information regarding their preparation is cited from Remy *et al.* [131]. The starting material, CBV300, is a Na-Y zeolite ammonium-exchanged for over 80%. CBV500 is a typical USY catalyst prepared by steaming of CBV300. CBV712 is obtained by a mild acid leaching while the other samples (CBV720, CBV740, and CBV780) were steamed a second time at higher temperature and leached with a mineral acid.

The number of framework Al (N_{al}), extra-framework Al (N_{EFAL}), unit cell formula, and zeolite pore volume are given in Table 4.4. The correlations used are the same as in Moljord *et al.* [132]. The micro- and mesopore volumes were estimated from the N_2 adsorption isotherm by extrapolating the quasi-linear part of the curve to $p/p_0=0$ and $p/p_0=1$, respectively.

The NH_3-TPD profiles are given in Fig. 4.1, showing a peak centered around 180°C attributed to physically adsorbed NH_3 after comparing with the desorption profile of a non-acidic NaY-sample (LZY-52). This curve also shows that the physically adsorbed NH_3 desorbs below 250°C, thus the amount of strong acid sites was estimated from the NH_3-desorption above 250°C and is given in Table 4.5. As expected the number of strong acid sites decreases with increasing Si/Al ratio.

Table 4.4: The unit cell formula, amount of extra-framework Al per unit cell (N_{EFAL}), pore volume, and Na content of the Y-zeolite samples [132].

Sample	unit cell formula	N_{EFAL}	Pore volume (cc/g)		Na	Si/Al	Si/Al
			micro	meso	ppm	global	fr.work
CBV500	$Na_{0.4}H_{38.8}Al_{39.2}Si_{152.8}O_{384}$	9.6	0.310	0	700	2.9	3.9
CBV712	$Na_{0.25}H_{20.85}Al_{21.1}Si_{170.9}O_{38}$	7.1	0.295	0.075	500	5.8	8.1
CBV720	$Na_{0.3}H_{11.0}Al_{11.3}Si_{180.7}O_{384}$	2.4	0.275	0.065	560	13.0	16.0
CBV740	$Na_{0.05}H_{9.45}Al_{9.5}Si_{182.5}O_{384}$	0.1	0.290	0.065	100	19.0	19.2
CBV780	$Na_{0.15}H_{6.05}Al_{6.2}Si_{189.8}O_{384}$	0.0	.0275	0.060	300	30.6	30.6

The desorption peaks are wide, indicating a large distribution of acid strength typical for Y-zeolites [133-137].

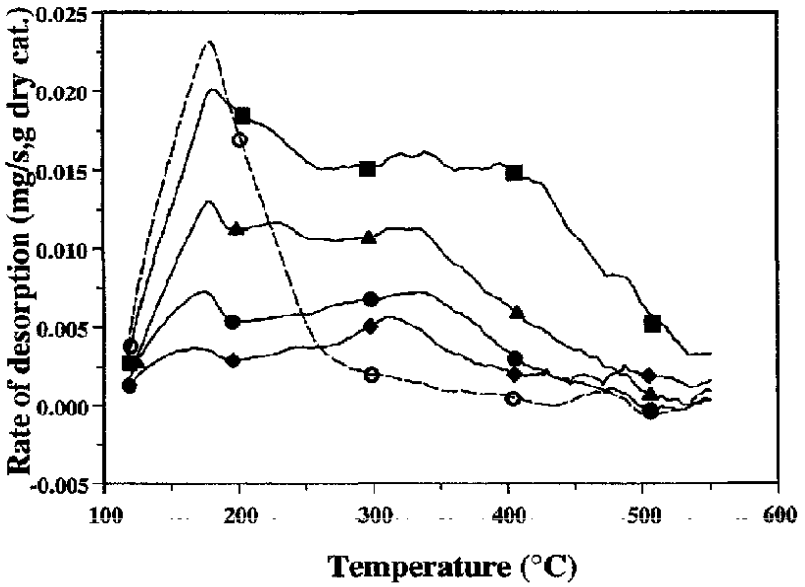

Figure 4.1: NH_3-TPD curves for CBV500 (■), CBV712 (▲), CBV720 (●), CBV740 (◆), and LZY-52 (○). LZY-52 is a non-acidic NaY.

The amount desorbed is low, and constitutes about 30-40% of the theoretical number of acid sites based on calculations of framework Al per unit cell. This is in line with other reports [133,134,137-139]. From Table 4.5 it is also evident that incorporation of metal into the support does not change the acidity in a significant way.

Table 4.5: Acidity of the Y-zeolite supports defined as the amount of NH_3 desorbed between 250 - 550°C.

Support	Si/Al (global)	Amount desorbed (250 - 550°C) mmoles/g	Peak temp. °C
CBV500	2.9	1.28	340
0.3Pt-CBV500	2.9	1.24	340
CBV712	5.8	0.56	310
CBV720	13.0	0.27	335
CBV740	19.0	0.23	335
CBV780	30.6	0.19	310

4.1.3 THE METAL FUNCTION

Report on the measured metal dispersions from the chemisorption studies and the metal particle sizes observed by TEM.

The H/Pt ratios measured by pulse titration and volumetric chemisorption are in close agreement for the investigated catalyst samples. The H/Pt ratios depend on the temperature of calcination and reduction, and on the zeolite itself. The rather low H/Pt ratios found indicates platinum located in both supercages and the larger mesopores. The estimated Pt particle sizes from chemisorption measurements were partly confirmed by transmission electron microscopy.

Chemisorption

A description of the sample pretreatment is given in Chap. 3.1.2 and the apparatus and procedures used in the chemisorption measurements are described in Chap. 3.2.1.

The total amount of hydrogen adsorbed in the volumetric chemisorption measurements was used to calculate the H/Pt ratio believing this to be the best method in order to have reproducible results. The H/Pt ratios reported in Table 4.6 were measured on catalyst samples

Table 4.6: Metal dispersions calculated from chemisorption measurements.

Catalyst	NH_4 : Pt	H : Pt (pulse)	H : Pt (volumetric)	Particle size[1] (nm)
3PtC500	200	0.28	0.20	3.9
3PtC712	0	0.05	0.03	21.6
3PdC712	0	0.06	-	18
3PtC720	0	0.33	0.39	3.3
3PtC740	0	0.23	0.29	4.7
3PtC780	0	0.22	-	4.9
3Pt/Al_2O_3	-	0.51	0.75	2.1

[1] :Calculated from pulse measurements assuming sperical particles.

tested in toluene hydrogenation. The samples were calcined at 400°C and reduced at 500°C. The H/Pt ratios measured by puls H_2-O_2 titration and volumetric chemisorption are in qualitative agreement giving similar trends for the investigated samples. At low dispersions the H_2-O_2 titration method gives slightly higher values than the volumetric method does, while the opposite is true for higher dispersions. One explanation why the pulse method is lagging behind at the higher H/Pt ratios may be that the adsorption equilibrium state is not reached at increasing Pt dispersions (above H/Pt=0.20). The chemisorption results show a large variation in the measured chemisorption of hydrogen, with 3 samples falling in the range 3-4 nm particle diameter, while the other samples have larger particles. The larger values would indicate that the metal might be located in mesopores formed during the dealumination of the supports, since the particle sizes are too large to be accommodated in supercage cavities.

The reference catalyst demonstrated the metal dispersion previously found by Prestvik [1] (0.65 and 1.44 (tot. ads.) by pulse and volumetric methods respectively).

Factors influencing the metal dispersion

The catalysts were prepared with the goal of making well-dispersed, active hydrogenation catalysts. The conditions chosen were selected to give a high Pt dispersion, both during the metal introduction step (ion exchange) and during the calcination step [59,61]. The large variation in the metal dispersion seen in Table 4.6 and the absent of highly dispersed Pt samples motivated a more extensive investigation on the influence of pretreatment conditions which are known to be crucial in obtaining small metal particles inside the zeolite cavities [54,62,63,65]. The effect of varying the temperature of calcination and reduction on the metal dispersion is shown in Fig. 4.2 and Fig. 4.3 respectively. The samples were prepared without adding the competing ion during the ion-exchange (NH_4 : Pt=0). The H/Pt ratios displayed are those obtained by the H_2-O_2 titration.

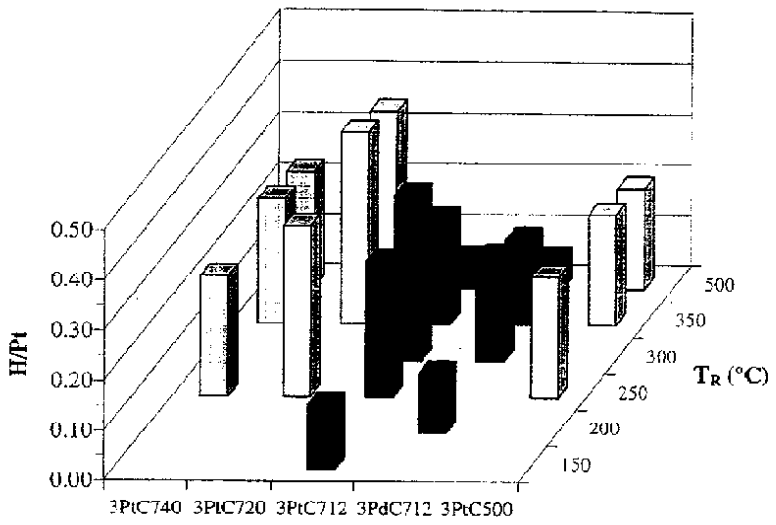

Figure 4.2: The H/Pt-ratio of Pt/HY reduced at various temperatures after calcination at 400°C. The H/Pt-ratios is measured by pulse titration.

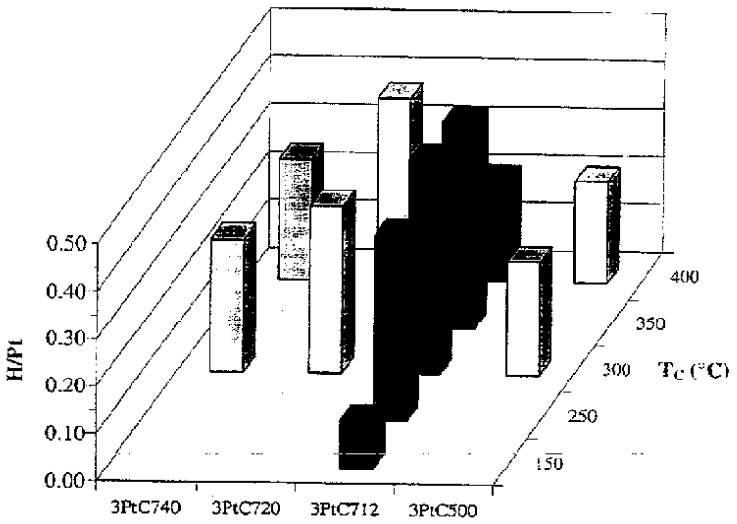

Figure 4.3: The H/Pt-ratio of Pt/HY calcined at various temperatures and reduced at 350°C. The H/Pt-ratios is measured by pulse titration.

It seems from studying Fig. 4.2 and 4.3 that three of the samples (3PtC500, 3PtC720, 3PtC740) are little affected in the range of pretreatment temperatures applied here. It is however differences in the H/Pt ratios between the zeolite supports with the dispersion increasing in the order 3PtC500< 3PtC740< 3PtC720. 3PtC712 on the other hand shows a vulcano-type response with distinct drops in the hydrogen adsorption capacity at low and high temperature of calcination and reduction. The data suggest an optimum pretreatment consisting of calcination at 325°C and reduction at 300°C for this catalyst sample.

The main purpose of the calcination step is to strip the percusor metal-complex of its ligands and place the metal-ions in favorable positions (supercages) for the following reduction. The temperature plays an important role in controlling the undesirable metal-ion migration from supercages towards the smaller sodalite cages (see Chap. 2.2.2). The fact that the measured H/Pt ratios are nearly unaffected by the varying pretreatment temperatures for three of the samples indicate that the location and size of the metal particles are altered only to a limited extent. This lead to the assumption that the Pt ions are located in the supercages and mesopores of the zeolite and that the reduction sequence proposed by Homeyer and Sachtler [63] (Chap. 2.2.2) is applicable. The H/Pt ratios indicate particles too large to be fitted in the zeolite supercages and point to the mesopores as a more plausible location. Although the measured mesopore volume is rather small (Table 4.4) the small amount of platinum applied in these catalysts can be accomodated here. This fact does not exclude the possibility of some platinum being located in supercages. The observed differences in H/Pt ratios between the samples may reflect the differences in mesopore size and the distribution of metal particles between mesopores and supercages.

In the case of the 3PdC712 and 3PtC712 samples it also seems as if the metal ions are located in the supercages and mesopores up to a calcination temperature of 300°C and 350°C respectively. The low H/Pt ratio for the samples calcined below 200°C is a result of incomplete decomposition of the ammine complex, the remainder being reduced by H_2 releasing ammonia which neutralizes acid sites, thus preventing these sites from becoming chemical anchors, subsequently giving a poorer and more agglomerated catalyst [59,140]. The formation of an unstable, neutral, and mobile species, e.g. $Pt(NH_3)_2H_2$ take place allowing agglomerization to occur [54]. Figure 4.3 suggests that a calcination temperature of 400°C

initiate migration of metal ions to the sodalite cages where the highly charged bare M^{2+} ions establish a more stable energetic configuration [62,70]. At 400°C this process is not expected to be complete and so metal ions co-exist both in supercages and sodalite cages. The increased stability of the M^{2+} ions together with the fact that the kinetic diameter of the H_2 molecule (2.9 Å) is larger than that of the O_6 rings (2.2 Å), necessitates a higher reduction temperature than for the M^{2+} ions remaining in the supercages [62]. In Figure 4.2 this is observed as an increase in the H/Pt ratio for increasing T_R up to 300°C reflecting the increasing degree of reduced Pt atoms leaving the sodalite cavities and becoming available for chemisorption. A further increase in the reduction temperature is accompanied by a significant drop in the dispersion. The reduced metal atoms combine to particles and there is a thermodynamic driving force for further growth of these particles and heating in reducing atmosphere therefore result in loss of dispersion [65,141]. This phenomenon is most pronounced for low metal loadings in Pt/Y catalysts [142]. In the low metal load samples small primary particles migrate rapidly and move through the channels over large distances. Finally they will coalesce and form particles of much larger dimensions than the supercages possible on the outer surface.

Why the ion migration from supercages to sodalite cages commence at a lower temperature of calcination for the samples supported on CBV712 is most probably found in the structural properties of the zeolite framework.

TEM

To be able to say anything more about the metal particle size and also the size distribution transmission electron microscopy was performed on a selection of the Pt/Y catalysts. The results for samples pretreated at varios conditions are given in Table 4.7 together with the chemisorption results.

Table 4.7: Results from TEM in comparison with chemisorption measurements on 3PtC712.

sample	T_C (°C)	T_R (°C)	H:Pt pulse	H:Pt vol.	D_p (Å)[1]	TEM
3PtC712	250	350	0.08	0.25	120	Small particles, well-distrib. (10-25 Å).
3PtC712	325	350	0.38	1.2	26	Large particle distrib. From 10-25 Å, up to 200-400 Å.
3PtC712	400	500	0.05	0.65	150	Large particles/ansembles, 100-500 Å.

[1]: metal particle size from pulse measurements assuming spherical particles.

One of the 3PtC712 samples (T_C=400°C, T_R=500°C) show excellent agreement between the metal particle sizes estimated from chemisorption and TEM measurements. The particle size distribution observed for the sample calcined at 325°C and reduced at 350°C is indicative of some small particles located in supercages and larger ones residing in mesopores.

For the remaining sample calcined at 250°C and reduced at 350°C there is a large discrepancy between the metal particle size expected from the chemisorption measurements and the ones observed by TEM. The TEM observation indicates that calcination at 250°C is high enough to decompose the complex completely, with the following reduction at 350°C leading a to well dispersed catalyst. The particle size is in the range 10-25 Å, and at least 10 Å particles fit in the supercages of Y zeolite. The discrepancy between chemisorption measurements and TEM for this sample is understandable if the stoichiometry of adsorption is less than unity, as previously found for small Pt particles [118]. It may also come as a result of the lack of a representative selection of the specimen portrayed in the TEM micrographs. Large particles are few in number and thus may not be observed.

4.1.4 TOLUENE HYDROGENATION

An investigation on the feasibility of this model reaction for estimating the available metal area.

Measurement of the catalyst activity at initial and steady-state conditions specific for hydrogenation of toluene confirms the structure insensitivity of this model reaction. The deviating behavior at steady-state of the most acidic catalyst samples is caused by coke formation resulting in possible diffusional limitations situated in the zeolite interior.

The reaction study was performed under the standard conditions listed in Table 3.1. The reactor was run in the integral mode with high conversion of toluene. At these conditions the selectivity at steady-state for the hydrogenated product (methylcyclohexane) was in excess of 90% for all catalyst samples tested. Secondary products in the form of ethylcyclopentane and dimethylcyclopentanes from the isomerization of methylcyclohexan [143] accounted for the rest. The catalyst samples used and their given pretreatments are listed in Table 4.3 (the $3Pt/Al_2O_3$ sample was not used). The conversion of toluene into methylcyclohexane, i.e. the yield of methylcyclohexane versus time on stream is given in Fig. 4.4.

The deactivation is most pronounced for the Y-zeolites with the lowest Si/Al ratios (highest number of acid sites). In the case of the low acidity zeolite samples and the alumina catalyst very little deactivation occur at these reaction conditions. This is not surprising since the formation of carbonaceous compounds occur through a bifunctional mechanism [144]. By assuming that the reaction mechanism from benzene hydrogenation at atmospheric pressure [144] is valid also for toluene hydrogenation at high pressure, "coke" is formed from reactions between toluene and methylcyclohexane followed by isomerization of the methylcyclohexane unit. The decrease in the conversion is also reflected in the product distribution. The samples with little or no deactivation has only hydrogenation activity. The selectivity to cyclopentanes is, after 30 min on stream, 0.1 wt% over Pt/Al_2O_3 and 4 wt% over Pt/CBV780. The value after 5 hours on stream is 0.1 and 2 wt%, respectively. Over Pt/CBV500, the selectivity to cyclopentanes, which are the only isomerized products, is 31 wt% after 30 min. After 5 hours

on stream, the value is only 4 wt%. The values over Pt/CBV 712 is 15 wt% and 7 wt% respectively.

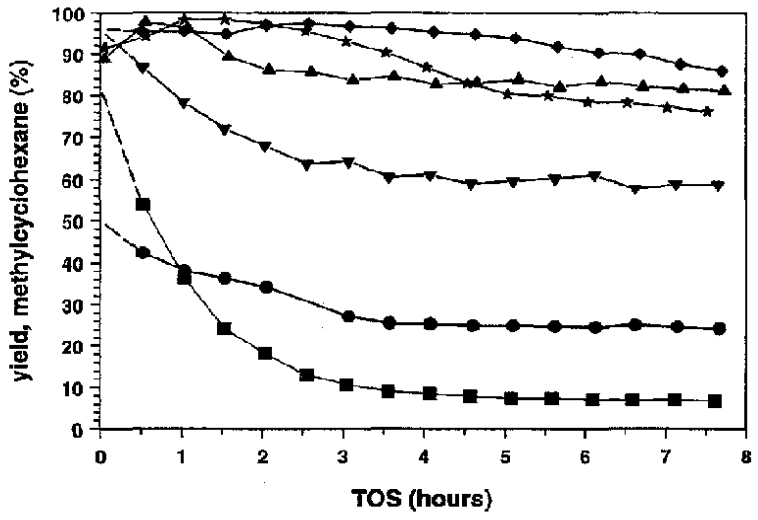

Figure 4.4. The yield of methylcyclohexane (wt%) with time on stream at 240°C. (■) PtCBV500, (●) PtCBV712, (▲) PtCBV720, (▼) PtCBV740, (★) PtCBV780, (◆) Pt/Al_2O_3.

In order to examine the effect of the different pretreatment temperatures on the hydrogenation activity of the metal, the Pt/CBV712 sample was exposed to varying temperatures of calcination and reduction. The yield of methylcyclohexane at 240°C and 30 barg total pressure versus time on stream is given in Fig. 4.5.

The extent of deactivation is similar for 3 of the 4 samples, and they end up at the same steady-state conversion. The selectivity to isomers is initially around 10 wt%. The H/Pt-ratio of these samples varies from 0.05 to 0.38 and 0.25 to 1.2 measured by pulse-titration or volumetric chemisorption, respectively. The steady-state conversion is similar on all samples, indicating that the deactivating effect of coke is the same on these samples, and thus only influenced by the zeolite acidity.

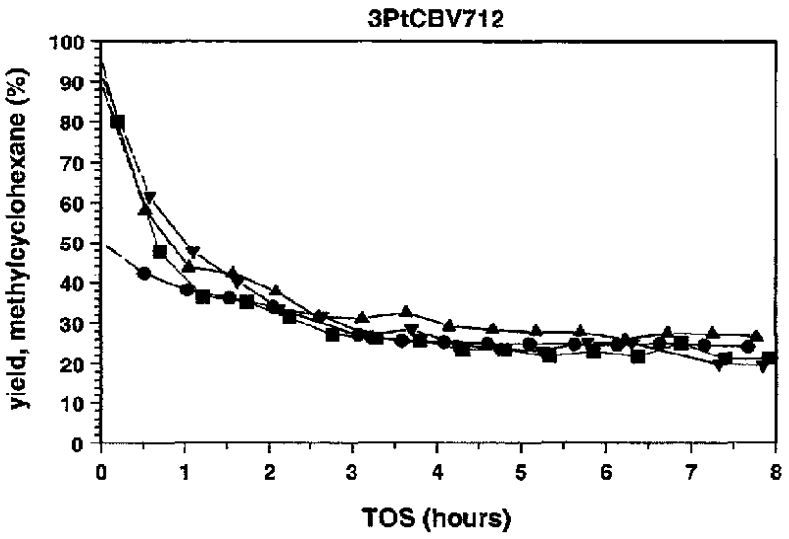

Figure 4.5. The yield of methylcyclohexane (wt%) with time on stream at 240°C. Pretreatment conditions: (▲)T_C=250°C and T_R=350°C, (■) T_C=325°C and T_R=350°C, (▼)T_C=400°C and T_R=350°C, (●)T_C=400°C and T_R=500°C.

If toluene hydrogenation is a structure insensitive reaction, the activity should be proportional to the Pt dispersion. The initial conversion of toluene into methylcyclohexane may be obtained by extrapolating the yield curves back to zero time on stream, as indicated by the dashed lines in Fig. 4.4 and Fig. 4.5. The specific activities were calculated using the integrated form of the plug-flow equation [145] utilizing the rate expression derived in Chap. 4.4.1. Considering the observed temperature increase (5-10°C) from the exothermic reaction, the true values for the initial conversion most probably lies somewhat lower than the extrapolated ones. Also, the initial hydrogenation activity might be influenced by bifunctional reactions involving the acid sites, and will in such a case not be representative of pure metal catalyzed hydrogenation. If the steady-state conversion is used instead, the hydrogenation activity might be too low, since formation of coke may hinder or block the access of toluene to some of the Pt particles, and also reduce the diffusion rate of toluene inside the Y zeolite. The third possibility is to extrapolate the quasi-linear part of the conversion-curve back to

zero, and use this value as the initial hydrogenation activity. As seen in Fig. 4.4 and 4.5, the hydrogenation activities found by alternative 2 and 3 will be almost the same, so the third alternative is excluded. The estimated activities is compared with the the H/Pt-ratio from the volumetric chemisorption measurements in Fig. 4.6a-b.

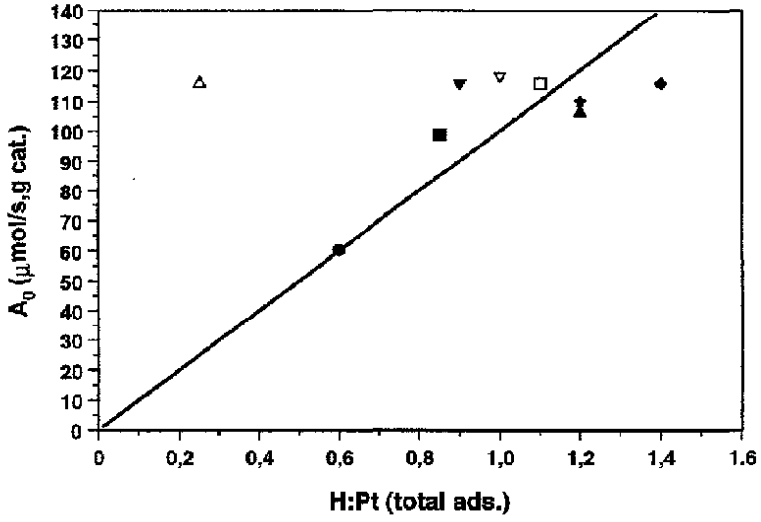

Fig. 4.6a. Initial hydrogenation activity based on extra-polation of the yield versus time-on-stream curve.

As seen in Fig. 4.6a, there is a reasonable good fit between the extrapolated initial hydrogenation activities and the H/Pt-ratio (measured in the Micromeritics ASAP 2010 unit). The value for PtCBV712 pretreated at 250°C/350°C (Δ) does not fit on the line. The high activity and low H/Pt-ratio can be explained if the small Pt particles, as observed by TEM, has an adsorption stoichiometry less than 1 [118]. Most of the zeolite supported samples show comparable dispersion and activity to the well-characterised Pt/Al_2O_3 reference catalyst (CK303). If the values found for PtCBV712 pretreated at 400°C/ 500°C (●) are omitted instead of the one at 250°C/350°C (Δ), a straight horizontal line would fit the rest of the data

points. In this case, the hydrogenation activity is independent of the Pt dispersion, which strongly suggests diffusional limitations in the zeolite pores. However, in such a case the activity of the Pt/Al_2O_3 should be significantly higher, because diffusional limitations in the macropores of this catalyst most likely are absent. Also, the apparent activation energies calculated from the steady-state activity in the temperature range 240°C to 160°C over the catalysts with high H/Pt (PtCBV 780 and Pt/Al_2O_3) are in the range 73-78 kJ/mol (Table 4.9). The deactivation of these catalysts at 240°C is rather low (Fig. 4.4), so the initial activity is approx. the same as the steady-state activity. Thus, the value of the apparent activation energy indicates the absence of diffusional limitations.

The hydrogenation activity at steady-state is compared with the H/Pt-ratio in Fig. 4.6b, and a good correlation is found only for the samples which show no deactivation. Pt/CBV500 pretreated at 400°C/500°C as well as the Pt/CBV712 pretreated at various temperatures has a very low and comparable hydrogenation activity. This can be explained by the formation of coke causing limitations or blocking of metal particles and inducing diffusional limitations.

From the initial hydrogenation activities, the turnover frequency is in the range between 5 and 7 s^{-1} at 240 °C and 30 bars. Reaction orders of zero and 1.5 for toluene and H_2 was used in the calculations, and these were determined over the PtCBV712 sample at 240°C and steady-state (Chap. 4.3.1). The WHSV was adjusted so that the conversion was kept below 15 %. Even though the conversion was relatively low, formation of coke might take place, resulting in falsified kinetics. Therefore, the given activities might be systematically too low over all the samples, but this error will not change the correlation to a straight line.The activity was measured after a TOS of 8 hours under steady-state conditions.

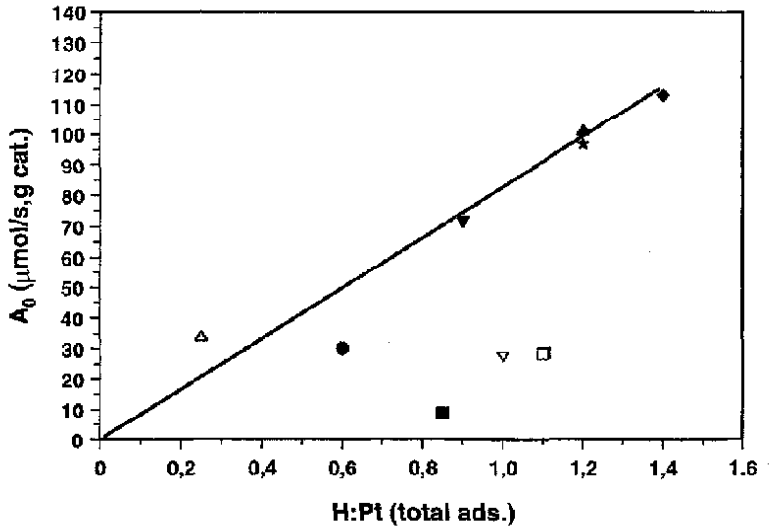

Fig. 4.6b. Hydrogenation activity based on the steady-state yield.

Figures 4.6. Hydrogenation activity calculated from the yield of methyl-cyclohexane at 240°C versus the H/Pt-ratio from volumetric chemisorption. (■): PtCBV500, T_C=400°C, T_R=500°C, (●): PtCBV712, T_C=400°C, T_R=500°C, (Δ): PtCBV712, T_C=250°C, T_R=350°C, (❑): PtCBV712, T_C=325°C, T_R=350°C, (∇):PtCBV712, T_C=400°C, T_R=350°C, (▲): PtCBV720, T_C=400°C, T_R=500°C, (▼): PtCBV740, T_C=400°C, T_R=500°C, (★) PtCBV780, T_C=400°C, T_R=500°C, (◆): Pt/Al_2O_3, T_C=450°C, T_R=450°C.

4.2 TRANSPORT LIMITATIONS

4.2.1 INTRAREACTOR GRADIENTS

A discussion on ways to ensure ideality of flow pattern and isothermality in the experimental reactor.

The common criteria for ensuring plug flow operation of the reactor are fulfilled at the reaction conditions used in this study. Remedies for minimizing the influence of radial temperature gradients like small reactor diameter, and diluting of the catalyst bed with inert particles were also applied in this study.

Ideality of flow pattern and isothermality are two of the most important requirements for simplifying the analysis of data obtained in a laboratory reactor. In a fixed bed catalytic reactor the assumption of plug flow, meaning that all reactants reside in the reactor a definite time determined by the flow rate and bed volume is used in the evalution of kinetic data. In experimental reactors with shallow beds this is not automatically the case.

Axial gradients

In the axial direction in the reactor the existence of concentration and temperature gradients are inevitable by virtue of the conversion of reactants accompanied by heat release/consumption. At high conversion and short beds this can lead to diviations from plug flow due to axial eddy dispersion, also called backmixing [146]. An effective remedy for avoiding this phenomenom is increasing the bed length and/or reducing the catalyst particle size. The calculations performed in Appendix III show that for the conditions applied ($L/d_p \sim 200$) the effect of axial dispersion is negligible for conversions below 80% (1. order reaction). From eq. AIII.3 One notice that a minimum bed length of zero is required for zero-order reactions, which are not affected by axial dispersion. One also notice the small Reynold numbers (Re_p) often common for laboratorty reactors [147]. Small particles reduces channeling resulting in non-uniform velocity profiles. Because the bed voidage is higher at the reactor wall a $d_r/d_p > 15$ is recomended for maintaining a flat profile [148]. In this study the $d_r/d_p \sim 90$, fulfilling this criteria.

Radial gradients

Due to the low flow rates in laboratory systems the importance of the various heat and mass transfer gradients decreases in the following way [147]:

-Intrareactor (radial) temperature gradients

-Interphase temperature gradients

-Intraparticle concentration gradients

-Interphase concentrations gradients

-Intraparticle temperature gradients

To minimize radial temperature gradients occuring because of the low thermal conductivity of the catalyst bed and the resistance to heat transfer between the inside wall and the catalyst bed, the following recomondations are made [148]:

-Low reactor diameter

-Low conversion levels

-High flow rates

-Dilute bed with inert particles possesing good heat conductivity (SiC).

Decreasing the reactor diameter increases the heat exchange area as well as the mass flow velocity. Beside improving the thermal conductivity, dilution with inert also reduces the rate per unit volume, and thus minimizes the intrareactor transport problems.

4.2.2 EXTERNAL AND INTERNAL GRADIENTS

Tests for finding kinetically controlled reactions conditions.

Experiments with varying the catalyst particle size showed that at the employed reaction conditions three different regimes of transport limitations exist in the range of catalyst samples and particle sizes studied. A particle size below 125 µm was necessary to avoid external and internal gradients. The location of the metal particles, either on the external surface of the support or homogeneously distributed inside the zeolite framework and the catalyst activity is determining on the degree of transport limitations observed.

To be able to correctly quantify the intrinsic catalyst properties, (catalyst activity, selectivity, deactivation etc.) the absent of transport limitations are a prerequisite. The often important role of the physical processes (mass- and heat-transport) has to be addressed separately.

Transport limitations

An experimental test to verify whether gradients exist is to change the catalyst particle size. Varying the particle size alter the ability of the catalyst to transfer mass or heat to and from the catalyst sites. If a dependency between the reaction rate (conversion) and the particle size is observed, external or internal gradients exist. The effect of changing the catalyst particle size on the conversion of toluene is given in Table 4.8. The reaction conditions are given in Table 3.1.

Table 4.8: Toluene conversion (%) as a function of catalyst particle size.

Catalyst	Particle size (µm)		
	125-500	74-297	74-125
3PtC500		8	
3PtC712	25	23	
3PtC720	70		81
3PtC740	46		61
3PtC780	98	80	77

The toluene conversion was measured at steady-state after a TOS of 8 hours. The catalyst samples shows a set of different behaviors to decreasing particle size: The 3PtC712 sample activity seems to be independent of the particle size, the 3PtC720 and 3PtC740 show an increasing activity, while the 3PtC780 sample exhibit high toluene conversion activity over the largest particles and lower, constant activity for the smaller particles.

If one concider the 3PtC712 sample first the absent of gradients may be explained by the location of the metal particles on the support. In Chap. 4.1.3 it was concluded that this sample hosted large platinum particles located on the outer surface of the zeolite support. The active hydrogenation sites are thus readily accessible and no internal diffusion of reactants/products is necessary for the reaction to proceed.

In the case of the two samples 3PtC720 and 3PtC740 the observed behavoir is a strong indication of the existence of internal diffusion limitations, the rate being proportional to d_p^{-1} [145]. The accessibility of the metal sites inside the zeolite framework varies with location (supercages, mesopores, diffusion distance within the particle) the result being an internal effectiveness factor less than unity for the larger catalyst particles. The presence of extra framework aluminium in the pores of these samples may also obstruct the diffusion of molecules in and out of the zeolite channels.

The 3PtC780 sample showed a high initial activity giving close to complete conversion of toluene over the 125 - 500 μm particle fraction. An high initial activity for this catalyst is not surprising considering the fact that the 3PtC780 sample have a metal loading which is 11% higher than the other samples (Table 4.2). With a metal dispersion comparable to the 3PtC720 and 3PtC740 samples (Table 4.6) the increased metal area gives a more active catalyst. For vapor-phase systems, the greater part of the resistance to heat transfer is often in the boundary layer around the particle, rather than within [149]. Thus the evolved heat from the exothermic hydrogenation reaction sets up a external temperature gradients resulting in a particle temperature higher than the surrounding fluid. The strong dependency of the reaction rate on temperature can cause large deviations from the intrinsic rate. Due to the low flow rates in laboratory reactors, external temperature gradients is an often encountered problem. Decreasing the particle diameter increases the heat transfer coefficient ($h \propto d_p^{-1}$ [145]) and from Table 4.8 it is clear that the external temperature gradient is eliminated using the fraction containing the smallest particles.

4.3 HYDROGENATION OF SULFUR-FREE TOLUENE

4.3.1 KINETICS

Report of kinetic experiments to determine empirical reaction orders.

The kinetic behavior of two of the catalysts were studied at moderate temperature and pressure. Using power rate law kinetics the observed reaction orders are close to 0 in toluene and 1.5 in H_2. The kinetic behavior does not seem to be influenced by the support acidity. The results support a reaction model involving the slow addition of hydrogen atoms to the adsorbed aromatic species as the rate determining step. This model also invoke the presence of hydrogen-deficient aromatic compounds on the metal surface.

The hydrogenation of toluene over different supported metal catalysts has been studied by several groups [19, 17,18,124,150]. These studies were all performed at atmospheric pressure and rather low temperatures (below 210°C). Investigations done at elevated pressures were not found and the need for kinetic information with the purpose of comparing the catalytic activity of the prepared samples motivated a closer examination of the kinetic behavior.

Pressure effects

The kinetic behavior of two of the catalysts were studied at moderate temperature and pressure using power rate law kinetics (eq. 4.1):

$$r = k \times P_{H_2}^{m} \times P_{tol}^{n} \qquad (4.1)$$

The experimental conditions are given in Chap. 3.3.2, Table 3.2. Figure 4.7 shows plots of the data obtained over the 3PtC500 and 3PtC712 catalysts, keeping either the partial pressure of toluene or that of H_2 constant and varying the pressure of the other component, always maintaining differential conditions in the reactor (conversion below 10%).

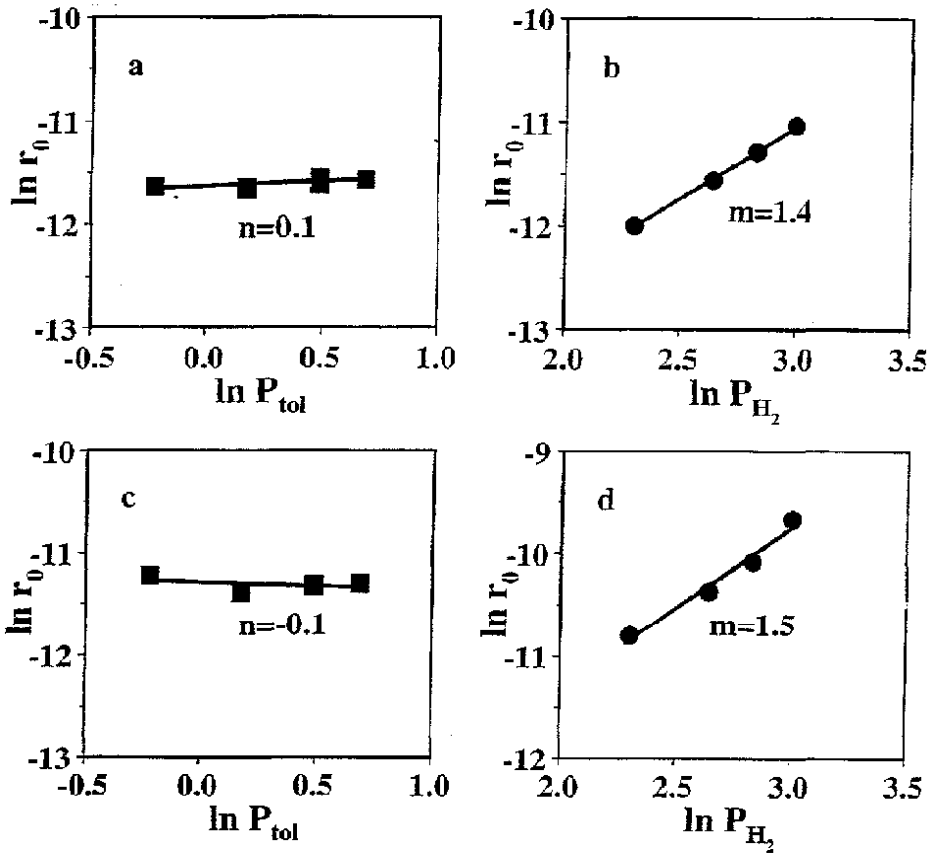

Figure 4.7: Kinetic plots of toluene hydrogenation over 3PtC500 (a,b) and 3PtC712 (c,d). Conditions: P_{tot} = 31 bar, T = 240°C. a,c: order in toluene with constant pressure of hydrogen = 14.7 bar, b,d: order in hydrogen with constant partial pressure of toluene = 1.7 bar.

With sulfur-free toluene feed the observed reaction orders are close to 0 in toluene and 1.5 in H_2. These values can be compared to hydrogenation kinetics reported in literature. Lin and Vannice [19] studied toluene hydrogenation over supported Pt catalysts at total pressure close to atmospheric and found a zero order dependency in toluene, and a pressure dependency in H_2 that varied with temperature. At low temperatures (60°C) they reported an order m<0.7,

wheras at 100°C m was found to be >1. Lindfors *et al.* studied supported Ni catalysts and also found similar results [17,18].

In Figure 4.8 the experimental reaction rates are compared with the rates calculated using the power-law rate model (eq. 4.1) and an acceptable fit is observed.

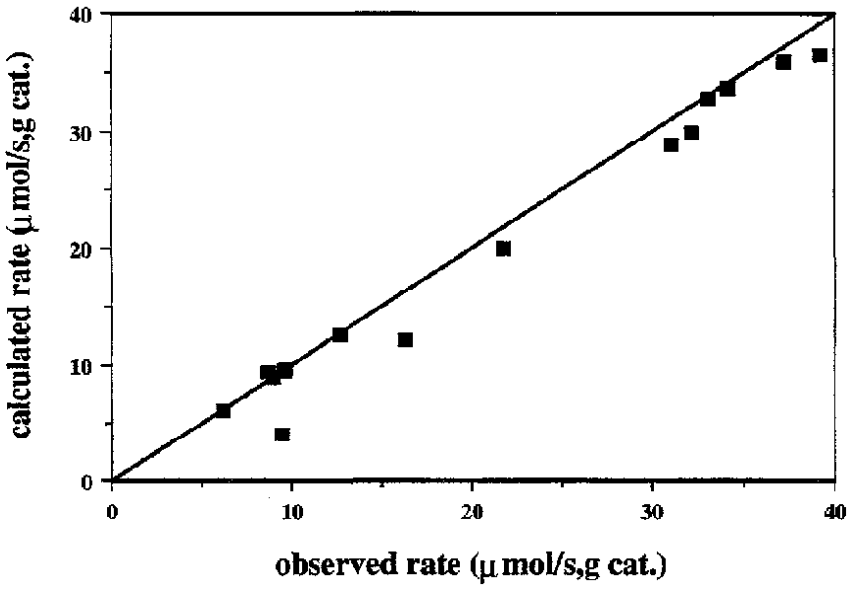

Figure 4.8: Comparison of the experimental and calculated reaction rates according to the power-law rate model.

The close to zero-order dependence in toluene is attributed to the surface coverage of toluene being near saturation. The fact that the two types of support used does not seem to influence the reaction orders suggests that the slow step for hydrogen addition to the ring is similar in both cases. The increase in H_2 reaction order with temperature is explained by a surface dehydrogenation reaction taking place concurrently with hydrogenation to form hydrogen-deficient species (tolyl) on the metal surface [124,151].

4.3.2 TEMPERATURE

Experiments to determine the effect of temperature on catalyst activity.

When the reaction temperature was varied in the range between 160 - 400°C a maximum in the toluene conversion was observed. The temperature of maximum reaction rate varied with catalyst support and reaction pressure. Such behavior is attributed to changes in the number of active sites due to inhibition by carbonaceous species formed under different reaction conditions. Activation energies estimated from the temperature response experiments were in agreement with observations in literature except one low value indicating diffusional limitations for one of the catalyst samples.

Many studies involving the hydrogenation of aromatics over supported metal catalysts have reported similar kinetic behavior, such as a temperature-dependent maximum and changes in reaction orders with temperature [17-19,22-24,152]. To obtain a more comprehensive picture of the kinetic behavior of the catalysts investigated, the effect of temperature on catalyst activity was studied.

Temperature effect

A series of experiments were conducted varying the reaction temperature over a wide range (160 - 400°C). Apart from that the reaction conditions were identical to those given in Table 3.1. Figure 4.9 shows a plot of the toluene conversion as a function of the reaction temperature for three of the catalyst samples. Upon increasing the reaction temperature there is detectable conversion of toluene from about 160°C in the case of the zeolite-supported catalysts. A further increase in temperature leads to increasing toluene conversion up to about 275 - 325°C, where there is a maximum in the conversion. A wide difference in maximum conversion exist at these conditions. The maximum conversion is obtained at the lowest temperature over the alumina-supported sample. Upon a further increase in the temperature to 400°C the conversion drops significantly approaching the equilibrium conversion at these conditions.

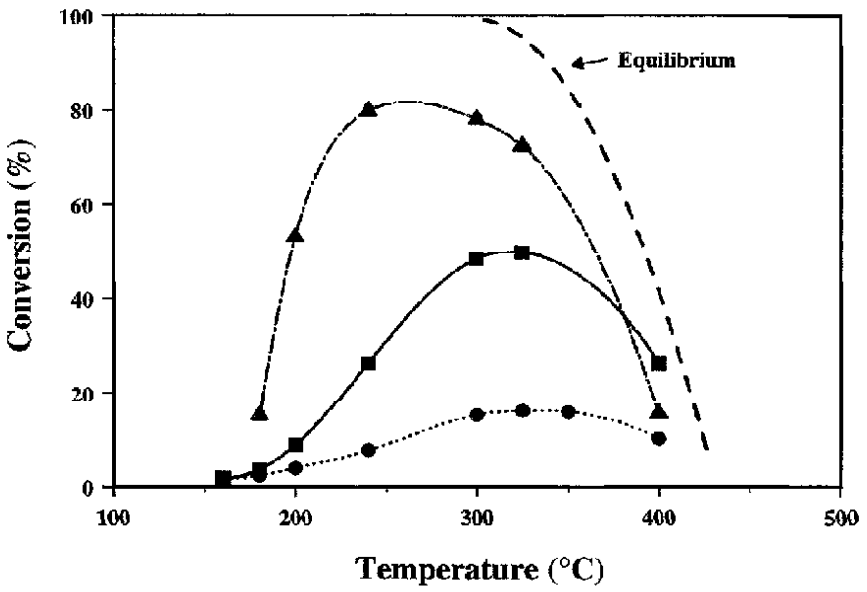

Figure 4.9: Temperature response in toluene hydrogenation over $3Pt/Al_2O_3$ (▲), 3PtC712 (■), and 3PtC500 (●).

This behavior has been observed earlier over supported Ni-catalysts. Van Meerten and Coenen [152] observed this behavior in the hydrogenation of benzene over Ni/SiO_2, and excluded effects such as poisoning, diffusion limitations, and approach to equilibrium as the cause of this effect. In their studies of toluene and ethylbenzene hydrogenation, Salmi *et al.* [17,18,20] attributed such behavior to a reduction in the hydrogen coverage with increasing temperature. The maximum in rate is then a consequence of the combined effects of the temperature dependence of the rate constant k, and the heat of adsorption, leading to a reduction in the coverage of adsorbed reactants with increasing temperature. Vannice *et al.* [19,24,124,151] have performed extensive studies on benzene and toluene hydrogenation over both unsupported and supported noble metal catalysts. They found only one reaction model consistent with all the data. The model invoked the addition of the first H atom to the aromatic ring as the rate-determining step as well as the simultaneous formation of a predominant H-deficient surface species. With acidic supports the model also involved

spilled-over hydrogen and aromatic molecules adsorbed on acidic sites. The results reported here, although obtained at much higher pressures, are comparable, showing very similar trends, and would support such a model.

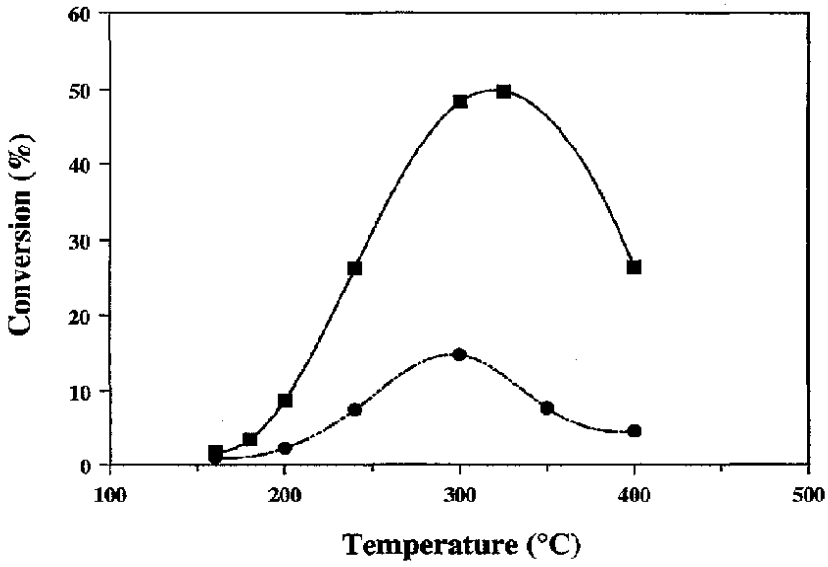

Figure 4.10: Temperature response in toluene hydrogenation over 3PtC712. Conditions: P_{tot} = 31 bar (■), P_{tot} = 11 bar (●).

In Figure 4.10 the effect of pressure on the position in the rate maximum is plotted. A shift in the reaction rate maximum to higher temperatures with increasing pressure is observed. This was also found earlier [152] and may be contributed to less formation of carbonaceous species from the reversible dehydrogenation of adsorbed toluene (endothermic process) which inhibits the reaction rate.

Activation energies

An Arrhenius plot of the toluene hydrogenation over the Pt catalysts is given in Figure 4.11. The activation energies were estimated from the temperature response experiments, taking the data in the region 160 - 240°C. The observed kinetic parameters are summarized in Table 4.9.

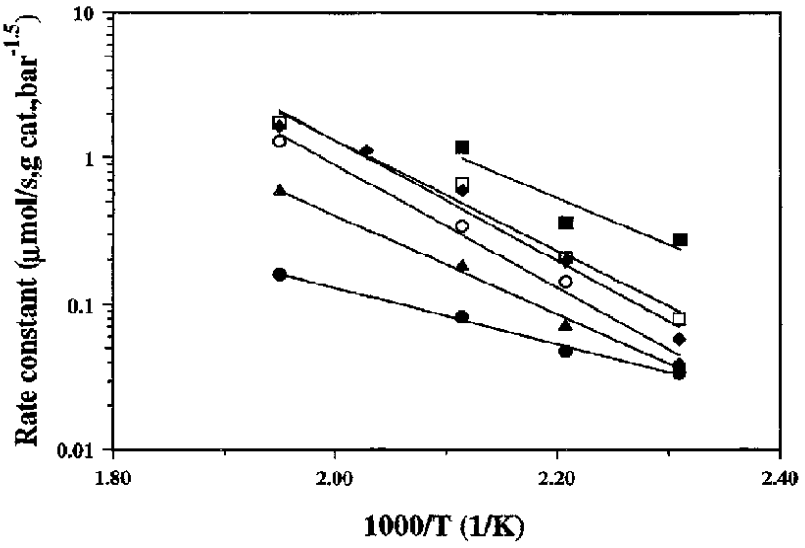

Figure 4.11: Arrhenius plot of toluene hydrogenation over Pt catalysts: $3Pt/Al_2O_3$ (■), 3PtC720 (□), 3PtC780 (◆), 3PtC740 (○), 3PtC712 (▲), and 3PtC500 (●).

Table 4.9: Observed kinetic parameters in toluene hydrogenation over supported Pt catalysts.

Catalyst	E (kJ/mol)	T_{MAX} (°C)	n	m
$3Pt/Al_2O_3$	59	275		
3PtC500	36	325	0,1	1,4
3PtC712	64	325 (300[a])	-0,1	1,5
3PtC720	72			
3PtC740	80			
3PtC780	78			

[a]: Total pressure 11 bars.

The activation energies are in the region from 36 - 80 kJ/mol. Lin and Vannice [19] studied toluene hydrogenation at total pressures close to atmospheric and reported activation energies of 12 ± 2 kcal/mol (50 ± 8 kJ/mol) for toluene hydrogenation over Pt supported on a range of

oxidic supports (Al_2O_3, SiO_2, SiO_2-Al_2O_3, TiO_2). This is in good agreement with the value of 59 kJ/mol observed for the Pt/Al_2O_3. The zeolite-supported catalysts show higher activation energies with the exception of the 3PtC500 sample.

When internal diffusion limitations are present the measured reaction order and activation energy are not the true values. This is referred to as disguised or falsified kinetics [145]. Under such conditions the relationship between the true and apparant values is given by:

$$n_T = 2 \times n_{App} - 1 \tag{4.2}$$

$$E_T = 2 \times E_{App} \tag{4.3}$$

Assuming that the activation energy and the reaction order in toluene determined in Chap. 4.3.1 for 3PtC500 were measured under internal diffusion limitations, the true order in toluene is -0.8 while the true activiation energy becomes 72 kJ/mol. This value of the activation energy is in agreement with the values found for the other zeolite supported catalysts.

4.4 HYDROGENATION OF SULFUR-SPIKED TOLUENE

4.4.1 KINETICS

Report of experiments to determine the effect of adding sulfur to the feed on the kinetic behavior.

The reaction orders with respect to toluene and hydrogen change when trace amounts of sulfur is added to the feed. The order with respect to toluene is more sensitive to the level of sulfur in the feed than the order in hydrogen supporting a reaction model asuming non-competitive adsorption at different sites for toluene and hydrogen. The effect of reaction temperature when using a toluene feed containing sulfur is similar to the sulfur-free feed although a maximum in the conversion cannot be determined with absolute certainty.

The kinetic properties of the socalled sulfur-tolerant noble metal catalysts when used in the presence of sulfur are not well described. Thus studying the effect of sulfur on the reaction kinetics may lead to information on how sulfur species influence the adsorption and bonding of reactants on the catalyst surface.

Pressure effects

To further explore the kinetic behavior of these catalysts again a simplefied kinetic study was conducted, using power rate law kinetics (eq. 4.1). The experimental conditions are given in Chap. 3.3.2, Table 3.2. Figure 4.12 shows plots of the data obtained over the 3PtC712 catalyst. The observed kinetic parameters are summarized in Table 4.10 including data for some other catalysts.

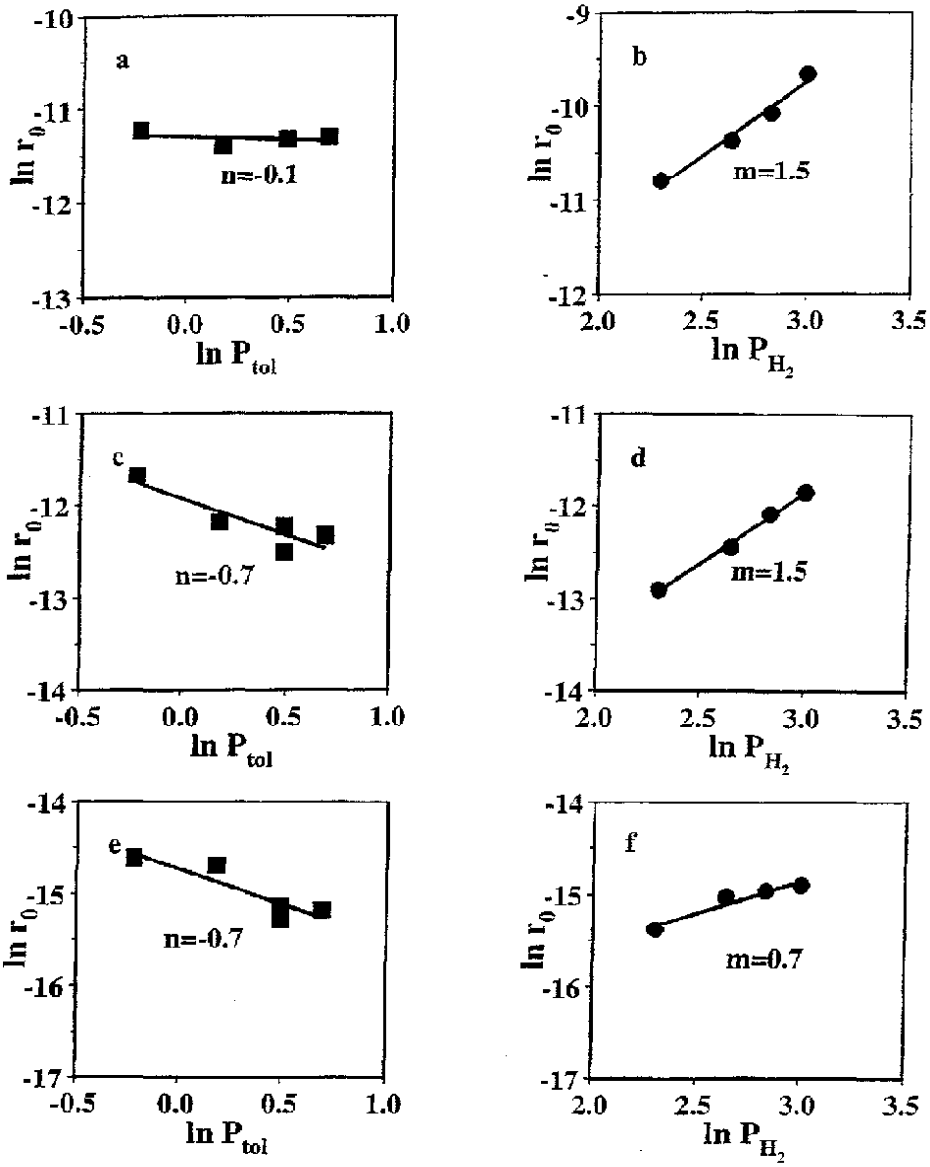

Figure 4.12: Kinetic plots of toluene hydrogenation over 3PtC712. a, b: Sulfur-free toluene, c, d: 20 ppm S, e, f: 200 ppm S. a,c,e: order in toluene with constant partial pressure of hydrogen, b,d,f: order in hydrogen with constant partial pressure of toluene.

With 20 ppm sulfur present in the liquid feed (added as 100 ppm benzothiophene) a slightly negative order in toluene is observed (n = -0.7), whereas the order in H_2 is unchanged relative to sulfur-free toluene (m =1.5). Increasing the sulfur concentration to 200 ppm S leads to no further change in the observed order in toluene (n =-0.7), but reduces the observed order in H_2 to m = 0.7. Although a comprehensive study has not been completed, the summary in Table 4.10 indicates that these trends are independent of the support within the range used.

Table 4.10: Observed kinetic parameters in toluene hydrogenation over supported Pt catalysts. Sulfur added in the form of benzothiophene.

	Sulfur-free feed		20 ppm Sulfur		200 ppm Sulfur	
Catalyst	n	m	n	m	n	m
3PtC500	0,1	1,4				
3PtC712	-0,1	1,5	-0,7	1,5	-0,7	0,7
3PtC780			-0,7	1,5		

In Figure 4.13 the experimental reaction rates with 20 ppm S in the feed are compared with the rates calculated utilizing the power-law rate model (eq. 4.1) and an acceptable fit is observed.

The addition of sulfur to the feed has the effect of partly or completely sulfiding the surface, not only covering the active Pt sites but leading to different adsorption sites with different adsorption properties. From a thermodynamic point of view a complete sulfidation of the Pt to bulk PtS or PtS_2 is not expected at these conditions. A surface sulfide is formed, first on the high coordination sites followed by the development of a 2-dimentional surface sulfide [83].

As discussed in Chap. 2.3.2 compounds of high electronic densities like aromatics bond stronger to sulfur poisoned metals because sulfur acts like an electron-acceptor and decrease the electron density of the unpoisoned metallic surface area [86,101-103]. The decrease in the reaction order in toluene with sulfur addition observed indicates stronger adsorption of the hydrocarbon and thus supports these findings.

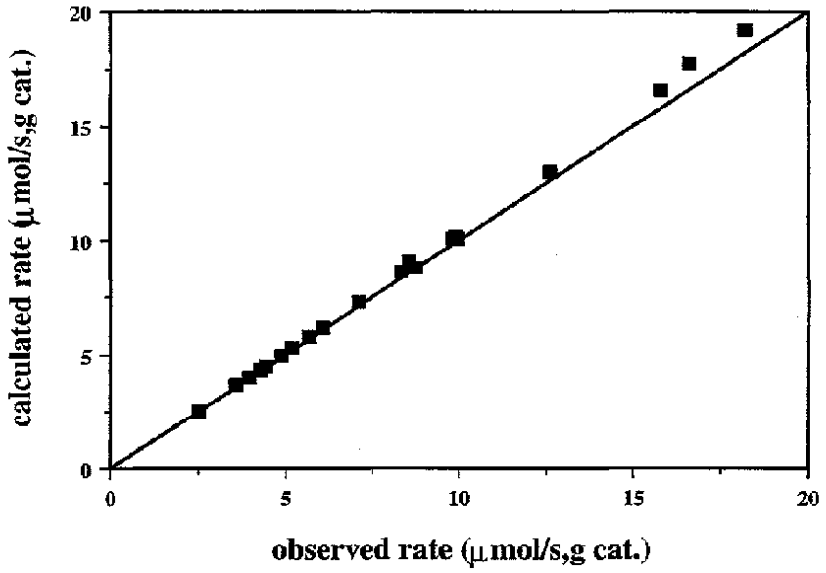

Figure 4.13: Comparison of the experimental and calculated reaction rates according to the power-law rate model.

The fact that the adsorption of hydrogen is unaffected at the lowest level of sulfur contamination is in agreement with the reaction model developed by Vannice *et el.* [124] assuming dissociative, noncompetitive H_2 adsorption on sites different from those adsorbing toluene. According to this model the hydrogen adsorb on three-fold or four-fold hollow sites, while the aromatic molecule adsorbs on an on-top site.

The change to lower reaction order in hydrogen at the highest sulfur level is surprising since inhibition in the hydrogen adsorption due to geometric and electronic effects caused by sulfurization of the metal has been reported (Chap. 2.3.2). On the other hand the hydrogenation reaction involves the rupture of Pt-H bonds resulting in higher hydrogenation activity for weakly adsorbed hydrogen atoms. Studies [24] have indeed shown that a nearly saturated surface containing weakly adsorbed hydrogen is needed before the reaction begins. A decrease in the fraction of this weakly adsorbed hydrogen through a sulfur-induced

modification of the chemisorption site leading to more strongly held hydrogen could explain the observed decrease in the hydrogenation activity caused by sulfur poisoning.

Temperature effects

An experiment was conducted where the reaction temperature was varied over the same range as previously using a toluene feed containing 20 ppm S (100 ppm BT). Figure 4.14 shows a plot of the toluene conversion as a function of the reaction temperature. The plot also contain the data obtained for sulfur-free toluene. Similar trends can be seen but the activity is now much lower, and a reaction temperature of 240°C is necessary to obtain a detectable conversion. At 400°C the conversion is close to the equilibrium. Because of the few data points the existent of a maximum in the conversion caused by the reaction kinetics cannot be determined with certainty.

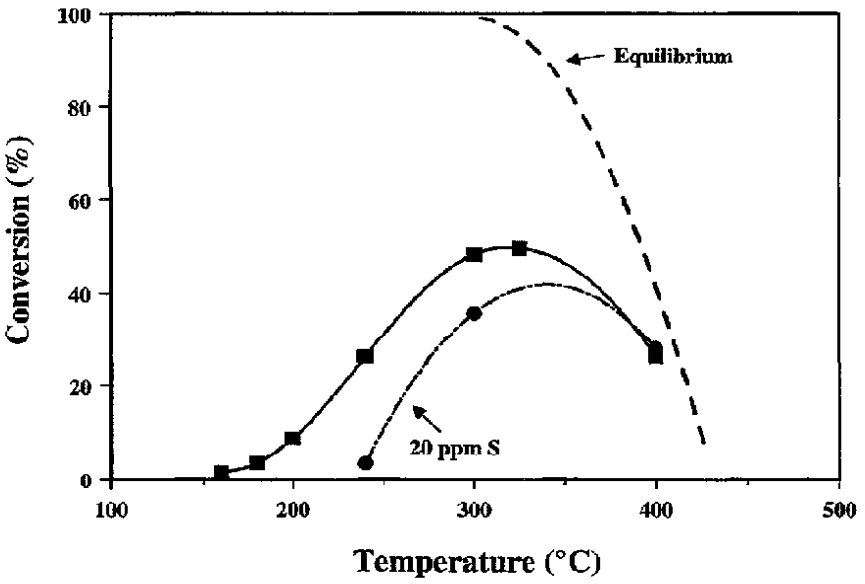

Figure 4.14: Temperature response in toluene hydrogenation over 3PtC712. Reaction conditions as in Table 3.1.

4.4.2 SULFUR-TOLERANCE

Report of experimental studies on the effect of different sulfur-compounds on the catalyst activity.

Platinum supported on Y-zeolites gives considerably more sulfur-tolerant catalysts compared to Al_2O_3 as a support. High Si/Al-ratios give high specific activity due to higher Pt dispersion, while the intrinsic activity (TOF) in the presence of sulfur is highest at low Si/Al-ratio. The sulfur-tolerance seems to be independent of the Si/Al-ratio. There are no clear differences in the effect of the various sulfur-compounds (BT, DBT, and DMDS) on the catalyst activity.

One purpose of this work was to study the sulfur tolerance as a function of Si/Al ratio (acidity) of Y-zeolite supported platinum. The model sulfur compounds chosen were benzothiopene (BT) and dibenzothiophene (DBT) which represents the aromatic thiophenes, the most difficult sulfur compounds to remove from the feed. These compounds would therefore prevail in the feed after a traditional first-stage hydrotreating. Dimethyldisulfide (DMDS) decomposes easily to H_2S under the reducing conditions used and simulates the dissociative adsorption all sulfur compounds undergoes to a certain extent depending on the reaction conditions.

Effect of catalyst support

The experimental conditions and procedures used for the hydrogenation of sulfur-spiked toluene are given in Chap. 3.3.3. Two typical experimental runs are visualized in Figures 4.15 and 4.16. After the initial lining out of the system in sulfur-free toluene a switch to sulfur-spiked (benzothiophene) liquid feed is made and an almost instant drop in the toluene conversion is observed before a new steady-state conversion is reached. In the case of the Pt/Al_2O_3 catalyst (Figure 4.15) the addition of 92 ppmwt BT (approx. 20 ppm S) leads to an almost inactive catalyst, and no further addition of sulfur was attempted. For the zeolite supported catalyst (Figure 4.16) a step-wise increase up to 943 ppmwt BT (approx. 200 ppm S) could be made while still maintaining a detectable activity. When a switch back to sulfur-free toluene is made, some regeneration of the catalytic activity occurs. The activity gain is

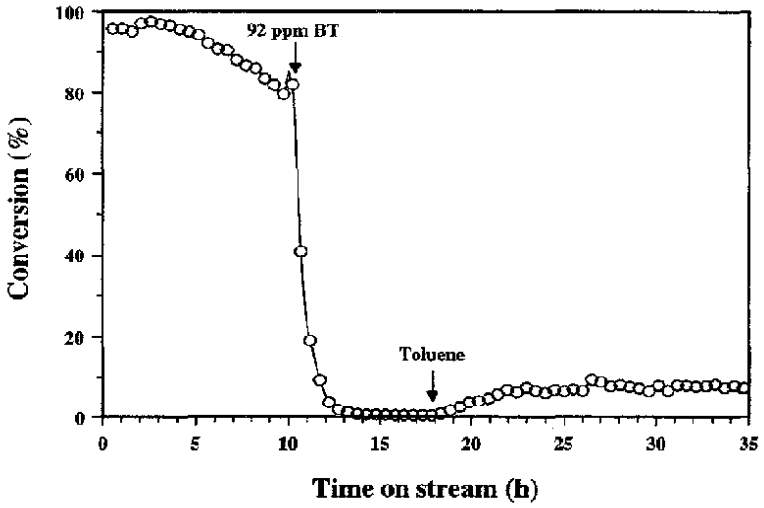

Figure 4.15: Toluene hydrogenation over $3Pt/Al_2O_3$. The effect of sulfur-spiked feed Bezothiophene) on the conversion.

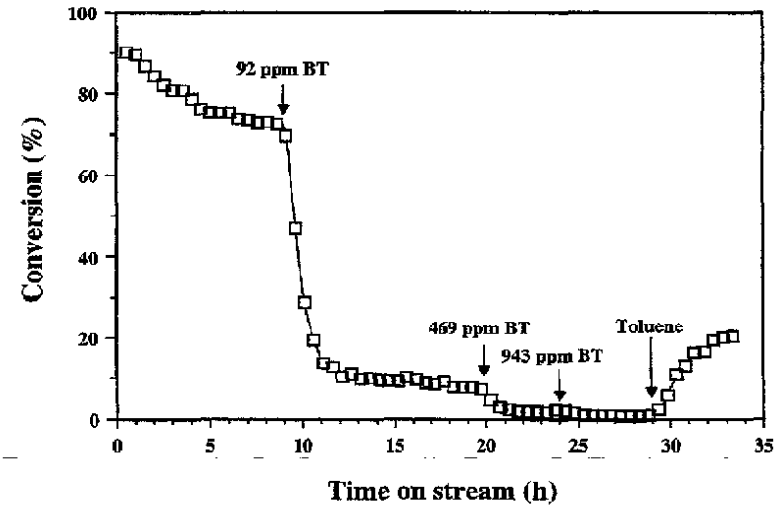

Figure 4.16: Toluene hydrogenation over 3PtC720. The effect of sulfur-spiked feed (Benzothiophene) on the conversion.

most pronounced for the zeolite supported sample. A permanent deactivation caused by the sulfur poisoning seems to be the result, at least with the experimental setup and within the time scale used in this work. Sulfur analysis of the liquid product showed a conversion of the sulfur compounds in excess of 90% in all cases. Although no complete mass-balance on sulfur was established, one can imagine a distribution between the gas phase (H_2S), the liquid product and the catalyst surface.

As described in Chap.2.2.2 there are many reports of the enhanced sulfur tolerance of zeolite supported noble metals [53-56]. These properties are believed to originate from the intimate interaction of the metal with protons in the zeolite cavities. The higher degree of reactivation of the zeolite supported catalyst when exposed to sulfur-free toluene after sulfur poisoning, is an indication of a less strong bonding between sulfur and platinum explained in terms of electron-deficient Pt particles [54,55].

Specific activity

Experimental runs identical to the ones described in the preceding paragraphs were performed on zeolite supported catalysts with different Si/Al ratios (acidity) exposing them to the different sulfur compounds at various concentration levels. The specific activity of the catalysts is reported in Table 4.11, Table 4.12, and Table 4.13. Turnover frequencies based on dispersion measurements of unpoisoned samples are also reported.

Table 4.11: Specific activity and turnover frequency (TOF) for hydrogenation of toluene spiked with benzothiophene.

	sulfur-free toluene		92 ppmwt BT		469 ppmwt BT		943 ppmwt BT	
Catalyst	r_0[a]	TOF[b]	r_0	TOF	r_0	TOF	r_0	TOF
PtC500	9,01	1,6	3,65	0,7	0,79	0,1	0,24	0,04
PtC712	27,59	25,6	4,08	4,5	0,87	1,0	0,34	0,4
PtC720	97,97	18,8	8,71	1,5	3,25	0,6	1,67	0,3
PtC740	73,19	22,8	7,66	2,0	1,67	0,4	0,36	0,1
PtC780	92,90	21,1	9,82	2,2	2,46	0,6	0,54	0,1
Pt/Al_2O_3	97,58	12,4	0,54	0,07	-	-	-	-

[a]: specific activity [µmol/s,g cat.], [b]: turnover frequency [s^{-1}] based on H_2-O_2 titration, pulse mode of fresh unpoisoned samples.

The specific activities for hydrogenation of pure toluene were calculated using the integrated form of the plug-flow equation [145] utilizing the rate expression derived in Chap. 4.4.1. When sulfur was added to the liquid feed the toluene conversion was low (below 10%) and differential conditions were assumed.

Table 4.12: Specific activity and turnover frequency (TOF) for hydrogenation of toluene spiked with dimethyldisulfide.

	sulfur-free toluene		17 ppmwt DMDS		144 ppmwt DMDS		317 ppmwt DMDS	
Catalyst	r_0[a]	TOF[b]	r_0	TOF	r_0	TOF	r_0	TOF
PtC500	9,01	1,6	4,34	0,8	0,99	0,2	0,37	0,07
PtC712	27,59	25,6	7,72	8,6	1,25	1,4	0,50	0,6
PtC720	97,97	18,8	10,11	1,7	3,01	0,5	1,25	0,2
PtC740	73,19	22,8	9,20	2,4	1,71	0,4	0,63	0,2
PtC780	92,90	21,1	15,98	3,6	4,25	0,9	2,17	0,5

[a]: specific activity [µmol/s,g cat.], [b]: turnover frequency [s^{-1}] based on H_2-O_2 titration, pulse mode of fresh unpoisoned samples.

Table 4.13: Specific activity and turnover frequency (TOF) for hydrogenation of toluene spiked with dibenzothiophene.

	sulfur-free toluene		133 ppmwt DBT		663 ppmwt DBT		1326 ppmwt DBT	
Catalyst	r_0[a]	TOF[b]	r_0	TOF	r_0	TOF	r_0	TOF
PtC712	27,59	25,6	3,71	4,1	0,92	1,0	0,41	0,5
PtC780	92,90	21,1	9,07	2,1	1,56	0,4	0,39	0,1

[a]: specific activity [µmol/s,g cat.], [b]: turnover frequency [s^{-1}] based on H_2-O_2 titration, pulse mode of fresh unpoisoned samples.

From the preceding tables it is clear that the specific activity for toluene hydrogenation is highest at high Si/Al ratios. This is also true when sulfur is present in the feed. From Table 4.6 it is evident that they are very active catalysts due to their higher Pt dispersion. The increased metal surface area can accommodate the adsorbed sulfur and still maintain a high number of unpoisoned sites active for hydrogenation.

Intrinsic activity (TOF)

In order to access how the sites active in toluene hydrogenation are affected by sulfur induced deactivation, the rates referred to the number of active sites were calculated. Such a rate expresses the rate at which the catalytic cycle turns over and is defined as the turnover frequency [152].

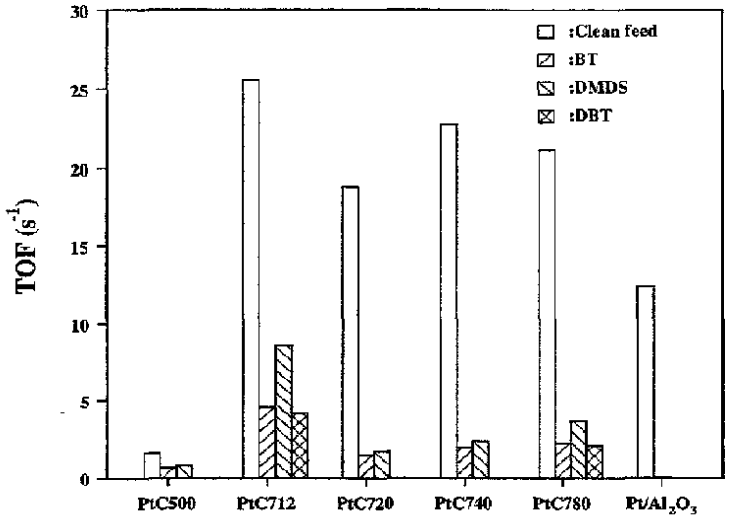

Figure 4.17: TOF of the catalyst samples for the hydrogenation of sulfur-free toluene and toluene spiked with different sulfur compounds to the amount of approx. 20 ppm sulfur.

The turnover frequencies tabulated in Table 4.11 through 4.13 are shown in a graphical view in Figures 4.17, 4.18, and 4.19.

Four of the zeolite supported catalysts possess a fairly constant TOF for the hydrogenation of sulfur-free toluene (Figure 4.17). The true rate for the PtC500 catalyst is limited by mass transfer as discussed before. The effect of adding 20 ppm sulfur to the feed can be seen as a marked fall in the TOF for all the catalysts samples. The rest activity falls in the range between 8 - 18% of initial activity for the zeolite supported catalysts. In the case of the sulfur poisoned alumina supported catalyst the activity is only 0.5% of the initial (hardly visible on the graph).

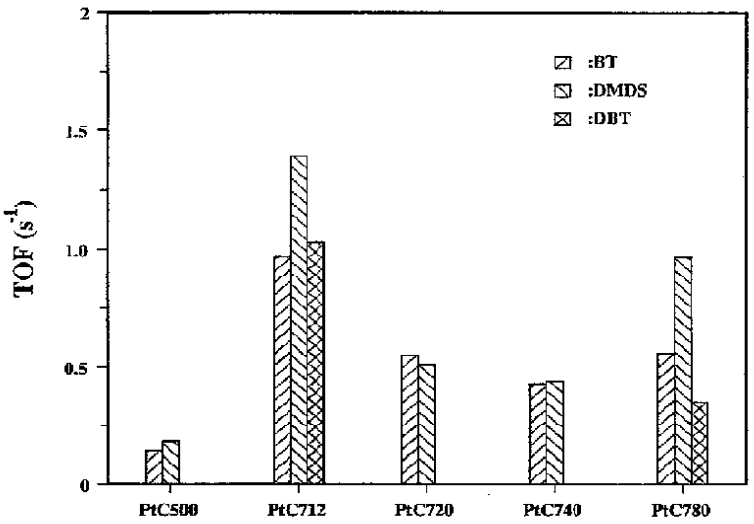

Figure 4.18: TOF of the catalyst samples for the hydrogenation of toluene spiked with different sulfur compounds to the amount of approx. 100 ppm sulfur.

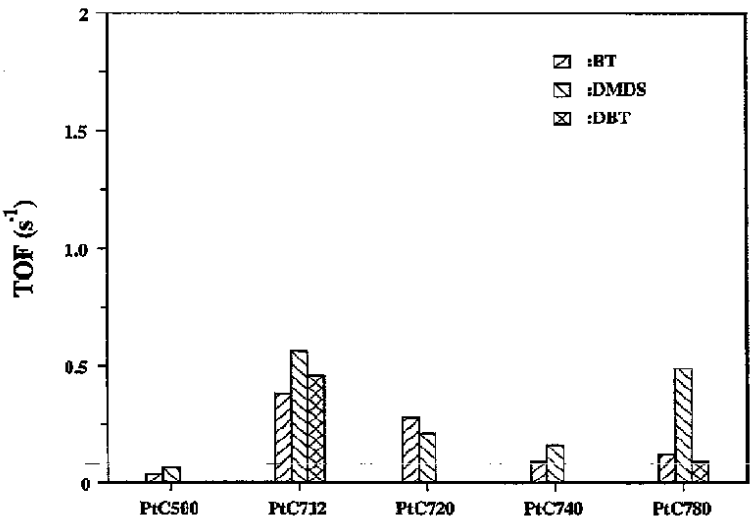

Figure 4.19: TOF of the catalyst samples for the hydrogenation of toluene spiked with different sulfur compounds to the amount of approx. 200 ppm sulfur.

Decreasing values of TOF most probably do not imply a change in the activity of the individual sites. Leclerq and Boudart [153] studied the hydrogenation of cyclohexen over Pt/γ-Al_2O_3 poisoned with sulfur (sulfates on the support). They found that values of TOF calculated by counting surface platinum atoms not covered with sulfur by means of hydrogen adsorption remains constant. The decrease in TOF values therefore reflects the reduced number of active, unpoisoned hydrogenation sites.

A further increase in the feed sulfur concentration leads to a subsequent decrease in the calculated TOF values as depicted in Figures 4.18 and 4.19. With 100 ppm sulfur the TOF values are in the range between 2 - 5% of the TOF for hydrogenation of sulfur-free toluene, decreasing to between 0.5 - 2% at the highest sulfur level. The fact that the most active zeolite supported catalyst posses a TOF five times that of Pt/Al_2O_3 at a sulfur level one order of magnitude greater illustrates the superiour sulfur tolerance of these catalysts.

Assuming that the turnover frequency is constant for the unpoisoned hydrogenation sites the percentage of initial activity (sulfur tolerance) indicated above reflects the degree of surface metal sulfide formation.

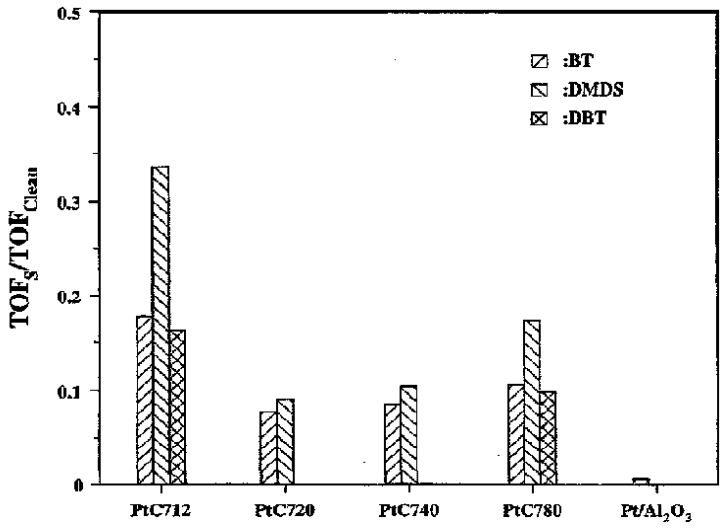

Figure 4.20: Sulfur tolerance of the catalysts with approx. 20 ppm sulfur in the feed.

It must be mentioned that although traditional metalsulfide hydrotreating catalysts are known to show poor hydrogenation activity [5,11,34-36], the platinumsulfide may also to some extent contribute to the overall hydrogenation activity. If the sulfur tolerance is defined, as above, as the ratio TOF_S / TOF_{Clean} where TOF_S denotes the activity on sulfur spiked feed, and TOF_{Clean} stands for the intrinsic activity on sulfur-free toluene a plot like the ones in Figures 4.20 and 4.21 can be made.

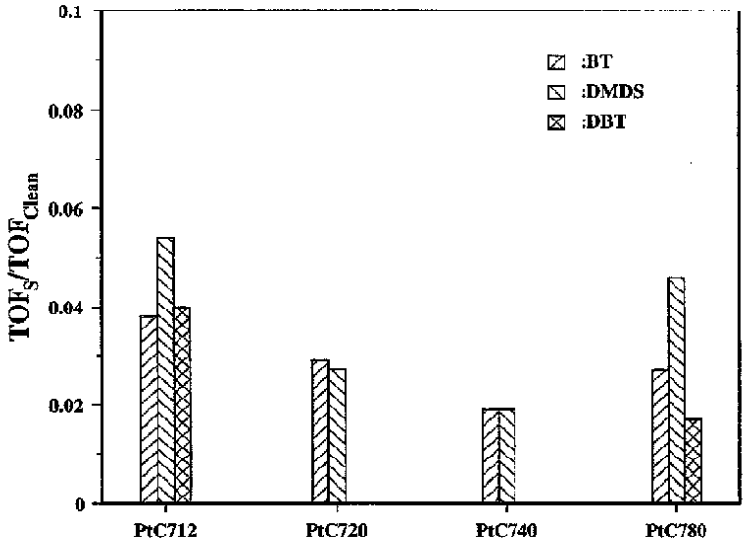

Figure 4.21: Sulfur tolerance of the catalysts with approx. 100 ppm sulfur in the feed.

It seems to be no pronounced effect of the Si/Al ratio of the zeolite support on the sulfur tolerance. Considering the NH_3-TPD measurements reported in Table 4.5, Chap. 4.1.2 the differences in acidity between the CBV720, CBV740, and CBV780 are very small. Although there are differences in the dispersion of platinum on these carriers, the sum of these two factors (acidity and dispersion) seems to give a comparable affinity for sulfur [92]. Much in the same way the higher acidity of the CBV712 sample is canceled out by the lower Pt-dispersion of this catalyst resulting in a comparable sulfur tolerance of all the zeolite supported catalysts examined.

Effect of sulfur compound

There are no clear differences in the effect of of the various sulfur compounds (BT, DBT, and DMDS) on the catalyst activity. This means that under the reducing conditions applied here the temperature is sufficiently high to provide dissociative adsorption of all the sulfur-containing molecules on the metal. Size and geometrical effects no longer prevail and the poisoning reaction is thus given by eq. 2.10 with H_2S acting as the common sulfiding agent. The high hydrogenolysis activity of small platinum particles is well known [1] and would support such a conclusion.

4.4.3 PRESULFIDING

Report of experiments studying its influence on catalyst activity and kinetic behaviour.

Presulfiding of the zeolite supported catalyst in 5% H_2S/H_2 results in a lower activity for hydrogenation of sulfur spiked toluene than that of the reduced catalyst. The reaction order in H_2 is identical for the sulfided and the reduced catalysts, while the order in toluene is less negative in the case of the presulfided sample. The temperature response also show similar features following the two different pretreatments.

As discussed in the previous chapter it is not expected that the sulfur levels and the limited time scale of the experiments used here results in the formation of a completely sulfided catalyst. To be able to study the activity and kinetic behaviour of such a catalyst, presulfiding at severe conditions (high temperature and sulfur concentration) was applied.

Effect on activity

After reduction the catalysts were presulfided in 5% H_2S/H_2 as described in chap. 3.3.3. All experiments were carried out using sulfurcontaining feed in order to keep the catalyst in the sulfided state. The toluene conversion as a function of TOS for the presulfided PtC780 catalyst is outlined in Figure 4.22. The reaction conditions are given in table 3.1, chap. 3.3.2.

Starting with 92 ppmwt BT in the feed steady-state conditions are reached after 1 hour on stream. Increasing the sulfur concentration to 469 ppmwt BT results in a nearly inactive catalyst at the choosen reaction conditions. When a switch to pumping sulfur-free toluene is made a marked increase in toluene conversion take place. This is due to the desorption of reversibly bound sulfur in the form of H_2S regenerating the reduced metal surface. In table 4.14 the specific activity and TOF of presulfided and reduced PtC780 are compared. The activity of the presulfided sample is clearly lower which is in accordance with the low hydrogenation activity found for other metal sulfides [5,11,34-36].

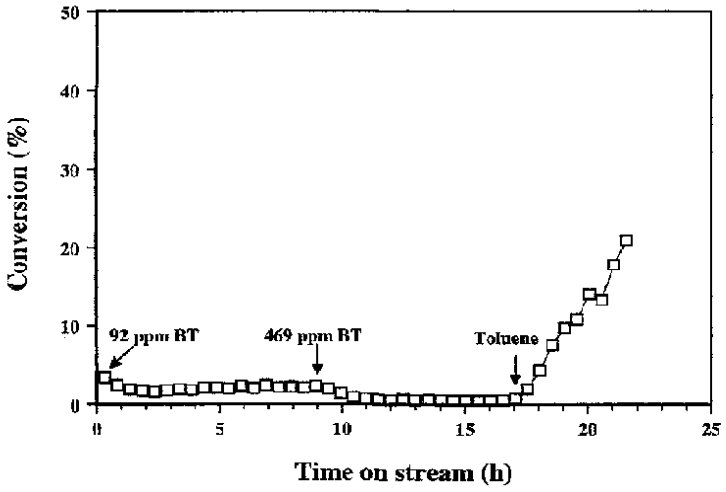

Figure 4.22: Conversion of toluene spiked with benzothiophene over presulfided PtC780.

Table 4.14: Specific activity and turnover frequency (TOF) for hydrogenation of toluene spiked with dibenzothiophene over presulfided PtC780.

	92 ppmwt BT		469 ppmwt BT	
Catalyst	r_0[a]	TOF[b]	r_0	TOF
PtC780	9,82	2,3	2,46	0,6
PtC780[c]	2,51	0,6	0,51	0,1

[a]: specific activity [µmol/s,g cat.], [b]: turnover frequency [s^{-1}] based on H_2-O_2 titration, pulse mode of fresh unpoisoned samples, [c]: presulfided sample.

Pressure effects

The kinetic behaviour of the presulfided catalysts was studied using power rate law kinetics (eq. 4.1). The experimental conditions are given in table 3.2, Chap. 3.3.2. Figure 4.23 shows plots of the data obtained over the 3PtC712 and 3PtC780 catalysts. The observed kinetic parameters are summerized in Table 4.15.

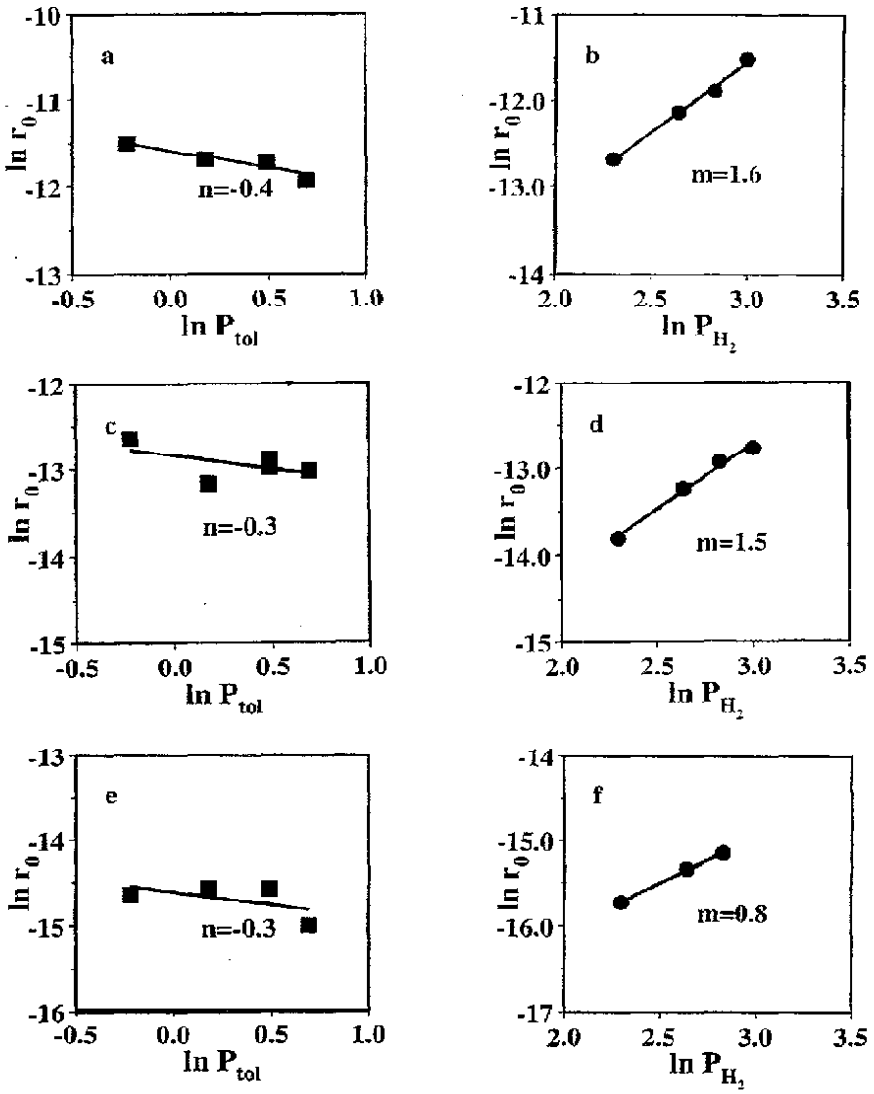

Figure 4.23: Kinetic plots of toluene hydrogenation over 3PtC780 (a,b), and 3PtC712 (c,d,e,f). a,b,c,d: 20 ppm S, e,f: 200 ppm S. a,c,e: order in toluene with constant partial pressure of hydrogen, b,d,f: order in hydrogen with constant partial pressure of toluene.

Table 4.15: Observed kinetic parameters in toluene hydrogenation over supported Pt catalysts. Sulfur added in the form of benzothiophene.

	20 ppm Sulfur		200 ppm Sulfur	
Catalyst	n	m	n	m
3PtC712	-0,3	1,5	-0,3	0,8
3PtC780	-0,4	1,6		

With 20 ppm sulfur in the feed (added as 100 ppm wt BT) a slightly negative order in toluene is observed (n=-0.4 and n=-0.3), wheras the order in H_2 is found to be 1.5. Increasing the sulfur concentration to 200 ppm sulfur leads to no change in the observed order in toluene (n=-0.3), but reduces the observed order in H_2 to m=0.8. If a comparison between these values and the values given in table 4.10 for hydrogenation of sulfurspiked toluene over reduced catalysts is made, it is observed that the orders in H_2 are close to identical. The orders in toluene are shifted to a less negative value (from n=-0.7 to n=-0.3) when going from the reduced to the presulfided catalyst.In Figure 4.24 the experimental reaction rates with 20 ppm sulfur in the feed are compared with the rates calculated utilizing the power-law rate model (eq.4.1) and an acceptable fit is observed.

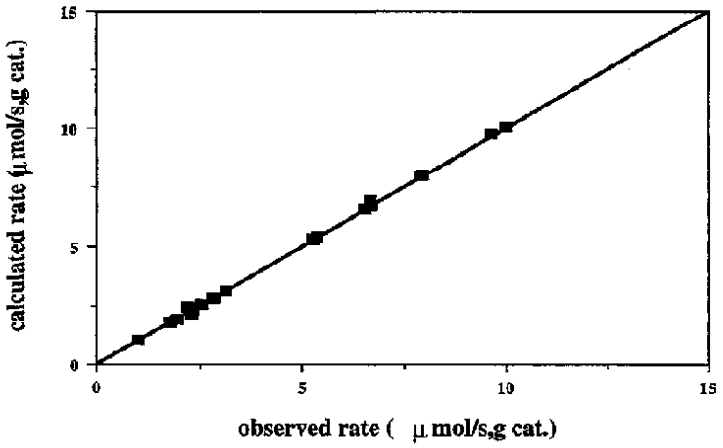

Figure 4.24: Comparison of the experimental and calculated reaction rates.

The similar dependency of the rection rate on the partial pressures of toluene and hydrogen between the reduced and presulfided catalysts is a clear indication of the close resemblance of the working state of the two.

Temperature effects

An experiment studying the temperature response over one of the sulfided catalysts was conducted using the toluene feed containing 100 ppmwt BT. Figure 4.25 shows a plot of the toluene conversion as a function of the reaction temperature. For the purpose of comparison the data for hydrogenation of sulfur-free and sulfurspiked toluene over the reduced catalyst are also included. A reaction temperature of 240°C is also here necessary to obtain a detectable conversion. The conversion increases steadily with temperature approaching the equilibrium conversion at 400°C.

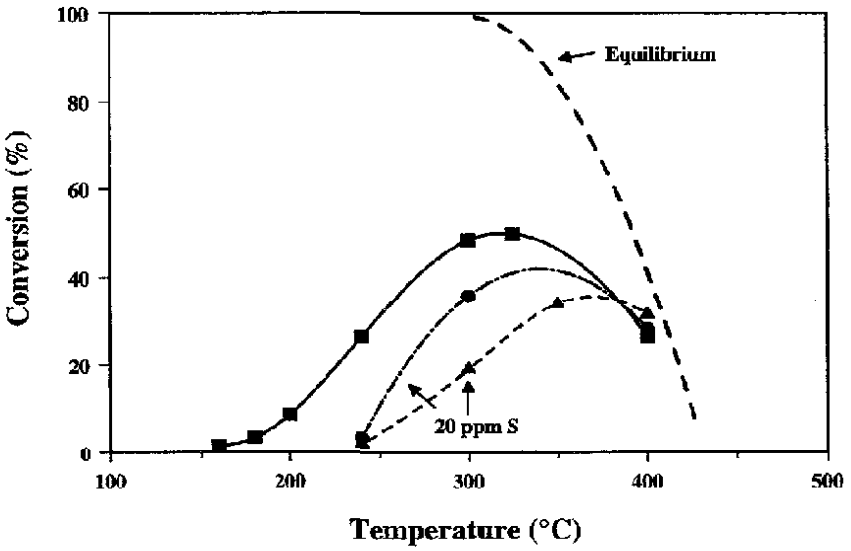

Figure 4.25: Temperature response in toluene hydrogenation over 3PtC712. Reduced catalyst (■, ●), presulfided catalyst (▲).

Allthough comprehensive data in the upper region of the temperature range are lacking there seems to be no maximum in the conversion which can be ascribed to the kinetic properties of the catalyst. Neither have examples of such behaviour of metal sulfide catalysts been found reported in literature.

5. CONCLUSIONS

A summary account of the main results and findings

Zeolite supported platinum catalysts have been prepared and both the metal and acid functions were characterized utilizing various experimental techniques. Hydrogenation of toluene was used as a model reaction and the effect of sulfur adsorption on the activity and kinetic behavior of the catalysts was investigated. The catalyst samples showed hydrogenation activities comparable to a commercial Pt/Al_2O_3 catalyst. There were no clear differences in the effect of the various sulfur compounds studied. Platinum supported on zeolite Y gave considerably more sulfur tolerant catalysts compared to Al_2O_3 as support.

Catalyst preparation and characterization. Noble metal catalysts supported on Y-zeolite were successfully prepared by ion-exchange. The metal content was 0.3 wt% and the Si/Al ratio of the zeolite supports varied in the range between 2.6 and 40. Characterization of the catalyst samples were performed utilizing several techniques. Ammonia TPD profiles showed wide desorption peaks indicating a large distribution in acid strength.

The metal function was characterized by chemisorption (H_2-O_2 titration in the pulse mode, and H_2 chemisorption in a volumetric apparatus), TEM, and toluene hydrogenation. Volumetric chemisorption resulted in higher H/Pt ratios than found with pulse titration. For the PtCBV712 zeolite the optimum pretreatment conditions were calcination at 325°C and reduction at 350°C resulting in the highest H/Pt ratios.

TEM micrographs of the PtCBV712 samples did not support the chemisorption measurements for all the samples. The sample calcined and reduced at 325°C/350°C had a calculated metal particle size from pulse titration of 26 Å, but TEM revealed a broad size distribution (10-400 Å). Calcination and reduction at 250° and 350°C resulted in small particles (10-25 Å) as seen by TEM, but the calculated particle size from chemisorption was large (150Å). The discrepancy is understandable if the stoichiometry of adsorption is less than unity on the smallest Pt particles.

Toluene hydrogenation at 31 bars and 240°C was used to assess the metal activity and thus the metal dispersion. Estimated initial activities correlated well with the H/Pt ratios measured by chemisorption. The Pt/HY with the highest H/Pt ratios had comparable activities to a well dispersed commercial Pt/Al_2O_3 catalyst. The steady state activity for hydrogenation did not correlate with the chemisorption measurements on the most acidic samples. This is due to the formation of coke deactivating the catalyst by blocking or limiting the access of toluene into the interior of the zeolite.

Hydrogenation of toluene. The effects of temperature and pressure on the kinetic behaviour of the platinum catalysts were studied in a high pressure fixed bed micro reactor. The reaction orders in toluene and hydrogen were determined at 240°C and 31 bars total pressure. An order close to 0 in toluene and 1.5 in hydrogen was found. A temperature dependent maximum in the reaction rate was also found. The temperature of maximum reaction rate varied with catalyst support and reaction pressure.The kinetic behavior does not seem to be influenced by the support acidity. The results support a reaction model involving the slow addition of hydrogen atoms to the adsorbed aromatic species as the rate determining step. This model also invoke the presence of hydrogen-deficient aromatic compounds on the metal surface.

Hydrogenation of sulfur-spiked toluene. The reaction orders with respect to toluene and hydrogen change when trace amounts of sulfur is added to the feed. The order with respect to toluene is more sensitive to the level of sulfur in the feed than the order in hydrogen supporting a reaction model asuming non-competitive adsorption at different sites for toluene and hydrogen. The effect of reaction temperature when using a toluene feed containing sulfur is similar to the sulfur-free feed although a maximum in the conversion cannot be determined with absolute certainty.

Sulfur-tolerance. Platinum supported on Y-zeolites gives considerably more sulfur-tolerant catalysts compared to Al_2O_3 as a support. High Si/Al-ratios give high specific activity due to higher Pt dispersion, while the intrinsic activity (TOF) in the presence of sulfur is highest at low Si/Al-ratio. The sulfur-tolerance seems to be independent of the Si/Al-ratio. There are no clear differences in the effect of the various sulfur-compounds (BT, DBT, and DMDS) on the catalyst activity.

REFERENCES

[1] Prestvik, R. Thesis, *Characterization of the metal function of a Pt-Re/Al_2O_3 reforming catalyst,* The Norwegian Institute of Technology, Trondheim, **1995.**

[2] Topsøe, H.; Clausen, B. S.; Massoth, F. E. *Hydrotreating Catalysis,* Catalysis-Science and Technology *11*; Springer Verlag **1996**.

[3] Douaud, A. *Hydrocarbon Processing.*, **1995**, (February) 55.

[4] Walsh, M. *Soc. Automot. Eng. (Spec. Publ.).* **1995**, (1073), 1.

[5] Lee, S. L.; Jonker, R. J. *Akzo Catalysts Symposium;* 1991, 25.

[6] Cooper, B. H.; Stanislaus, A. *Catal. Rev. Sci. Eng.* **1994**, *36*(1), 75.

[7] Suchanek, A. J. *1990 NPRA Annual Meeting.;* pp AM-90-21.

[8] Unzelman, G. H. *Oil Gas J.* **1987**, (June 29), 55.

[9] Jaffe, S. B. *Ind. Eng. Chem. Process Des. Dev.* **1974**, *13*(1), 34.

[10] Gully, A.; Ballard, W. P. Advances in Petroleum Chemistry and Refining.; Interscience Publ.: London, **1963**; *7*, 241.

[11] Cooper, B. H.; Stanislaus, A.; Hannerup, P. N. *ACS Preprints, Div. Fuel Chem.* **1992**, *37*(1), 41.

[12] Page, J. F. *Applied Heterogenous Catalysts: design-manufacture-use of solid catalysts.* Technip **1987**

[13] Dufresne, P.; Bigeard, P. H.; Billon, A. *Catal. Today.* **1987**, *1*, 367.

[14] Girgis, M. J.; Gates, B. C. *Ind. Eng. Chem. Res.* **1991**, *30*, 2021.

[15] Cooper, B. H.; Donnis, B. B. L. *Appl. Catal. A:General.* **1996**, *137*, 203.

[16] Kasztelan, S.; Guillaume, D. *Ind. Eng. Chem. Res.* **1994**, *33*, 203.

[17] Lindfors, L. P.; Salmi, T. *Ind. Eng. Chem. Res.* **1993**, *32*(1), 34.

[18] Lindfors, L. P.; Salmi, T.; Smeds, S. *Chem. Eng. Sci.* **1993**, *48*(22), 3813.

[19] Lin, S. D.; Vannice, A. M. *J. Catal.* **1993**, *143*, 554.

[20] Smeds, S.; Murzin, D.; Salmi, T. *Appl. Catal.* **1995**, *125*, 271.

[21] Van der Steen, P. J.; Scholten, J. J. F. *Appl. Catal.* **1990**, *58*, 291.

[22] Orozco, J. M.; Webb, G. *Appl. Catal.* **1983**, *6*, 67.

[23] Bandiera, J.; Meriaudeau, P. *React. Kinet. Catal. Lett.* **1988**, *37*(2), 373.

[24] Chou, P.; Vannice, A. M. *J. Catal.* **1987**, *107*, 140.

[25] Sapre, A. V.; Gates, B. C. *Ind. Eng. Chem. Process Des. Dev.* **1981**, *20*, 68.

[26] Kokayeff, P. *Catalytic Hydroprocessing of Petroleum and Distillates.*; Oballa, M. C.; Shih, S. S., Chem. Ind. **1994**; *58*, 253.

[27] Bouchy, M.; Dufresne, P.; Kasztelan, S. *Ind. Eng. Chem. Res.* **1992**, *31*, 2661.

[28] Bouchy, M.; Peureux-Denys, S.; Dufresne, P.; Kasztelan, S. *Ind. Eng. Chem. Res.* **1992**, *32*, 1592.

[29] Yui, S. M. *Catalytic Hydroprocessing of Petroleum and Distillates.*; Oballa, M. C.; Shih, S. S., Chem. Ind. **1994**; *58*, 235.

[30] Wilson, M. F.; Fisher, I. P.; Kriz, J. F. *J. Catal.* **1985**, *95*, 155.

[31] Yui, S. M.; Sandford, E. C. *Proceedings of API Refining Dept., 50th Midyear Meeting, Kansas City;* **1985**; 290.

[32] Cooper, B. H.; Hannerup, P. N.; Søgaard-Andersen, P. *Erdøl & Kohle.* **1994**, *47*(9), 330.

[33] Cooper, B. H.; Søgaard-Andersen, P.; Nielsen-Hannerup, P. *Catalytic Hydroprocessing of Petroleum and Distillates.*; Oballa, M. C.; Shih, S. S., Chem. Ind. **1994**; *58*, 279.

[34] van den Berg, J. P.; Lucien, J. P.; Germaine, G.; Thilemans, G. L. B. *Fuel Proc. Tech.* **1993**, *35*, 119.

[35] Nash, R. M. *Oil Gas J.* **1989**, (May 29), 47.

[36] Yoes, J. R.; Asim, M. Y. *Oil Gas J.* **1987**, (May 11), 54.

[37] Lucien, J. P.; van den Berg, J. P.; Germaine, G.; van Hooijdonk, H. M. J. H.; Gjers, M.; Thielemans, G. L. B. *Catalytic Hydroprocessing of Petroleum and Distillates.*; Oballa, M. C.; Shih, S. S., Chem. Ind. **1994**; *58*, 291.

[38] Minderhoud, J. K.; Lucien, J. P. *Eur. Patent 303, 332* **1988**.

[39] Haun, E. C.; Thompson, G. J.; Gorawara, J. K.; Sullivan, D. K. *US Patent.* **1990**, *5,114,562*.

[40] Hamilton, G. L.; Suchanek, A. J. *Oil Gas J.* **1991**, (July 1), 55.

[41] Peries, J. P.; Billon, A.; Hennico, A.; Kressmann, S. *1991 NPRA Annual Meeting;* pp AM-91-38.

[42] Søgaard-Andersen, P.; Cooper, B. H.; Hannerup, P. N. *1992 NPRA Annual Meeting.;* pp AM-92-50.

[43] Lee, S. L.; de Wind, M. *Oil Gas J.* **1992**, 88.

[44] Del Rossi, K. J.; Jablonski, G. A.; Marler, D. O. WO 95/28459, *PCT Int. Appl.*

[45] Schuit, G. C. A.; Gates, B. C. *AIChE J.* **1973**, *19*(3), 417.

[46] Voorhoeve, R. J. H.; Stuiver, J. C. M. *J. Catal.* **1971**, *23*, 243.

[47] Farragher, A. L.; Cossee, P. *5th Int. Congr. on Catalysis.;* North-Holland: Amsterdam, **1973**; 1301.

[48] Delmon, B. *Bull. Soc. Chim. Belg.* **1979**, *88*, 979.

[49] Wivel, C.; Candia, R.; Clausen, B. S.; Mørup, S.; Topsøe, H. *J. Catal.* **1981**, *68*, 453.

[50] Prins, R.; De Beer, H. J.; Somorjai, G. A. *Catal. Rev.-Sci. Eng.* **1989**, *31*(1-2), 1.

[51] Vivier, L.; Kasztelan, S.; Perot, G. *Bull. Soc. Chem. Bel.* **1991**, *100*(11-12), 801.

[52] Lowe, B. M. *Educ. Chem.* **1992**, *29*(1), 15.

[53] Rabo, J. A.; Schomaker, V.; Pickert, P. E. *Proc. 3th Int. Congress on Catalysis.;* North Holland, Amsterdam, **1965**; 1264.

[54] Dalla Betta, R. A.; Boudart, M. *Proc. 5th Int. Congress on Catalysis.;* North Holland, Amsterdam, **1973**; 1329.

[55] Gallezot, P.; Datka, J.; Massardier, J.; Primet, M.; Imelik, B. *Proc. 6th Int. Congr. on Catalysis.;* **1976**, 696.

[56] Vedrine, J. C.; Dufaux, M.; Naccache, C.; Imelik, B. *J. Chem Soc., Faraday Trans.* **1978**, *74*, 440.

[57] Tran Manh Tri; Massardier, J.; Gallezot, P.; Imelik, B. *Stud. Surf. Sci. Catal.*; Imelik, B. et al., elsevier **1980**; *5*, 279.

[58] Stakheev, A. Y.; Sachtler, W. M. H. *J. Chem. Soc. Faraday. Trans.* **1991**, *87*(22), 3703.

[59] Sachtler, W. M. H.; Zhang, Z. *Adv. Catal.* **1993**, *39*, 129.

[60] Bai, X.; Sachtler, W. M. H. *J. Catal.* **1991**, *129*, 121.

[61] Gallezot, P. *Catal. Rev. Sci. Eng.* **1979**, *20*(1), 121.

[62] Tzou, M. S.; Teo, B. K.; Sachtler, W. M. H. *J. Catal.* **1988**, *113*, 220.

[63] Homeyer, S. T.; Sachtler, W. M. H. *Stud. Surf. Sci. Catal.* **1989**, *49*, 975.

[64] Homeyer, S. T.; Sachtler, W. M. H. *J. Catal.* **1989**, *117*, 91.

[65] Sachtler, W. M. H.; Tzou, M. S.; Jiang, H. J. *Solid State Ion.* **1988**, *26*, 71.

[66] Gallezot, P.; Alarcon-Diaz, A.; Dalmon, J. A.; Renouprez, A. J.; Imelik, B. *J. Catal.* **1975**, *39*, 334.

[67] Arai, H.; Seiyama, T.; Marakawa, M.; Tominaga, T. *Stud. Surf. Sci. Catal.* **1980**, *6*, 167.

[68] Park, S. H.; Tzou, M. S.; Sachtler, W. H. M. *Appl. Catal.* **1986**, *24*, 85.

[69] Tzou, M. S.; Sachtler, W. H. M. *Stud. Surf. Sci. Catal.* **1988**, *38*, 233.

[70] Chmelka, B. F.; Rosin, R. R.; Went, G. T.; Bell, A. T.; Radke.C.J.; Petersen, E. E. *Stud. Surf. Sci. Catal.* **1989**, *49*, 995.

[71] Chmelka, B. F.; Rosin, R. R.; Went, G. T.; Bell, A. T.; Radke.C.J.; Petersen, E. E. *Stud. Surf. Sci. Catal.* **1989**, *49*, 995.

[72] Kuo, Y.-J.; Tatarchuk, B. J. *J. Catal.* **1988**, *112*, 229.

[73] Kuo, Y.-J.; Cocco, R. A.; Tatarchuk, B. J. *J. Catal.* **1988**, *112*, 250.

[74] Breysse, M.; Afonso, J.; Lacroix, M.; Portefaix, J. L.; Vrinat, M. *Bull. Soc. Chim. Belg.* **1991**, *100*(11-12), 923.

[75] Ledoux, M. J.; Kippelen, C.; Maire, G.; Szabo, G.; Goupyl, J.; Krause, O. *Bull. Soc. Chim. Belg.* **1991**, *100*(11-12), 873.

[76] Ramanathan, S.; Oyama, S. T. *J. Phys. Chem.* **1995**, *99*, 16365.

[77] Sajkowski, D. J.; Oyama, S. T. *Appl. Catal. A:General.* **1996**, *134*, 339.

[78] Lee, J. S.; Yeom, M. H.; Park, K. I.; Nam, I. S.; Chung, J. S.; Kim, Y. G.; Moon, S. H. *J. Catal.* **1991**, *128*, 126.

[79] Lee, K. S.; Abe, H.; Reimer, J. A.; Bell, A. T. *J. Catal.* **1993**, *139*, 34.

[80] Koussathana, M.; Vamvouka, D.; Economou, H.; Verykios, X. *Appl. Catal.* **1991**, *77*, 283.

[81] Koussathana, M.; Vamvouka, D.; Tsapatsis, M.; Verykios, X. *Appl. Catal.* **1992**, *80*, 99.

[82] Koussathana, M.; Vamvouka, D.; Verykios, X. E. *Appl. Catal.* **1993**, *95*, 211.

[83] Bartholomew, C. H.; Agrawal, P. K.; Katzer, J. R. *Adv. Catal.* **1982**, *31*, 135.

[84] McCarty, J. G.; Wise, H. *J. Chem. Phys.* **1980**, *72*(12), 6332.

[85] McCarty, J. G.; Wise, H. *J. Catal.* **1985**, *94*, 543.

[86] Barbier, J.; Lamy-Pitara, E.; Marecot, P.; Boitiaux, J. P.; Cosyns, J.; Verna, F. *Adv. Catal.* **1990**, *37*, 279.

[87] McCarty, J. G.; Wise, H. *J. Catal.* **1983**, *82*, 92.

[88] Menon, P. G.; Prasad, J. *Proc. 6th. Int. Congr. on Catalysis.;* North-Holland: Amsterdam, 1977; p 1061.

[89] Apesteguia, C. R.; Barbier, J.; Plaza de los Reyes, J. F.; Garetto, T. F.; Parera, J. M. *Appl. Catal.* **1981**, *1*, 159.

[90] Apesteguia, C.; Barbier, J. *React. Kinet. Catal. Lett.* **1982**, *19*(3-4), 351.

[91] Schultze, J. W.; Koppitz, F. D. *Electrochim. Acta* **1976**, *21*, 327.

[92] Barbier, J.; Marecot, P.; Tifouti, L. *Appl. Catal.* **1985**, *19*, 375.

[93] Cini, M. *J. Catal.* **1975**, *37*, 187.

[94] Maxted, E. B. *Adv. Catal.* **1951**, *3*, 129.

[95] Aguinaga, A.; Montes, M.; de la Cal, J. C.; Asua, J. M. *Ind. Eng. Chem. Res.* **1992**, *31*, 155.

[96] Boitiaux, J. P.; Cosyns, J.; Verna, F. Stud. Surf. Sci. Catal.; **1987**; *34*, 105.

[97] Demuth, J. E.; Jepsen, D. W.; Marcus, P. M. *Phys. Rev. Lett.* **1973**, *31* (8), 540.

[98] Ng, C. F.; Martin, G. A. *J. Catal.* **1978**, *54*, 384.

[99] Bartholomew, C. H.; Pannell, R. B. *Appl. Catal.* **1982**, *2*, 39.

[100] Mahoungou, J. R. Thesis, Poitiers, 1990.

[101] Chiou, J. F.; Huang, Y. L.; Lin, T. B.; Chang.J.R. *Ind. Eng. Chem. Res.* **1995**, *34*, 4277.

[102] Lin, T. B.; Jan, C. A.; Chang, J. R. *Ind. Eng. Chem. Res.* **1995**, *34*, 4284.

[103] Marécot, P.; Mahoungou, J. R.; Barbier. *Appl. Catal.* **1993**, *101*, 143.

[104] Apesteguia, C.; Barbier, J. *Bull. Soc. Chim. (France).* **1982**, *5-6*(1), 165.

[105] Maurel, R.; Barbier, J. *J. Chim. Phys.* **1976**, *73*(11-12), 995.

[106] Kukes, S. G.; Clark, F. T.; Hopkins, D. *U.S. Patent 5,308,814.* **1994**.

[107] Winquist, B. H. C.; Miliam, S. N.; Murray, B. D.; Ryan, R. C. *Eur. Patent 519, 573* **1992**.

[108] Larsen, G.; Resasco, D. E.; Durante, V. A.; Kim, J.; Haller, G. L. *Stud. Surf. Sci. Catal.* **1994**, *83*, 321.

[109] Huang, T. C.; Kang, B. C. *J. Mol. Catal. A:Chemical.* **1995**, *103*, 163.

[110] Seoane, X. L.; L'Argentiere, P. C.; Figoli, N. S.; Arcoya, A. *Catal. Lett.* **1992**, *16*, 137.

[111] Rostrup-Nielsen, J. R. *J. Catal.* **1971**, *21*, 171.

[112] Oudar, J.; Pinol, S.; Pradier, C.-M.; Berthier, Y. *J. Catal.* **1987**, *107*, 445.

[113] Oudar, J.; Pradier, C.-M.; Vassilakis, D.; Berthier, Y. *Catal. Lett.* **1988**, *1*, 339.

[114] Figoli, N. S.; L'Argentiere, P. C.; Nicot, C.; Frety, R. *Catal. Lett.* **1996**, *38*, 171.

[115] Hoyos, L. J.; Primet, M.; Praliaud, H. *J. Chem. Faraday Trans.* **1992**, *88*(1), 113.

[116] Bartholomew, C. H. *Catalysis* **1994**, *11*, 93.

[117] Benson, J. E.; Boudart, M. *J. Catal.* **1965**, *4*, 704.

[118] O_Rear, D. J.; Löffler, D. G.; Boudart, M. *J. Catal.* **1990**, *121*, 131.

[119] Boudart, M.; Aldag, A.; Benson, J. E.; Dougharty, N. A.; Harkins, C. G. *J. Catal.* **1966**, *6*, 92.

[120] Dorling, T. A.; Moss, R. L. *J. Catal.* **1966**, *5*, 111.

[121] Aben, P. C.; Platteeuw, J. C.; Stouthamer, B. *Proc. 4th Int. Cong. Catal.;* Akademiai Kaido: Budapest, **1971**; 395.

[122] Basset, J. M.; Dalmai-Imelik, M.; Primet, M.; Mutin, R. *J Catal.* **1975**, *37*, 22.

[123] Franck, J. P.; Martino, G. *Progress in Catalyst Deactivation.*; NATO Advanced Study Institute Series E.; M. Nijhoff Pub.: The Hague, 1982; *54*, 355.

[124] Lin, S. D.; Vannice, A. M. *J. Catal.* **1993**, *143*, 563.

[125] Jacobs, P. A. Chemical Industries *Series. 15*; Marcel Dekker: New York, **1984.**

[126] Bednarova, L. *Characterization of NH4Y Zeolites*. Dept. of Industrial Chemistry, NTNU.: **1996.**

[127] Blekkan, E. A.; Holmen, A.; Vada, S. *Acta Chemica Scandinavia.* **1993**, *47*, 275.

[128] Bergene, E. Thesis, *Surface characterization of Pt and Pt/Rh gauze catalysts.* The Norwegian Institute of Technology, Trondheim, **1990.**

[129] Grønvold, A. G. Thesis, *Conversion of Methanol to Lower alkenes over Molecular Sieve-Type Catalysts*. The Norwegian Institute of Technology, Trondheim, **1994.**

[130] Heitnes Hofstad, K. A. Thesis, *Catalytical Partial Oxidation of Methane to Synthesis Gas.* NTNU, Trondheim, **1996.**

[131] Remy, M. J.; Stanica, D.; Poncelet, G.; Feijen, E. J. P.; Grobet, P. J.; Martens, J. A.; Jacobs, P. A. *J. Phys. Chem.* **1996**, *100*, 12440.

[132] Moljord, K.; Magnoux, P.; Guisnet, M. *Appl. Cat. A.* **1995**, *122*(1), 21.

[133] Hidalgo, C.; Itoh, H.; Hattori, T.; Niwa, M.; Murakami, Y. *J. Catal.* **1984**, *85*, 362.

[134] Shertukde, P. V.; Hall, W. K.; Dereppe, J.-M.; Marcelin, G. *J. Catal.* **1993**, *139*, 468.

[135] Spiewak, B. E.; Handy, B. E.; Sharma, S. B.; Dumesic, J. A. *Catal. Lett.* **1994**, *23*, 207.

[136] Zhang, D.-C.; Da, Z.-J. *Thermochim. Acta* **1994**, *233*, 87.

[137] Chauvin, B.; Boulet, M.; Massiani, P.; Fajula, F.; Figueras, F.; Des Courieres, T. *J. Catal.* **1990**, *126*, 532.

[138] Auroux, A.; Muscas, M.; Coster, D. J.; Fripiat, J. J. *Catal. Lett.* **1994**, *28*, 179.

[139] Iwamoto, M.; Tajima, M.; Kagawa, S. *J. Chem. Soc. Chem. Commun.* **1986**, 598.

[140] Reagan, W. J.; Chester, A. W.; Kerr, G. T. *J. Catal.* **1981**, *69*, 89.

[141] Homeyer, S. T.; Sachtler, W. M. H. *J. Catal.* **1989**, *118*, 266.

[142] Pandya, K. I.; Heald, S. M.; Hriljac, J. A.; Petrakis, L.; Fraissard, J. *J. Phys. Chem.* **1996**. *100*, 5070.

[143] Mignard, S.; Caillette, Ph.; Marchal, N. *Catalytic Hydroprocessing of Petroleum and Distillates.*; Oballa, M. C.; Shih, S. S., Chem. Ind. **1994**; *58*, 447.

[144] Fouche, V.; Magnoux, P.; Guisnet, M. *Appl. Catal.* **1990**, *58*, 189.

[145] Scott Fogler, H. *Elements of Chemical Reaction Engineering*. Prentice-Hall International Series in the Physical and Chemical Engineering Sciences.; Prentice-Hall, Inc.**1986**.

[146] Mears, D. E. *Chem. Eng. Sci.* **1971**, *26*, 1361.

[147] Dautzenberg, F. M. *ACS Symp. Series*. **1989**, *411*, 99.

[148] Moulijn, J. A.; Tarfaoui, A.; Kapteijn, F. *Catal. Today*. **1991**, *11*, 1.

[149] Mears, D. E. *Ind. Eng. Chem. Proc. Dev.* **1971**, *10*(4), 541.

[150] Lindfors, L. P.; Salmi, T.; Whitty, K. *Ind. Eng. Chem. Res.* **1994**.

[151] Poondi, D.; Vannice, M. A. *J. Catal.* **1996**, *161*, 742.

[152] van Meerten, R. Z. C.; Coenen, J. W. E. *J. Catal.* **1975**, *37*, 37.

[153] Leclercq, G.; Boudart, M. *J. Catal.* **1981**, *71*, 127.

[154] Oehme, M. *Kapillargasskromatografi i Praksis.* **1993.**

[155] Bjørnstad, P, Bjørnstad, T. *NIVÅMETODEN for bedre skriving i arbeidslivet.* **1993.**

APPENDIX I

GASES[1] AND CHEMICALS

---

a. Pulse chemisorption	Air (kl. 2 pkt. A)
	O_2 2.5 (99.5%)
	H_2 5.0 (99.999%)
	Ar 6.0 (99.9999%)[2]
	7% H_2 in Ar
b. Volumetric chemisorption	Air (kl. 2 pkt. A)
	N_2 5.0 (99.999%)
	H_2 5.0 (99.999%)
	He 6.0 (99.9999%)
c. Activity measurements	Toluene (p.a. Prolabo)
	Benzothiophene (95%, Aldrich)
	Dibenzothiophene (98%, Aldrich)
	Dimethyldisulphide (Elf Aquitane)
	N_2 5.0 (99.999%)
	H_2 5.0 (99.999%)
	5% H_2S in H_2
d. TPD of NH_3	He 6.0 (99.9999%)
	5% NH_3 in He 4.8 (99.998%)
e. Thermogravimetric analysis	Air (kl. 2 pkt. A)
	N_2 5.0 (99.999%)

[1] All gases were dilivered by HydroGas except for [2], delivered by Air Products.

APPENDIX II

THE HYDROGENATION APPARATUS

Description of components and parts.

The lines of the apparatus consists of 1/4" 316s stainless steel, except the liquid feed lines which are made of 1/16" 316s stainless steel. The reactor is constructed of a 316s stainless steel tube (9 mm i.d.) with flanges at the top and bottom. The remaining components are standard equipment from commercial suppliers applying with the prescribed requirements. The apparatus is mounted on a aluminium plate attached to a aluminium frame supported on wheels for mobility.

Parts with specifications. The placement of the different components is indicated in fig. 3.5.

1. Gas flask valve
   Norgas

2. Pressure reduction valve with needle valve
   Norsk Hydro

Material	: Stainless steel
Medium	: H_2S
Pressure range	: 0-300 bar at inlet
	: 0-5 bar at outlet
Connection	: Gyrolok 4N-316 at outlet

3. Needle valve
   Hoke D3752 G4Y 316SS

Connection	: Gyrolok 4N-316 at inlet and outlet

4. Micron filter

Hoke 6311 G4Y 316SS

Filterelement	: 80410-1
Max pressure	: 5000 PSIG at 70°F
Temperature range	: -51°C - 232°C
Cv-factor	: 0.006
Connection	: Gyrolok 4N-316 at inlet and outlet

5. Manometer

Bourdon Sedeme, MIX100

ø=100 mm

Pressure range	: 0-250 bar
Connection	: Gyrolok 4AF8-316

6. Pressure reduction valve

Tescom Pressure Regulator

Serie	: 44-1100
Model	: 44-1125-24
Max pressure inlet	: 10 000 PSI
Pressure outlet	: 25-4000 PSI
Connection	: Gyrolok 4N-316 at inlet and outlet

7. Manometer

Bourdon Sedeme, MV3X

ø=150 mm

Pressure range	: 0-250 bar
Connection	: Gyrolok 4AF8-316

8. Ball valve

Hoke 7115 G4Y 316SS

Max pressure	: 6000 PSIG
Temperature range	: -18°C - 149°C
Cv-factor	: 0.80
Orifice	: 0.187
Connection	: Gyrolok 4N-316 at inlet and outlet

9. Ball valve

Hoke 7122 G4Y 316SS

Max pressure	: 1500 PSIG
Temperature range	: -18°C - 176°C
Cv-factor	: 0.80
Orifice	: 0.187
Connection	: Gyrolok 4N-316 at inlet and outlet

10. Oxygen trap

Alltech's High Pressure Oxisorb

Cat. no.	: 60679
Max pressure	: 3000 PSI
Connection	: 1/4" NPT at inlet and outlet

11. Metering valve

Hoke 1335G4Y

Max pressure	: 5000 PSI
Temperature range	: -54°C - 232°C
Cv-factor	: 0.010
Orifice	: 0.047
Connection	: Gyrolok 4N-316 at inlet and outlet

12. Check valve

Hoke 6133G4Y 316SS

Max pressure	: 6000 PSIG
Cv-factor	: 0.187
Connection	: Gyrolok 4N-316 at inlet and outlet

13. Pressure regulator

Tescom Back Pressure Regulator

Serie	: 26-1700
Model	: 26-1723-24-090
Max pressure inlet	: 10000 PSI
Pressure outlet	: 25-4000 PSI
Connection	: Gyrolok 4N-316 at inlet and outlet

14. Mass flow controller (MFC)

Hi-Tec Mass Flow Controller

Model	: F-230C-FA-22-V MFC
Connection	: Gyrolok 4N-316 at inlet and outlet
Operating data	
Medium	: N_2
Temperature	: 20°C
Pressure inlet	: 150 bar
Pressure outlet	: 144 bar
Max pressure	: 300 bar
Capacity	: 6-300 cc/min.

15. Mass flow controller (MFC)

Hi-Tec Mass Flow Controller

Model	: F-230C-FA-22-V MFC
Connection	: Gyrolok 4N-316 at inlet and outlet
Operating data	
Medium	: H_2
Temperature	: 20°C
Pressure inlet	: 150 bar
Pressure outlet	: 144 bar
Max Pressure	: 300 bar
Capacity	: 6-300 ml/min.

16. Gas flow regulator

Vögtlin Flow Meter

Model	: V100.140A-PV
Connection	: Gyrolok 4N-316 at inlet and outlet
Operation data	
Medium	: H_2S/H_2
Temperature	: 20°C
Pressure	: 1 bara
Capacity	: 0-440 ml/min.

17. Oven

Matriale	: 2 Fibrothal heatmodules type HAS 70/250/110
Inner diameter	: 70 mm.
Outer diameter	: 220 mm.
Length	: 250 mm.
Effect	: 450 W.
Power	: 110 V pr. module

18. Absorber

19. Liquid feed reservoir

20. Pump

Model	: HP 1050 Isocratic Pump
Connection	: 1/16" HPLC fittings
Operating data	
Medium	: non-corrosive liquids (pH: 1.0 - 9.5)
Temperature range	: 10°C - 55°C
Pressure range	: 0 - 200 bar
Capacity	: 0,001 - 9,999 cc/min.

21. Pump

Model	: Altex 100A Isocratic Pump
Connection	: 1/16" HPLC fittings
Operating data	
Medium	: non-corrosive liquid (pH: 1.0 - 9.5)
Temperature range	: 10°C - 55°C
Pressure range	: 0 - 700 bar
Capacity	: 0,01 - 9,999 cc/min.

22. Gas Chromatograph

Model	: Chrompack CP9000
Detectors	: Channel A - TCD
	: Channel B - FID
Columns	: Channel A-PoraplotQ, 10 m*0,53 mm.
	: Channel B-CP-5 CB, 10 m*0,53 mm.

23. 3-way, 2-stem manifold

Autoclave Engineers 10V2075-316

Max pressure	: 11500 PSI
Temperature range	: -54°C - 232°C
Cv-faktor	: 0.18

Orifice	: 0.094
Connection	: 1/16" fittings at inlet and outlet

24,25. Gas regulators

Flow Meter

Model	: RA 4 81 599/83
Temperature	: 20°C
Pressure	: 1bara
Capacity	: 0 - 500 cc/min.

26. Condensation pot

APPENDIX III

AXIAL DISPERSION

Calculation of the required L/d_p for ensuring plug flow operation in the reactor.

The viscosity of the fluid medium at reactor conditions is estimated by:

$$\mu = 0{,}3838T + 167{,}3534 \qquad [10^{-7}\ \text{m kg}^{-1}\ \text{s}^{-1}] \qquad \text{(AIII.1)}$$

viscosity for N_2 [154] (50% of the fluid medium).

The particle Reynolds number is given by:

$$Re_p = G\, d_p / \mu \qquad \text{(AIII.2)}$$

The minimum L/d_p follows from [143]:

$$\frac{L}{d_p} > (92.0)\,Re_p^{-0.23}\, n \ln\frac{1}{1-x} \quad \text{(for gas-phase operation)} \qquad \text{(AIII.3)}$$

Equations AIII.1 - AIII.3 applied on the reaction conditions given in table 3.1 gives:

$Re_p = \underline{0.40}$ and $L/d_p > \underline{184}$ $\quad (d_p = 10^{-4}\ \text{m},\ G = 0.10\ \text{kg m}^{-2}\ \text{s}^{-1},\ n = 1,\ x = 0.8)$

Increasing the temperature to 350°C gives:

$Re_p = \underline{0.34}$ and $L/d_p > \underline{190}$